

**The potential of high resolution regional
reanalyses COSMO-REA for renewable
energy applications**

Inaugural-Dissertation

zur

Erlangung des Doktorgrades

der Mathematisch-Naturwissenschaftlichen Fakultät

der Universität zu Köln

vorgelegt von

Christopher W. Frank

aus Bad Honnef

Köln, 2019

Berichterstatter/in: Prof. Dr. Susanne Crewell
Prof. Dr. Roel A.J. Neggers

Tag der mündlichen Prüfung: 15.01.2020

Für meinen Sohn Leonas Lars, seine Generation und alle Folgenden.

Contents

1	Introduction	1
1.1	Motivation	1
1.2	Contribution within this thesis	2
2	Material and methods	7
2.1	Regional reanalyses COSMO-REA6 and COSMO-REA2	7
2.2	PV simulation chain	9
2.2.1	Module orientation estimate	9
2.2.2	Transposition model to plane of array	12
2.2.3	PV simulation model	14
3	Bias correction of a novel European reanalysis data set for solar energy applications	17
3.1	Introduction	18
3.2	Data sets	20
3.2.1	COSMO-REA6	20
3.2.2	ERA-Interim	22
3.2.3	MERRA-2	23
3.2.4	Surface measurements	23
3.3	Assessment of COSMO-REA6 GHI	26
3.4	GHI post-processing	29
3.5	Evaluation of the new GHI data set	32
3.5.1	Marginal distribution	33
3.5.1.1	Separate evaluation for clear sky and cloudy conditions	33
3.5.2	Joint distribution	34
3.5.3	Cross-validation of the new GHI data set	35
3.5.4	Daily mean values	37
3.5.4.1	Comparison to previous studies	37
3.5.5	Spatio-temporal representation	38
3.5.6	Ramp rates	40
3.6	Summary	41
3.7	Conclusion	43
4	The added value of high resolution regional reanalyses for wind power applications	45
4.1	Introduction	46
4.2	Reanalyses and observations	48
4.2.1	High resolution regional reanalyses	48
4.2.2	Global reanalyses	49

4.2.3	Tower measurements	49
4.2.4	Assimilated observations	51
4.3	Methods	52
4.3.1	Matching of model and measurements	52
4.3.2	Uncertainty estimates	53
4.3.3	Vertical extrapolation of measurements	55
4.3.3.1	Wind extrapolation set-up	56
4.4	Results	57
4.4.1	Marginal distributions	57
4.4.1.1	Wind speed	57
4.4.1.2	Temporal wind speed changes	58
4.4.1.3	Vertical wind speed gradients	60
4.4.1.4	Low wind persistence	62
4.4.2	Joint distributions	65
4.4.2.1	Bias and bias corrected MAE	65
4.4.2.2	Correlations	65
4.4.2.3	Stability dependent validation	66
4.4.3	Accumulated relative power estimates	71
4.5	Discussion	73
4.6	Conclusion	74
4.7	Annex	76

5 Hybrid wind-solar balancing effects: An European study using post-processed regional reanalysis 79

5.1	Introduction	79
5.2	Material and methods	83
5.2.1	Regional reanalysis for PV and wind power estimates	83
5.2.2	Post-processing of COSMO-REA6 direct and diffuse radiation components	84
5.2.3	PV reference data	87
5.2.4	PV fleet information	87
5.2.5	PV simulation set-ups	88
5.3	Results	89
5.3.1	The added value of post-processed irradiance for PV power estimates	89
5.3.1.1	Assessment of post-processed radiation components	91
5.3.1.2	PV estimates with and without post-processed radiation components	95
5.3.1.3	Summary and discussion	96
5.3.2	Assessment and calibration of real fleet PV power simulations	98
5.3.2.1	Assessment with Open Power System Data	99

5.3.2.2	Calibration	100
5.3.2.3	Variability assessment	103
5.3.2.4	Summary and discussion	104
5.3.3	Balancing effects and potentials of hybrid wind-solar production	106
5.3.3.1	Inland balancing	107
5.3.3.2	Cross-border balancing	111
5.3.4	Discussion	116
5.4	Conclusion	117
5.5	Annex	120
6	Conclusions and Outlook	123
6.1	Conclusions	123
6.2	Overall picture and outlook	127
	Bibliography	129
	Danksagung	141

Abstract

Atmospheric reanalyses, a synthesis of meteorological observations and weather models, provide best estimates of past weather information in a physically consistent way on a temporal and spatial grid. These characteristics make reanalyses an established tool for a variety of weather related applications. In the field of renewable energies reanalyses are used to simulate production variabilities of existing or theoretical power plants and their impact on the energy system, which leads to a steadily growing interest in such products.

However, the application potential of reanalyses depends highly on their ability to describe atmospheric phenomena accurately. Thus, with each new reanalysis product assessment studies of its potential for specific applications becomes necessary. At this point, the thesis at hand contributes to assess the accuracy of reanalyses with respect to renewable energy applications. Herein, the novel high resolution regional reanalyses COSMO-REA6 and COSMO-REA2 developed within the Hans-Ertel-Centre for weather research at the German weather service are assessed, post-processed, and further exploited for renewable energy related applications.

The first part investigates global horizontal irradiance (GHI), which is relevant for photovoltaics (PV). In order to assess which reanalysis provides best estimates of GHI, the two regional reanalyses are compared comprehensively to measurements as well as to the frequently used global reanalyses ERA-Interim and MERRA-2. Here, multiple validation metrics like the bias, the root mean square error and the correlation show that the COSMO reanalyses significantly outperform the global reanalyses. For instance, the median bias of daily average GHI is shown to be improved from about 10 Wm^{-2} for global reanalyses to roughly 3 Wm^{-2} in COSMO-REA6. Beside the bias, in particular variance related scores are found to be improved in the higher resolved products. Especially a spatio-temporal representativity study which investigates the representation of spatial cloud distributions shows significant improvements regarding the regional products.

However, the comparisons of the GHI from the COSMO reanalyses to measurements reveal systematic shortcomings in the reanalyses: (1) an underestimation of GHI in clear sky situations and (2) an overestimation of GHI in cloudy sky situations. Motivated by the need for reliable radiation information in the PV sector a cloud dependent post-processing is developed. Therein, GHI values are scaled by either clear or cloudy sky specific adjustment factors. The factors are determined by applying orthogonal distance regressions between modeled and measured GHI for the two different cloud regimes. With systematic bias improvements by the post-processing in clear sky from roughly -47 Wm^{-2} to -2 Wm^{-2} and in cloudy sky from 15 Wm^{-2} to -1 Wm^{-2} significant improvements are achieved. Further, the post-processed GHI significantly improves temporal ramp rates which are of special interest for the energy sector in order to estimate power

variations over time. A central advantage of the developed post-processing method is its applicability to the entire reanalysis domain. A cross-validation exhibits a significant improvement of the post-processed GHI also at independent locations.

The second main study of this thesis complements the radiation assessment by a wind speed assessment. A comprehensive evaluation of wind speed from regional reanalyses compared to global reanalyses is conducted. Here, reference measurements of wind speed obtained from four wind towers with maximum measurement heights up to 280 m in Central Europe are used. Main improvements from the global to the regional reanalyses are found for the representation of ramp rate- and vertical wind gradient distributions. Considering joint distribution scores like the bias, mean absolute error, and the correlations most significant improvements are found close to the ground or at sites where surface effects are more prominent.

With the confidence gained from the first two parts, that the regional reanalyses add information to the global reanalyses products, the third study focuses on European wide balancing potentials of wind and solar power by using COSMO-REA6. The central goal is to determine to which extend decorrelations of wind and PV can balance extreme situations on a country-wise level, but also across different countries in Europe. Therefore, fixed fleet distributions of wind- and PV plants are simulated for the time period 1995-2014. An additional scaling of the installed capacities of the different technologies gives the opportunity to further investigate balancing potentials in an optimized PV to wind allocation ratio scenario. The simulations show that the potential of variability reductions of hybrid wind-PV production caused by decorrelations of wind and PV power varies between 29 and 42% per country, with a slight tendency to higher potentials for northern than for southern countries. The corresponding optimized ratios of installed capacity between wind and PV are found to vary between 32-42% for the former and 58-68% for the latter technology. Moreover, a simultaneous extreme production analysis of wind and PV from country to country showed high cross-border balancing potentials in Europe. Highest probabilities of simultaneous wind and PV extremes between countries are mainly less than 10%.

To summarize, all studies in this work show that the novel regional reanalyses bring an additional value for the renewable energy sector compared to global reanalyses products. Thus, this thesis provides a solid basis for the user community of reanalyses to decide which reanalysis might be the best for the particular application.

Zusammenfassung

Atmosphärische Reanalysen, eine Synthese aus meteorologischen Beobachtungen und Wettermodellen, liefern beste Schätzungen vergangener Wetterinformationen auf physikalisch konsistente Weise in einem zeitlichen und räumlichen Raster. Diese Eigenschaft macht Reanalysen zu einem etablierten Werkzeug für eine Vielzahl von wetterbezogenen Anwendungen. Im Bereich der erneuerbaren Energien, welcher ein stetig wachsendes Interesse an Reanalysen zeigt, werden Reanalysen beispielsweise zur Simulation von Produktionsvariabilitäten bestehender oder theoretischer Kraftwerke sowie deren Auswirkungen auf das Energiesystem genutzt.

Das Anwendungspotenzial von Reanalysen hängt jedoch von ihrer Fähigkeit ab, atmosphärische Phänomene genau zu beschreiben. So werden mit jeder neuen Reanalyse Produktbewertungsstudien über ihr Potenzial für spezifische Anwendungen notwendig. An dieser Stelle setzt die vorliegende Arbeit an. Die aktuellen hochauflösenden und regionalen Reanalysen COSMO-REA6 und COSMO-REA2, die im Hans-Ertel-Zentrum für Wetterforschung beim Deutschen Wetterdienst entwickelt wurden, werden bewertet, post-prozessiert und für Anwendungen im Bereich der erneuerbaren Energien genutzt.

Der erste Teil untersucht die für die Photovoltaik (PV) relevante globale horizontale Bestrahlungsstärke (GHI). Um zu beurteilen, welche Reanalyse die besten Schätzungen des GHI liefert, werden die regionalen Reanalysen umfassend mit Messungen sowie mit den etablierten globalen Reanalysen ERA-Interim und MERRA-2 verglichen. Hier zeigen mehrere Validierungsmetriken wie der Bias, der Root Mean Square Error und die Korrelation, dass die COSMO-Reanalysen die globalen Reanalysen deutlich übertreffen. Der Bias von GHI Tagesmitteln beispielsweise verbesserte sich von ca. 10 Wm^{-2} in den globalen auf etwa 3 Wm^{-2} in den regionalen Reanalysen. Neben dem Bias werden vor allem varianzbezogene Scores in den höher aufgelösten Produkten verbessert. Insbesondere eine raumzeitliche Repräsentativitätsstudie, die basierend auf GHI-Korrelationen die Darstellung räumlicher Wolkenverteilungen untersucht, zeigte signifikante Verbesserungen von den globalen zu den regionalen Produkten.

Die Evaluierung des GHI der COSMO-Reanalysen mit Messungen zeigt jedoch verbleibende systematische Mängel: (1) eine Unterschätzung des GHI in Situationen mit "wolkenfreiem" Himmel und (2) eine Überschätzung des GHI in Situationen mit "bewölktem" Himmel. Motiviert durch den Bedarf an zuverlässigen Strahlungsinformationen, insbesondere im PV-Bereich, wird hier eine wolkenabhängiges post-processing entwickelt. Darin werden die GHI-Werte mit einstrahlungsabhängigen Anpassungsfaktoren skaliert. Die Faktoren werden durch die Anwendung orthogonaler Distanzregression zwischen modelliertem und gemessenem GHI für die beiden verschiedenen Wolkenregime bestimmt. Mit systematischen Bias-Verbesserungen durch die Nachbearbeitung von ca. -47 Wm^{-2} auf -2 Wm^{-2} im Falle klarer Himmelssituationen und von 15 Wm^{-2} auf -1 Wm^{-2} in bewölkten Situationen werden signifikante Verbesserungen erzielt.

Darüber hinaus zeigt die nachbearbeitete GHI auch eine signifikante Verbesserung zeitlicher Variabilität, die für den Energiesektor von besonderem Interesse ist, um Erzeugungsschwankungen abzuschätzen. Ein zentraler Vorteil der entwickelten Nachbearbeitungsmethode ist ihre Anwendbarkeit auf die gesamte Reanalyseudomäne. Eine Kreuz-Validierung zeigt, dass die Nachbearbeitung des GHI auch an unabhängigen Standorten signifikante Verbesserung erzielt.

Im zweiten Hauptteil dieser Arbeit wird eine umfassende Bewertung der Windgeschwindigkeit aus regionalen Reanalysen im Vergleich zu globalen Reanalysen durchgeführt. Hierbei werden Referenzmessungen der Windgeschwindigkeit von vier etablierten Windtürmen mit maximalen Messhöhen von bis zu 280 m in Mitteleuropa verwendet. Im Vergleich zu den globalen Reanalysen zeigen die regionalen Reanalysen, insbesondere in den Verteilungen von zeitlichen Windrampen und vertikalen Windgradienten, signifikante Verbesserungen. Unter Berücksichtigung gemeinsamer Verteilungskennzahlen wie dem Bias, mittlerer absoluter Fehler und Korrelationen zeigen sich die signifikantesten Verbesserungen vor allem in Bodennähe und in Gebieten mit vergleichsweise komplexen Oberflächeneffekten.

Mit den Erkenntnissen der ersten beiden Teile, dass die regionalen Reanalysen im Vergleich zu den globalen Reanalysen einen signifikanten Mehrwert liefern, konzentriert sich die dritte Studie auf europaweite Ausgleichspotenziale der Wind- und Sonnenenergie unter Verwendung von COSMO-REA6. Zentrales Ziel ist es, festzustellen, inwieweit Dekorrelationen von Wind und PV Extremsituationen auf Länderebene, aber auch zwischen verschiedenen Ländern in Europa ausgleichen können. Hierzu werden für den Zeitraum 1995-2014 feste Flottenverteilungen von Wind- und PV Anlagen auf Länderebene simuliert. Eine Skalierung der Installationskapazitäten der einzelnen Technologien bietet die Möglichkeit, die Ausgleichspotenziale in einem optimierten PV/Wind Installationsverhältnis zu untersuchen. Die Simulationen zeigen, dass das Potenzial von Variabilitätsreduktionen der hybriden Wind-PV-Produktion durch Dekorrelationen von Wind und PV-Leistung zwischen 29 und 42% pro Land liegt, mit einer leichten Tendenz zu höheren Ausgleichspotenzialen in nördlichen im Vergleich zu südlichen europäischen Ländern. Die entsprechenden optimierten Installationsverhältnisse zwischen Wind und PV variieren zwischen 58-68% für Solar und 32-42% für Wind. Darüber hinaus zeigt eine Produktionsanalyse von Wind und PV hohe grenzüberschreitende Ausgleichspotenziale von Land zu Land in Europa. Die höchsten Wahrscheinlichkeiten für gleichzeitige Wind- und PV-Extreme zwischen den Ländern liegen in der Regel unter 10%.

Zusammenfassend lässt sich sagen, dass alle Studien in dieser Arbeit zeigen, dass die neuartigen regionalen Reanalysen einen Mehrwert für den Sektor der erneuerbaren Energien im Vergleich zu globalen Reanalyseprodukten darstellen. So bietet diese Arbeit eine solide Grundlage für die Anwender-Community von Reanalysen um zu entscheiden, welche Reanalyse die beste für die jeweilige Anwendung sein könnte.

1 Introduction

1.1 Motivation

Reanalyses represent the synthesis of state-of-art numerical weather prediction (NWP) models with weather observations and provide best estimates of the past weather. Herein, the NWP model combines a multitude of arbitrarily distributed observations in a physically consistent way and complements the observations by all other meteorological relevant variables on an homogeneous spatial and temporal grid. With this characteristic reanalyses provide a prerequisite for a variety of climate related questions. Examples are: How do global temperature, precipitation or weather characteristics change over time and how are these changes spatially distributed [e.g. Simmons et al., 2017; Lan et al., 2019]. But when thinking one step further, reanalyses also provide a profound basis for many more weather related application questions. Of special interest for this thesis is the potential of reanalyses to answer questions related to renewable energies. With novel reanalyses products, namely COSMO-REA6 [Bollmeyer et al., 2015] and COSMO-REA2 [Wahl et al., 2017], these particularly high resolved products are investigated with respect to their added information for the energy sector (PV and wind) in comparison to already existing reanalyses and observations. Moreover, the new product COSMO-REA6 is exploited in terms of European balancing potentials of wind and photovoltaic (PV) power.

COSMO-REA6 and COSMO-REA2 are novel high resolution regional reanalyses developed within the Hans-Ertel-Centre (HErZ) for weather research [Simmer et al., 2016]. Compared to conventional reanalyses, so called global reanalyses which come at relatively coarse resolution (30-100 km), the novel regional reanalyses are developed with significantly reduced grid spaces of 6 km and 2 km, respectively. The advantage of the finer resolution is the potential to resolve weather phenomena on smaller scales (especially mesoscale) and therefore to estimate realistic local atmospheric conditions with improved reliability. The assessment of this expected improvement is one central objective of this work.

With the release of first European regional reanalyses products only a few years ago in 2014 [Bollmeyer et al., 2015], most studies today still rely on the well established global reanalyses, at least in the wind power sector [e.g. Staffell and Pfenninger, 2016; Ritter et al., 2015; Cannon et al., 2014]. The reason for the excessive use of reanalyses for wind power estimates is the need for spatially resolved wind information at typical hub-heights (50-150 m above ground) which is up to now only covered by reanalyses products. Thus, with reanalyses spatially resolved site assessment studies for wind turbines become possible. In the field of solar power reanalyses have been less often used [e.g. Boilley and Wald, 2015]. The reason for this is the availability of alternative products, i.e. gridded radiation estimates derived from satellite observations.

Different studies showed by direct comparison with ground based observations that satellite products are more reliable than global reanalyses estimates [Jia et al., 2013]. Yet, with the availability of new regional reanalyses it has to be investigated whether this conclusion holds also for these higher resolved products.

Beside site assessment studies, a central reason for the interest of the energy sector in reanalyses is the problem of destabilizing effects on the electricity system by highly variable renewable energies [VRE, Graabak and Korpås, 2016]. The basic prerequisite for a reliable energy supply is the steadily guaranteed balance between power supply and power demand. Thus, when replacing steerable energy suppliers by weather dependent VRE technologies the power system needs to be adapted towards the possibility to balance VRE induced over- and under supplies. While for current shares this issue is a manageable problem, further expansions of VRE are expected to aggravate the risk of destabilizing and therefore enforces the need for technical adaptations like storage expansions or improved exploitation of balancing potentials of the VRE technologies [Graabak and Korpås, 2016]. Especially, potential studies of balancing effects of wind and solar forced power are expected to benefit from reanalyses as they are the only source providing physically consistent time-series of VRE relevant variables. Thus, reanalyses provide the opportunity to simulate and investigate consistent wind and PV power scenarios.

The central aim of the thesis at hand is to supply fundamental information on renewable energy characteristics based on regional reanalyses. Therein three conducted studies act in principle three fold. They provide...

- *new insights* of the applicability of the reanalyses. That means by analyzing the quality of wind and solar radiation provided by the COSMO reanalyses, new insights in terms of their application potential to solve VRE related problems is generated.
- *improvements*. Meaning, radiation estimates from the newest regional reanalyses are post-processed in order to improve the reliability of future PV studies based on reanalyses.
- *hints on the balancing potentials* of wind and solar power on an European scale.

1.2 Contribution within this thesis

To address the overall aim three studies presented in three chapters were conducted. While the first two studies focus on the quality assessment and on the post-processing of VRE related variables of COSMO-REA6 and COSMO-REA2 the third exploits the post-processed reanalyses in terms of wind and PV power balancing potentials in Europe. The following Sections provide an overview and detailed introduction of the individual studies.

Study I - Radiation study

The first study (Frank et al. [2018], Ch. 3) deals with the comprehensive assessment and post-processing of the global horizontal irradiance (GHI) provided by both COSMO reanalyses. Therein, the regional as well as global reanalyses are compared to high quality ground measurements obtained from the baseline surface radiation network [BSRN, Ohmura et al., 1998], and from SYNOP stations of the German weather service.

The assessment of regional reanalyses compared to global reanalyses is conducted by the use of the well established global reanalyses ERA-Interim [Dee et al., 2011] and MERRA-2 [Molod et al., 2015]. With horizontal resolutions of about 80 km and 50 km, respectively, these reanalyses are much coarser resolved than the COSMO reanalyses and therefore not able to resolve mesoscale processes that are relevant for cloud simulations and therefore for PV simulations. ERA-Interim is of special interest as it is the product which provides boundary conditions for the limited area reanalysis COSMO-REA6. Thus, in comparison to ERA-Interim the added value can only be caused by the changed resolution or by different data assimilation methods. MERRA-2 is used as it is one of the most established reanalyses in the energy sector [e.g. Zhang et al., 2018; Pfenninger and Staffell, 2016].

By investigating the performance of the COSMO reanalyses, systematic deficits in GHI due to clouds and aerosols were found that lead to the development of a post-processing scheme for GHI provided by COSMO-REA6. The focus on COSMO-REA6 is motivated by its coverage of whole Europe and the goal to study European wide balancing potentials of wind and PV power. For the validation of the performance of the post-processed GHI fields compared to the original reanalyses product a cross-validation assessment is applied. Moreover, the global reanalyses as well as the regional reanalyses and the post-processed product are assessed and discussed in their potential to answer energy related questions. Especially the reanalyses potential to represent temporal GHI changes (ramp rates) are in detail investigated and discussed.

The central questions addressed in this study can be summarized to:

1. How accurate is COSMO-REA6 GHI with respect to ground observations?
2. Does COSMO-REA6 GHI improve compared to global reanalyses, i.e. ERA-Interim and MERRA-2, in bias and variability metrics?
3. Can the systematic biases found in COSMO-REA6 be corrected with a post-processing algorithm?

Study II - Wind study

The second study (Frank et al. [2019], Ch. 4) assesses wind speed profiles provided by the COSMO reanalyses and compares its performance to that of the global reanalyses ERA-Interim and MERRA-2. A second central point of the study is to assess the application potentials of the COSMO-REA products in the field of site assessment for wind power plants.

Similar to study I, one of the main goals of this study is to investigate whether the COSMO reanalyses better represent already existing and well established reanalyses products. Therefore, vertically resolved wind speed measurements obtained from four well established meteorological towers in central Europe are used as reference. Like in study I, the COSMO reanalyses are compared to the reanalysis providing boundary conditions (ERA) which gives the opportunity to investigate the added value of resolution. The comparison of the COSMO-REA products to MERRA-2 is of special interest as MERRA-2 is one of the most often used reanalyses in wind power related studies [e.g. Pfenninger, 2017; Cannon et al., 2014]. The reason for the frequent use of MERRA-2 in VRE studies can be found in the unique characteristic of MERRA-2 compared to other global reanalyses to provide wind information with hourly resolution, at least for the specific heights of 10 m and 50 m above ground level. Other global reanalyses provide the meteorological output fields in intervals of six or three hours which is also the case for the general output of MERRA-2. Note, the general output interval of the COSMO reanalyses is hourly (3D fields) down to quarter hourly (2D fields) [Bollmeyer, 2015].

For the assessment of the reanalyses products typical statistical wind power metrics are applied. In addition to common metrics, the study also comprises investigations on the ability of reanalyses to represent ramp rates (i.e. wind speed changes in defined time windows), persistent low wind situations, and vertical wind gradients. These three metrics are in particular motivated by the wind sector as they are closely related to power generation extremes.

A second focus of the study is the potential of the COSMO reanalyses for site assessment studies. Economically accepted uncertainties in wind information used for site assessment correspond to that of vertically extrapolated wind measurements obtained from a tower with a minimum height of at least 2/3 of the target height [Fördergesellschaft Windenergie und andere Erneuerbare Energien, 2011]. This results in a minimum requirement for the quality of the reanalyses, which should at least correspond to that of the extrapolated estimates.

The main questions of this study can be summarized to:

1. How accurately do COSMO-REA6 and COSMO-REA2 reproduce realistic wind characteristics relevant for the energy sector?
2. Do regional reanalyses perform better in representing hub-height wind characteristics than global reanalyses?

3. What is the application potential of reanalyses, especially for site assessment studies?

Study III - Balancing study of wind and PV power

Increasing shares of renewable energy come with destabilizing effects for the electricity system. One possibility to reduce the destabilizing effect of wind and PV power is to adapt the electricity grid and the installed power fleet in order to exploit spatial but also wind-to-PV related balancing potentials in an optimal way. At this point, reanalyses become of special interest, as they have up to now been the only source providing both, wind and irradiance physically and spatially consistent. Thus, by applying conversion models to convert COSMO-REA output to wind and PV power, conclusions with respect to wind-PV balancing potentials can be drawn.

Given the lack of European hybrid wind-PV balancing potential studies with a focus on natural balancing effects based on one consistent reanalysis only, here the regional reanalysis COSMO-REA6 is exploited and used to tackle this issue (Cha. 5). Motivated by the structure of the electricity market and questions of practicability, conducted investigations are based on country level. A first necessary step to investigate balancing potentials of power quantities is the estimation of the respective quantities. Concerning wind power, the power estimates based on COSMO-REA6 conducted by Henckes et al. [2018] can be easily applied. In the case of PV, a new power data set for PV power plants distributed all over Europe is generated. For this issue a PV modeling chain based on the power conversion scheme developed by Huld et al. [2011] is applied (for details see Sec. 2.2).

By aiming to use most realistic irradiance estimates for PV power derivations used in the balancing analysis, the first part of study III is concerned with the development of a post-processing of the radiation components, direct and diffuse radiation. As a result the components allow a precise estimation of the radiation on inclined PV module surfaces. With the development and application of the post-processed radiation components in the balancing potential investigation the central questions tackled in study III are:

1. Do PV power simulations profit from the developed post-processing of the COSMO-REA6 radiation components?
2. How do extremes smooth out per country when considering hybrid wind-solar production compared to individual source productions?
3. Do specific countries benefit more from hybrid production than other countries?
4. Which countries are particularly suited to balance the extremes of other countries?

2 Material and methods

This chapter serves to introduce the central reanalyses products COSMO-REA and to present the simulation chain to estimate PV power. While the individual approximations and applied models are already published methods, the specific assembly of the models and its application to COSMO-REA data is new.

2.1 Regional reanalyses COSMO-REA6 and COSMO-REA2

In this chapter the two regional reanalyses COSMO-REA6 [Bollmeyer et al., 2015] and COSMO-REA2 [Wahl et al., 2017] are introduced. The development of these two reanalyses was carried out within the "Hans-Ertel Centre for Weather Research - Climate Monitoring Branch" which is funded by the Federal Ministry of Transport and Digital Infrastructure (BMVI) of Germany.

The fixed model used for the development of the two regional reanalyses are the COSMO forecast models operated at the DWD. In case of COSMO-REA6 the model COSMO-EU version 4.25.2 is used. In case of COSMO-REA2 version number 5.00.2 of the NWP model COSMO-DE is used. While the area covered by COSMO-REA6 comprises in principle whole Europe (CORDEX EUR-11), COSMO-REA2 is developed for an area covering generally Germany and border lands (extended COSMO-DE domain). The grid spacing of COSMO-REA6 is 6 *km* in horizontal and 40 layers in vertical direction. COSMO-REA2 comes with a 2 *km* horizontal resolution and 50 vertical layers. Temporally, COSMO-REA6 covers 23 years from 1995-2017 with continuous extension and COSMO-REA2 seven years from 2007-2013. Both reanalyses provide roughly 150 variables with hourly (3D variables) or quarter hourly (2D variables) output frequency.

Boundary conditions - spatial weather information to start and feed the regional models with boundary weather - are as typically provided by global or big brother reanalyses products. In case of COSMO-REA6 the initial- and boundary conditions are provided by the global reanalysis ERA-INTERIM [~ 80 km horizontal resolution, 60 vertical layer Dee et al., 2011]. For COSMO-REA2 the initial- and boundary conditions are given by COSMO-REA6.

The synthesis of NWP forecasts with observations is conducted by the application of the so called nudging approach. Nudging is a continuous four dimensional data assimilation scheme which adjusts the model state during the model integrations towards the observations (see Schraff [1997]). Assimilated variables in COSMO-REA6 and COSMO-REA2 are the pressure, the temperature,

the wind, and the humidity. Observations sources are SYNOP stations, aircrafts, buoys, radiosondes, wind profiler and ships (descending order). COSMO-REA2 contains an additional latent heat nudging of weather radar measurements [Bollmeyer et al., 2015].

2.2 PV simulation chain

Estimating the power generation of PV modules is a multi-step procedure. The procedure varies with the given input variables, starting with horizontal direct radiation (Q_{dir}), horizontal diffuse radiation (Q_{dif}), and unknown metadata of PV module orientation the central steps can be split into three main parts: (1) Estimating real world module orientation, (2) transposing the horizontal radiation to the plane of array (POA) orientation, (3) simulating the power generation of the PV module (see Fig. 2.1). The following describes the individual steps in detail. In this respect, additionally, simple studies are presented in order to motivate applied assumptions and to assess related uncertainties.

2.2.1 Module orientation estimate

Aiming to simulate realistic power generation of PV modules at any place in Europe needs assumptions on the installation orientation of the PV modules. Even if power register data are given they often do not contain information about orientation. Especially, on European scale uniform collections with comprehensive information are difficult to access.

A first guess for realistic module orientations is the orientation which maximizes the incidental radiation at the POA. Recently, some studies compared these optimized orientation estimates with real world installations. Saint-Drenan et al. [2018] found the optimal real world tilt angles α_{real} to be significantly smaller than optimized orientation estimates α_{opt} . With detailed installation information of about 2% of the total number of PV plants in Germany they found a mean deviation of

$$\alpha_{real} = 0.7 * \alpha_{opt}. \quad (2.1)$$

Saint-Drenan et al. [2018] explained this deviation by an economic reason: Investors aim to maximize the power generation per unit of surface. Here, mainly caused by less shadow effects modules installed with decreased tilt angles are found to increase the total power production. However, with a variety of dependencies like the land price, the solar resource and architectural characteristics the estimated factor 0.7 is known to vary from plant to plant [Saint-Drenan et al., 2018]. Therefore, recent studies started to estimate whole orientation distributions of real world installed PV modules [Saint-Drenan et al., 2018; Killinger et al., 2018]. However, due to the lack of studies examining the deviation factor and its variations at the European scale, here, as in [Saint-Drenan et al., 2018], a constant deviation factor of 0.7 is assumed.

Assumptions and methods applied in this thesis to estimate the optimal orientation are as follows. With respect to the azimuth angle, motivated by simplicity, constantly southwards-facing PV modules are assumed. The optimal tilt angle is estimated by maximizing the PV generation. Therein, caused by computational efforts only the year 2014 of COSMO-REA6

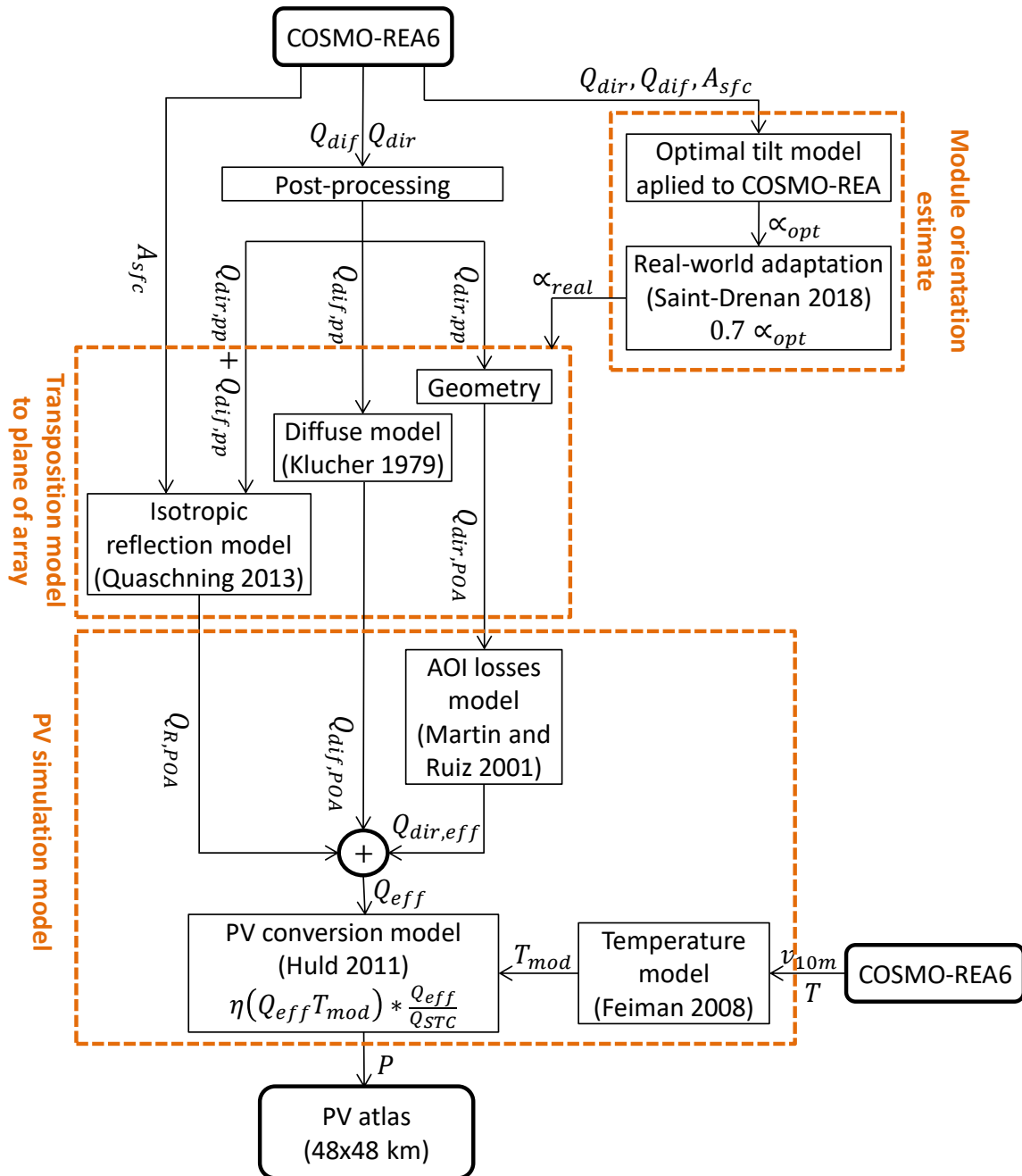


Figure 2.1: Modeling chain to estimate PV power based on reanalysis data.

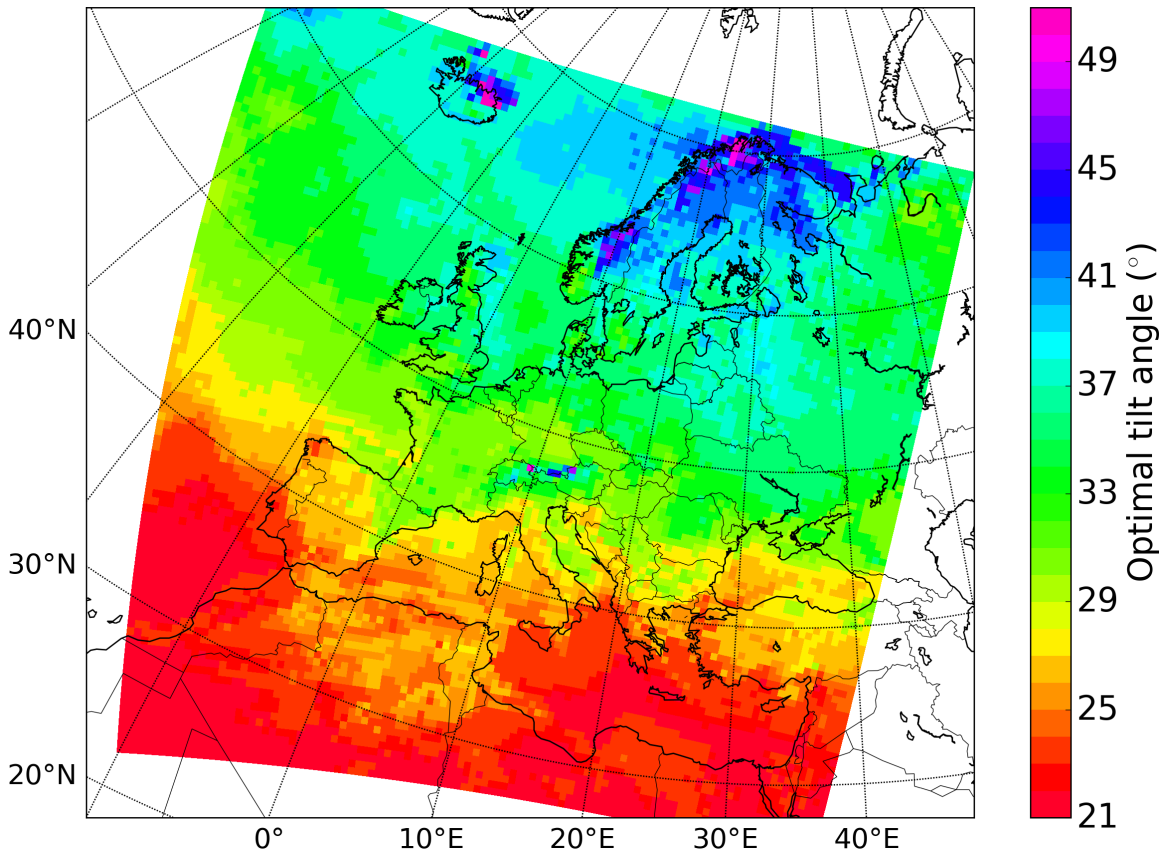


Figure 2.2: European distribution of optimal tilt angles estimated based on hourly radiation values of the year 2014 provided by COSMO-REA6.

radiation is used. Resulting optimal tilt angles vary between 21° and 50° (Fig. 2.2) in whole Europe which is in good accordance with the optimal tilt angles as available on the PV-GIS website (<http://re.jrc.ec.europa.eu/pvgis/>, illustrated by Saint-Drenan et al. [2018]). Also the general spatial distribution fits well. Larger differences only occur in the Asian area, where COSMO-REA6 derived optimal tilt angles are about 10° smaller.

In order to estimate the error of power estimates when using optimal tilt angles derived from just one year (2014) instead of using multiple year derived optimal tilt angles a sensitivity study is performed at ten exemplary BSRN stations in Europe (for the exact locations see Fig. 3.1). Therefore, three PV simulation runs are conducted: (1) A reference run with optimized tilt angles estimated based on 20 year time-series, (2) a positive perturbed run with the 20 year optimized angles perturbed by the simulated variation of single year optimal tilt estimates, and (3) a related negative perturbed run. For simplicity the surface albedo is set to 0.2 and the wind effects are ignored in this specific sensitivity study. Results show, maximum errors of aggregated power estimates due to the consideration of just one year of data when estimating the optimal tilt are below 0.35% (Fig. 2.3).

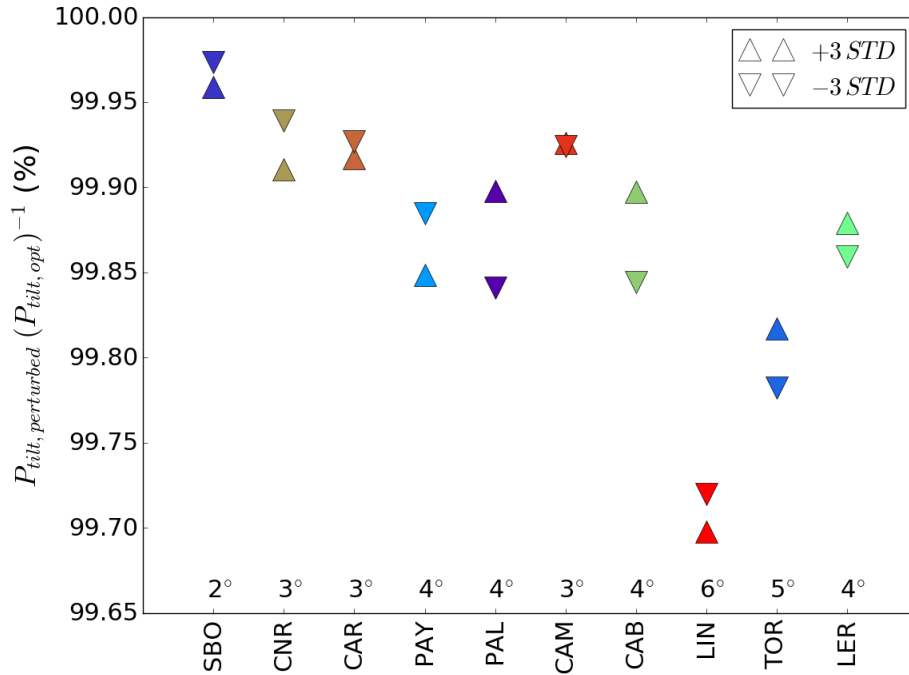


Figure 2.3: Relative aggregated power generation by using positive and negative perturbed optimal tilt angles with respect to the optimal tilt power generation at 10 BSRN sites. The sites are sorted by latitude from south to north. The numbers give the perturbation (three times the yearly standard deviation) per site in degree.

2.2.2 Transposition model to plane of array

The driving source of PV power is the irradiance on the tilted plane of the PV array. Thus, with radiation provided by reanalyses being typically the direct and diffuse radiation on the horizontal plain conversion models to tilted plains are necessary.

The irradiance to an arbitrary orientated plane Q_{POA} can be split in three parts

$$Q_{POA} = Q_{dir,POA} + Q_{dif,POA} + Q_{R,POA} \quad (2.2)$$

with $Q_{dir,POA}$ the direct radiation, $Q_{dif,POA}$ the diffuse radiation, and $Q_{R,POA}$ the at the ground and surroundings reflected radiation to the plane of array. The following describes how the individual parts can be calculated or estimated, respectively.

The direct radiation component propagates in a ray, thus the POA component can be calculated geometrically. For further information see e.g. Quaschnig [2013].

A variety of different models exist to calculate the diffuse radiation on the inclined plane. Here the analytic model proposed by [Klucher, 1979] is used. The advantage of this model compared to alternative models like those developed by Perez et al. [1986] (Perez-model) or Muneer [1990] is its computational efficiency. All mentioned models follow the anisotropic assumption. Meaning

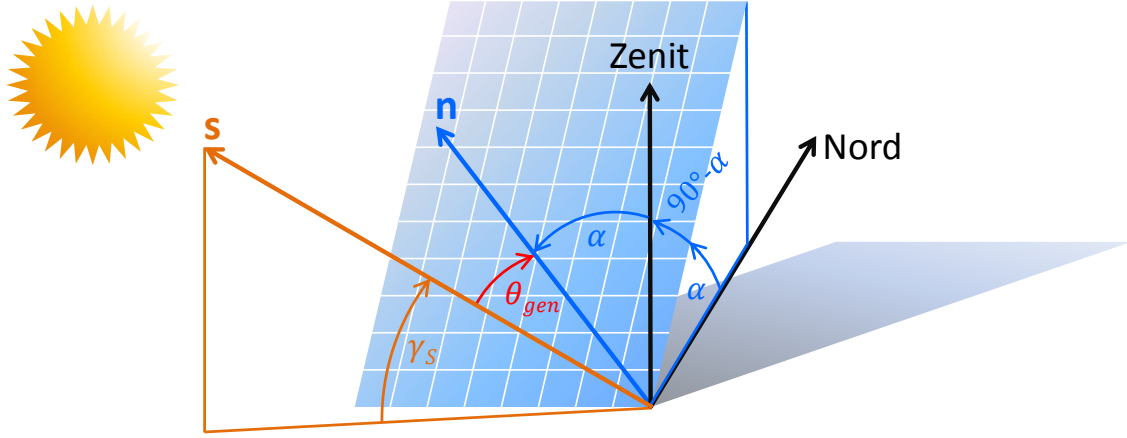


Figure 2.4: Angle overview of a tilted plane.

they assume for the upper hemisphere radiation a direction dependent distribution. Using the definition

$$F = 1 - \left(\frac{Q_{dif}}{Q_{GHI}} \right)^2 \quad (2.3)$$

Klucher [1979] estimates the diffuse radiation on a plane tilted by the angle α by

$$Q_{dif,POA} = \frac{1}{2} Q_{dif} (1 + \cos \alpha) (1 + F \sin^3 \frac{\alpha}{2}) (1 + F \cos^2 \theta_{gen} \cos^3 \gamma_s) \quad (2.4)$$

with γ_s the sun elevation, and θ_{gen} the angle between the normal POA vector (\mathbf{n}) and the vector pointing to the sun (\mathbf{s} , see Fig. 2.4).

In order to estimate the uncertainty of power estimates when using the more simple model from Klucher [1979] compared to the significant more complex model from Perez et al. [1986] a sensitivity study was carried out by Henckes et al. [2019]. A full PV power simulation model was implemented twice, once by using the Klucher- and once by using the Perez scheme. The results showed temporally aggregated power estimates differing less than 1% when using either the one or the other model.

The radiation reflected from the ground is estimated by following Quaschnig [2013] by using an isotropic approach which assumes an equal distributed radiation flux from all upper hemisphere directions. Thus, the radiation reflected from the ground which reaches the tilted plane is a function of the tilt angle α , the GHI and the surface albedo A_{sfc} :

$$Q_{R,POA} = 0.5 Q_{GHI} A_{sfc} (1 - \cos(\alpha)). \quad (2.5)$$

Note, that the albedo varies considerably with the environmental characteristic. Therefore, considering domain averaged albedo (6x6 km in case of COSMO-REA6 input) might result in

significant simulation errors for individual modules. Nevertheless, the effect is expected to be negligible if a sufficient number of power plants are aggregated.

2.2.3 PV simulation model

Besides the dependency on the incidental irradiance, the final power generation of a PV module also depends on module specific characteristics. Here, three models are used to deal with these effects. The first model treats irradiance reflections at the module's surface, the second estimates the temperature of the PV module as function of wind speed and ambient temperature, and the third model estimates the final power generation of the module considering technology dependent efficiency. Here, we focus on the silicon technology only, as they comprise the largest market share. Not considered are effects like spectral losses, shadow losses, snow losses, and dust or dirt losses. In accordance to Pfenninger and Staffell [2016], subsequent losses due to electricity components which are dominated by converter losses are roughly considered by assuming a constant electricity yield loss of 10%. The following describes the applied models to derive PV power estimates in detail.

In order to estimate the reflection losses at the module's surface the so called angle of incidence (AOI) model proposed by Martin and Ruiz [2001] is used. Therein, reflection losses (AL) of the direct radiation component are estimated by

$$AL(\theta_{gen}) = 1 - \left(\frac{1 - \exp(-\cos \theta_{gen}/a_r)}{1 - \exp(-1/a_r)} \right) \quad (2.6)$$

with a_r being an empirical dimensionless parameter describing the surface characteristic of the individual module. A comprehensive investigation conducted by Martin and Ruiz [2001] showed this coefficient (a_r) just slightly varying for different silicon modules. A rough value for typical silicon modules is $a_r = 0.16$ (see Tab. 1 in Martin and Ruiz [2001]). In accordance with Urraca et al. [2018] for the thesis on hand this value is assumed to be constant. Given the reflection losses as estimated in eq. 2.6, the effective radiation Q_{eff} which is finally available for the photoelectric effect can be estimated by:

$$Q_{eff} = (1 - AL) Q_{POA}. \quad (2.7)$$

A further module specific characteristic is the temperature dependent efficiency. To account for this effect a first step is to estimate the modules temperature (T_{mod}). T_{mod} is a function of the ambient temperature, the incident irradiance and the wind speed. Given the wind speed v_{10m} in

10 m above ground level (h_{10m}) wind speeds v_{mod} at the module's height h_{mod} can be estimated by (in accordance with Huld and Gracia Amillo [2015]):

$$v_{mod} = \left(\frac{h_{mod}}{h_{10m}} \right)^{0.2} v_{10m}. \quad (2.8)$$

Using the model of Faiman [2008] the modules temperature can be calculated as

$$T_{mod} = T_{amb} + \frac{Q_{eff}}{U_0 + U_1 * v_{mod}}. \quad (2.9)$$

Koehl et al. [2011] find the coefficients U_0 and U_1 just slightly varying with technology. For crystalline silicon modules they report values of U_0 and U_1 of $26.9 \text{ Wm}^{-2}\text{K}^{-1}$ and $6.2 \text{ Wm}^{-3}\text{sK}^{-1}$, respectively.

The PV conversion model describes the performance of the PV module and estimates the ideal generated power P_{ideal} as a function of the incident irradiance Q_{eff} and the module's temperature T_{mod} . Here, the empirical model proposed by Huld et al. [2011] is used. The authors show good model performance for several different crystalline silicon PV technologies. Dittmann et al. [2010] shows the model to be more accurate than alternative PV conversion models. The idea of the model is to multiply the theoretical power generation of the module under standard test conditions (STC) by factors which describe the instant deviation from the power production under STC conditions. The model has the form:

$$P_{ideal}(Q', T') = P_{STC} Q' \eta(Q', T') = P_{STC} Q' [1 + k_1 \ln(Q') + k_2 (\ln(Q'))^2 + k_3 T' + k_4 T' \ln(Q') + k_5 T' (\ln(Q'))^2 + k_6 T'^2] \quad (2.10)$$

with

$$Q' = \frac{Q_{eff}}{Q_{STC}} \text{ with } Q_{STC} = 1000 \text{ Wm}^{-2} \quad (2.11)$$

and

$$T' = T_{mod} - T_{STC} \text{ with } T_{STC} = 25^\circ\text{C}. \quad (2.12)$$

The coefficients k_1, k_2, \dots , and k_6 are estimated by a least-square optimization of the model with real world observations of 18 crystalline silicon modules (see Table 2.1).

In a last step subsequent electricity component losses dominated by converter losses are considered by reducing P_{ideal} by 10% [Pfenninger and Staffell, 2016]. According to Pfenninger and Staffell [2016] this assumption is rather conservative, since the PV systems used for the converter loss estimate are about 18 years old. Newer converter might work more efficient.

Table 2.1: For crystalline silicon modules optimized coefficients k_1 to k_6 used in Eq. 2.10 [Huld and Gracia Amillo, 2015]

k_1	-0.17237
k_2	-0.040465
k_3	-0.004702
k_4	0.000149
k_5	0.000170
k_6	0.000005

3 Bias correction of a novel European reanalysis data set for solar energy applications

This chapter is based on: Frank, C. W., S. Wahl, J.D. Keller, B. Pospichal, A. Hense, S. Crewell, 2018: Bias correction of a novel European reanalysis data set for solar energy applications, *Solar Energy*, 164, 12-24, doi.org/10.1016/j.solener.2018.02.012

One of the major challenges during the transition phase of the energy system is to maintain the balance between energy supply and demand. Rising questions are often related to site mapping, variability, extremes and compensation effects for example. A fundamental source of information to answer these questions are high quality data sets of renewable energy related variables. As reanalyses provide all relevant data to assess wind and solar power generation over a long period of time (decades) in a gridded consistent way, they exhibit great potential in the field of renewable energy. A new regional reanalysis is COSMO-REA6, which covers the European domain over the years 1995-2014 with a horizontal resolution of about 6 km and a temporal resolution of 15 minutes. In this paper, we first assess the quality of the Global Horizontal Irradiance (GHI) provided by COSMO-REA6. High quality GHI measurements obtained through the Baseline Surface Radiation Network (BSRN) are used as reference and reveal systematic short comings in the reanalysis: (1) an underestimation of GHI in clear sky situations and (2) an overestimation of GHI in cloudy sky situations. In order to reduce these systematic regime dependent biases, a post-processing is developed. The applied post-processing method is a scaling based on orthogonal distance regressions for two different regimes, i.e., "clear sky" and "cloudy sky". The two regimes are distinguished by the use of a transmissivity threshold. The post-processed GHI shows a significant reduction of the systematic biases and an improvement in representing the marginal distributions. A spatial cross-validation shows the applicability to the whole model domain of COSMO-REA6. Moreover, COSMO-REA6 as well as the post-processed GHI data reveal an added-value when compared to global reanalysis ERA-Interim and MERRA-2. The higher resolution reanalysis exhibits a significantly better performance of representing GHI variability, as well as biases, RMSE and other conventional scores. The post-processed GHI data are freely available for download.

3.1 Introduction

For a sustainable planning of the transition towards renewable energy production, the assessment of the solar energy potential and its variability has become more and more important [Kleissl, 2013]. Due to the high spatial and temporal variability of solar radiation long-term data over large domains are necessary to identify potentials for the production of renewable energy and risks regarding the growing dependency on this form of power generation. In this respect also the co-variability of solar and wind energy becomes more important, as its anticorrelation is expected to balance the volatility of the individual sources to some extent [e.g. Bett and Thornton, 2016; Santos-Alamillos et al., 2012; Grams et al., 2017]. More extensive studies simulate the electricity network in order to study the electricity grid as a whole system. In this context, realistic meteorological data allow studying for example the future need of storage and/or back-up capacity [e.g. Heide et al., 2010; Mulder, 2014].

Traditionally, solar energy potential has been assessed from measured time-series of solar irradiance at ground level. This is limited in its geographical distribution especially if high temporal resolution (< 1 hour) and high quality measurements are concerned. Most frequently, the Global Horizontal Irradiance (GHI) also called Surface Solar Irradiance (SSI), is measured within the networks of meteorological services. A spatially extended view is provided by satellite estimates like the HelioClim project by MINES ParisTech [Blanc et al., 2011] or the SARA (Solar surface Radiation Heliosat) data set [Müller et al., 2015] produced by the Satellite Application Facility on Climate Monitoring (CM-SAF). They exploit geostationary satellite measurements to derive GHI for the full disk with up to hourly temporal and 0.05 degree spatial resolution. Atmospheric reanalyses compiled from observations and numerical weather prediction models provide not only GHI but rather the complete state of the atmosphere including the vertical profiles of wind, temperature etc. in a physically consistent way. Therefore, these multi-year data sets which continually improve in resolution allow for a joint investigation of renewable energy resources [Bett and Thornton, 2016].

Global reanalyses that come at relatively coarse horizontal resolutions (40-100 km) are frequently used for investigating wind power generation [e.g. Staffell and Pfenninger, 2016; Ritter et al., 2015; Cannon et al., 2014; Kubik et al., 2013; Bett et al., 2013], but rarely for solar energy application [e.g. Boilley and Wald, 2015; Richardson and Andrews, 2014]. One of the first applications by Lohmann et al. [2006] revealed large differences among two global reanalyses for monthly mean values at horizontal resolutions of about 200 km. When comparing two state-of-the-art reanalyses and satellite derived (Helio-Clim-1) daily solar irradiance with surface measurements across the globe Boilley and Wald [2015] find that a large part of the variability in surface radiation is not captured by the reanalyses. A reason for the deviation between reanalysis and measurements might arise from the difficulty to parameterize small scale processes related to clouds and aerosols including interaction with solar radiation.

The work of Richardson and Andrews [2014] indicated the potential of reanalyses in PV applications. For Ontario, Canada, Richardson and Andrews [2014] evaluated the use of NASA's global reanalyses MERRA [Rienecker et al., 2011] as input for PV modeling. They found that the modeled PV yields driven by MERRA results in just slightly higher errors than ground-measured driven results, despite relatively larger errors in the MERRA GHI data. Later, Pfenninger and Staffell [2016] showed a comparable performance of PV output simulations based on MERRA and MERRA-2 [Molod et al., 2015] compared to satellite estimates when aggregated to country-level.

One reason for the few studies using radiation from reanalyses for solar energy applications is the availability of the high quality satellite products. Many publications in the past are based on either solar or wind energy which caused the use of different data sources in the two fields. In the field of wind energy reanalyses products are frequently used [Rose and Apt, 2015] while for solar energy satellite products are found to be most accurate [Jia et al., 2013], at least compared to global reanalyses. To our best knowledge up to now high resolution regional reanalyses are not considered in the solar energy community. In recent times the question of co-variability and compensation effects of wind and solar energy become more and more important. Thus, the need of a common data source for both variables increased. Reanalyses provide wind and radiation in a physically consistent way in space and time. This is crucial for studying joint distributions, otherwise results and interpretation might be distorted due to physical inconsistencies. Using both variables from one source causes the question which reanalysis performs best in representing wind speed and radiation? This study addresses this question concerning the radiation part and takes regional reanalyses into account.

While global reanalyses mainly resolve clouds associated with synoptic disturbances, high resolution regional reanalyses have the potential to better describe smaller scale clouds associated with mesoscale processes like thunderstorms or orographic circulations and therefore are more suitable for solar energy applications. This paper investigates the quality of the novel European regional reanalysis COSMO-REA6 [Bollmeyer et al., 2015] available with a horizontal resolution of 6 km over a time period of 20 years and a temporal resolution of 15 minutes. Evaluation of COSMO-REA6 meteorological variables such as precipitation, temperature and wind speed [Wahl et al., 2017; Bollmeyer et al., 2015; Kaiser-Weiss et al., 2015; Borsche et al., 2016; Henckes et al., 2018] has already shown a superior performance with respect to the European Centre for Medium-range Weather Forecasting (ECMWF) Re-Analysis Interim data set [ERA-Interim, Dee et al., 2011] but the representation of radiation has not been addressed so far.

An even higher resolution data set is available for Central Europe with a horizontal grid spacing of 2 km [COSMO-REA2, Wahl et al., 2017] albeit for a much shorter time period of seven years (2007 to 2013). However, due to its larger range of applicability, e.g., cross-country energy trading, we focus on the long-term European data set COSMO-REA6.

With this paper we focus on the following questions:

1. How accurate is COSMO-REA6 GHI compared to ground observations?
2. Does COSMO-REA6 GHI improve upon global reanalyses, i.e. ERA-Interim and MERRA-2, in bias and variability metrics?
3. Can the expected biases and deviations be corrected with a post-processing algorithm?

In order to address these questions the paper is structured as follows. Section 2 describes the reanalysis and observational data sets. A quality assessment of GHI from reanalyses is given in Section 3 which reveals some systematic deficits under clear and cloudy conditions. Therefore a post-processing procedure to correct these issues is developed in Section 4. An evaluation, including a cross-validation, of the post-processed radiation fields is presented in Section 5. Section 6 summarizes our findings followed by the conclusions in section 7.

3.2 Data sets

3.2.1 COSMO-REA6

COSMO-REA6 has been developed and produced within the Climate Monitoring Branch of the Hans-Ertel-Centre for Weather Research¹ and is based on the COnsortium for Small-Scale Modelling (COSMO) limited-area model [Schättler and Doms, 2011], which is part of the operational NWP model chain of the German Meteorological Service (DWD). It is a 20-year regional atmospheric reanalysis covering the European CORDEX EUR-11 domain with a horizontal resolution of 0.055° (approximately 6 km, see Fig. 3.1) and 40 vertical levels in terrain following coordinates. 3D model variables are archived every hour and 2D variables every 15 minutes. The most important variables, e.g. GHI, wind speed at the six lowest model level, can be downloaded via ftp (<http://reanalysis.meteo.uni-bonn.de>). In the reanalysis, a continuous nudging scheme is used to assimilate a wealth of observations into the model allowing for a detailed but temporally smooth representation of the prognostic variables [for further information the reader is referred to Bollmeyer et al., 2015].

The COSMO reanalyses uses the radiation scheme by Ritter and Geleyn [1992] based on the δ -two-stream approximation. The scheme is called every 15 min and calculates how solar radiation is modified in the atmosphere due to scattering and absorption by atmospheric gases, aerosol and clouds. The one dimensional radiative transfer is solved separately, once for the clear sky and once for the cloudy column which are subsequently combined according to cloud fraction. As the instantaneous distribution of clouds and water vapor are input to the radiation scheme, GHI reflects the strong dynamic variability of the atmosphere (Fig. 3.1).

¹<https://www.herz-tb4.uni-bonn.de>

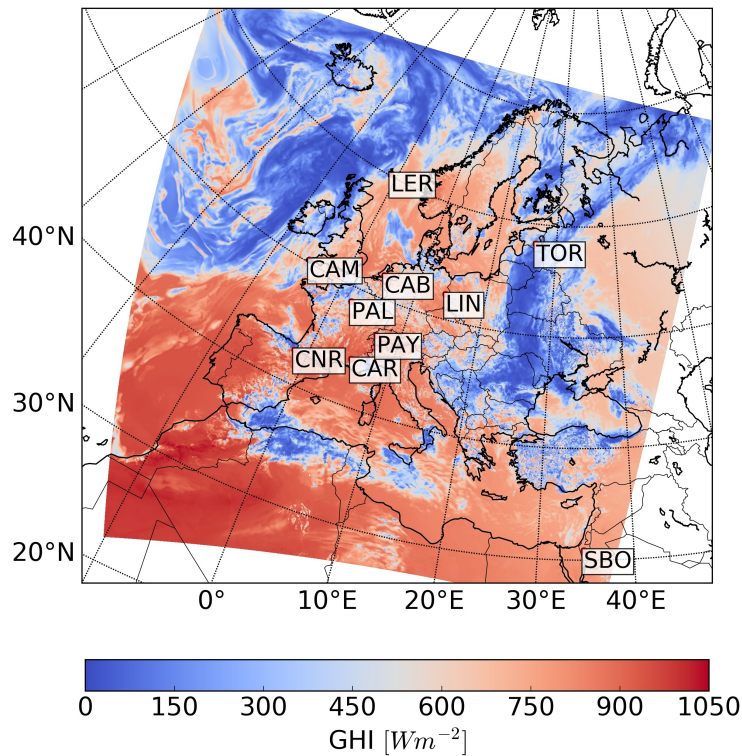


Figure 3.1: Example of GHI field as provided by COSMO-REA6 for 12 UTC, 01 June 2014. The abbreviations show the considered Baseline Surface Radiation Network (BSRN) stations and their locations. The stations are geographically located at the upper left corner of the abbreviation box. The associated station names and coordinates can be found in Tab. 3.1.

The aerosol input to the radiation scheme is based on the Tanre et al. [1984] climatology and combines the effect of five different types of aerosols: continental, maritim, urban, volcanic and stratospheric background aerosols. The horizontal distribution of the aerosol types is based on the Global Aerosol Data Set [GADS, Koepke et al., 1997]. Compared to other aerosol climatologies and observations, Zubler et al. [2011] showed that the Tanré climatology exhibits unrealistically high values of aerosol optical thickness for the European region (factor 2-3).

Despite the known disadvantages of the Tanré aerosol climatology it was used for the COSMO-reanalyses, as it is the standard input in the operational COSMO model setup at DWD. The aerosol climatology was not changed, as the COSMO model is known to provide good forecasts of e.g. precipitation, when using standard boundary fields. Nevertheless, within the framework of renewable energy research it might be advantageous to use a more realistic aerosol climatology, as already done in many other current NWP models.

Unless noted otherwise, we use the instantaneous output fields (every 15 minutes) of the short wave direct radiation Q_{dir} and the short wave diffuse radiation Q_{dif} at the surface from COSMO-REA6. The global horizontal irradiance Q_{GHI} is then obtained as

$$Q_{GHI} = Q_{dir} + Q_{dif} \quad (3.1)$$

by adding the direct and diffuse part of the short wave radiation at each grid point. Because GHI strongly depends on the solar elevation angle and thus on the diurnal and seasonal cycle, this dependency is eliminated by transforming GHI to transmissivity T , defined as

$$T = \frac{Q_{GHI}}{Q_{TOA}} \quad (3.2)$$

with Q_{TOA} the incoming irradiance at the Top Of the Atmosphere (TOA). The transmissivity is also called clearness index. Larger values refer to a clearer atmosphere, i.e. less radiation is extinguished mainly by aerosol and clouds. Considering transmissivity instead of GHI provides the benefit to be independent of the incoming TOA radiation amount. It should be noted that the ray path through the atmosphere is still a function of the solar elevation angle. Transmissivity is therefore positively correlated with this angle.

3.2.2 ERA-Interim

The global reanalysis ERA-Interim [Dee et al., 2011] provides data since 1979 to present. The hydrostatic model setup of ERA-Interim is based on the Integrated Forecasting System of the European Centre for Medium-Range Weather Forecasts (ECMWF) in the operational version of 2006 (IFS release Cy31r2). A four dimensional variational data assimilation scheme is applied for the assimilation of upper air variables, followed by separate schemes for near surface variables, soil moisture/temperature, snow and ocean waves. The 3D model fields are archived every 6 hours at a horizontal resolution of approximately 80 km and 60 vertical levels. Two-dimensional fields are available every 3 hours. For this study, we used the variable *Surface solar radiation downwards* with a temporal resolution of 3 hours (<http://apps.ecmwf.int/datasets/data/interim-full-daily/>). ERA-Interim is frequently used for retrospective analysis in the meteorological community [e.g. Linares-Rodríguez et al., 2011; Ranjha et al., 2013]. GHI fields from ERA-Interim are only available as three hourly averages and hence cannot resolve the variability due to clouds as is demonstrated in an example showing the diurnal cycle of GHI as obtained from ERA-Interim, COSMO-REA6, MERRA-2 and surface measurements (Fig. 3.2).

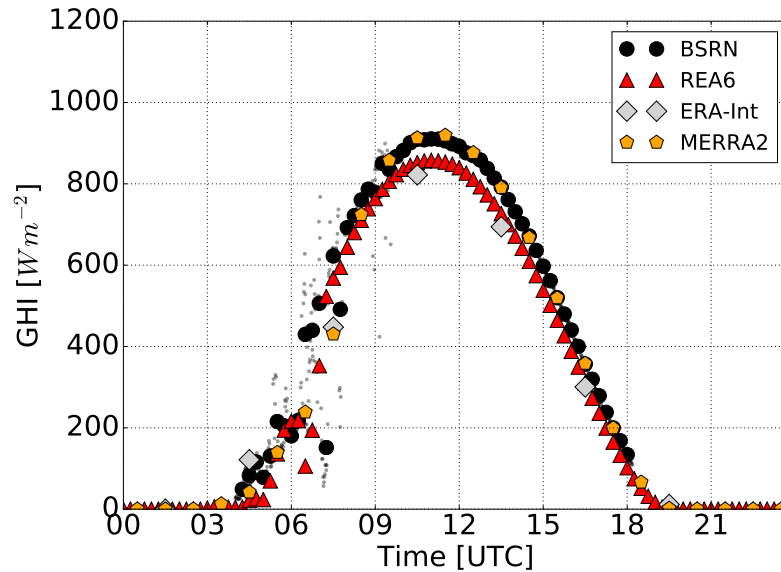


Figure 3.2: Time-series of GHI at Lindenberg, Germany, on June 23, 2008. BSRN measurements are given as 1 minute averages (small dots) and 10 min averages (large black dots). COSMO-REA6 provides instantaneous values every 15 minutes (red), MERRA-2 every 1 hour (orange), and ERA-Interim gives three hourly averages (grey).

3.2.3 MERRA-2

The Modern-Era Retrospective Analysis for Research and Applications-2 (MERRA-2) is the latest global reanalyses produced by the NASA Global Modeling and Assimilation Office [GMAO, Molod et al., 2015]. MERRA-2 is based on the Goddard Earth Observing System Model, Version 5 atmospheric general circulation model (AGCM). Observations are assimilated by the atmospheric data assimilation system (ADAS), version 5.12.4. MERRA-2 is the first global reanalyses assimilating space-based observations of aerosols [Randles et al., 2016].

MERRA-2 products are available since 1980 on a horizontal resolution of about 50 km in the latitudinal direction. For our study we use the global horizontal irradiation (name of variable: *surface_incoming_shortwave_flux*) which is provided half past each hour (hourly resolution). All MERRA-2 data are freely accessible online through the NASA Goddard Earth Sciences Data Information Services Center (GES DISC).

3.2.4 Surface measurements

In order to assess the quality of the reanalyses, we use the freely available GHI measurements of the Baseline Surface Radiation Network [BSRN, Ohmura et al., 1998, <https://dataportals.pangaea.de/bsrn/>]. The network was established in 1992 [Heimo et al., 1993] and contains measurements from 1992

to the present. The BSRN network is chosen as it comprises high temporal resolution measurements over long periods with high data quality. According to [Gueymard and Myers, 2009] it is crucial to use only the highest quality data as those from the BSRN network, since other suboptimal data might result in an incorrect assessment. The measurement accuracy of BSRN GHI is estimated to be about 5 Wm^{-2} [Ohmura et al., 1998]. Altogether ten sites of the BSRN network are located in the COSMO-REA6 model domain (see Fig. 3.1 and Tab. 3.1) comprising different climate regimes within Europe.

The high quality of the BSRN measurements is achieved by applying strict quality control and quality assurance protocols [König-Langlo et al., 2013]. In addition, König-Langlo et al. recommend that every user should consider further quality control. Therefore, we applied tests provided by Long and Dutton [2002], namely the so-called "Extremely Rare Limits" tests, and two comparison tests to check the consistency of the three measurements: GHI, direct and diffuse radiation. The application of these quality control tests leads to a reduction in the number of measurements of about 2.6%. When comparing gridded reanalyses data with local measurements one has to consider that the reanalyses data provide quantities representing a relative large model grid box area. Measurements, on the other hand, are affected by the local environmental conditions such as land cover and topography. In order to match the one minute resolution BSRN data with the instantaneous values from a COSMO-REA6 grid box, we applied a 10 minute average to the measurements with an averaging window centered around the COSMO-REA6 output time step. This is motivated by the fact that an air parcel with a typical horizontal wind speed of 10 ms^{-1} needs 10 min to cross a spatial distance of 6 km. Averages are only computed when all one minute values within a 10 min window are available and the corresponding solar elevation angles are larger than 10 degrees.

In order to separate cloudy and cloud free conditions we use measurements of the ceilometer network² operated by DWD. In total 87 sites, so-called SYNOP stations, in Germany provide measurements of GHI as 10 min averages and cloud base height (CBH) derived from lidar ceilometers. CBH is given as the lowest cloud base height (observed every 15 s) within a 10 min interval. Note that according to this definition CBH does not need to persist over the 10 minute interval, i.e. partly cloudy conditions are also included. In order to match the COSMO-REA6 instantaneous output we consider only two values per hour which are centered around the COSMO-REA6 output step ("quarter past" and "quarter to"). Considered CBH measurements are from the years 2007-2013.

²re3data.org: SAMD; editing status 2017-04-09; re3data.org – Registry of Research Data Repositories, doi:10.17616/R3D944, 2017.

Table 3.1: GHI statistics before (COSMO-REA6) and after applying the post-processing (COSMO-REA6pp) for all considered BSRN stations. Years states the time range and N_{obs} the number of available measurements. The bias, the root mean square error (RMSE), bias corrected RMSE (BC_RMSE), the mean absolute error (MAE), and the Pearson correlation (R) are based on the difference between modeled data and the BSRN measurements. The cross-validation results show the statistics when applying the post-processing to independent sites (see Sec. 3.5.3). The red marked sites are rejected from the estimation procedure of the scaling factors (see Sec. 3.4).

			COSMO-REA6 [Wm^{-2}]					COSMO-REA6pp [Wm^{-2}]					Cross-validation results [Wm^{-2}]				
Station name	Years	N_{obs}	R	Bias	RMSE	BC_RMSE	MAE	Bias	RMSE	BC_RMSE	MAE	Bias	BC_RMSE	MAE			
LIN	Lindenberg	95-09	202723	0.84	-2.9	129.8	129.7	87.4	5.2	136.6	136.5	86.9	5.4	136.6	87.0		
GAM	Camborne	01-14	183926	0.81	2.2	142.8	142.8	100.0	11.8	152.8	152.3	103.3	12.1	152.6	103.6		
CAR	Carpentras	96-14	253580	0.90	-29.8	122.2	118.5	86.1	-7.8	123.5	123.3	72.4	-9.8	123.0	72.8		
CNR	Cener	09-14	76731	0.85	-19.6	144.9	143.5	100.9	-2.8	151.9	151.9	95.3	-3.1	151.9	95.3		
CAB	Cabauw	05-14	134150	0.81	-18.4	138.8	137.5	94.6	-13.3	146.5	145.9	96.7	-14.2	146.2	97.0		
PAL	Palaiseau	05-14	123935	0.81	-7.6	144.4	144.2	99.8	1.0	152.4	152.4	100.0	0.7	152.6	100.1		
TOR	Toravere	99-14	163839	0.84	-8.2	121.3	121.0	81.1	1.5	126.8	126.7	79.5	2.0	126.8	79.6		
PAY	Payenne	95-11	208568	0.86	10.4	134.6	134.2	93.3	22.8	139.5	137.6	87.2	24.3	137.4	87.5		
Mean			1347452	0.84	-9.2	134.9	133.9	92.9	2.3	141.3	140.8	90.5	2.2	140.9	90.4		
STD			1347452	0.03	12.1	8.9	9.4	6.9	10.6	10.9	10.9	9.9	11.4	11.0	9.9		
LER	Lerwick	01-14	155356	0.75	12.6	136.3	135.7	97.9	18.5	147.1	145.9	102.5					
SBO	Sede Boger	03-12	131584	0.94	-49.7	109.3	97.3	83.2	-14.4	103.3	102.3	59.4					

Table 3.2: Transmissivity characteristics of observations, COSMO-REA6, and the post-processed transmissivity product COSMO-REA6pp for each BSRN site. The underlying dataset is the same as used for table 3.1, but transformed into transmissivity values.

Station name	Transmissivity obs		COSMO-REA6		COSMO-REA6pp		Cross-validation results		
	Mean	Var	Mean	Var	Mean	Var	Mean	Var	
LIN	Lindenberg	0.43	0.054	0.42	0.039	0.43	0.054	0.43	0.054
GAM	Camborne	0.42	0.054	0.42	0.043	0.43	0.059	0.43	0.059
CAR	Carpentras	0.55	0.048	0.51	0.031	0.53	0.045	0.53	0.045
CNR	Cener	0.51	0.055	0.48	0.039	0.49	0.055	0.49	0.055
CAB	Cabauw	0.42	0.052	0.39	0.041	0.40	0.055	0.40	0.055
PAL	Palaiseau	0.44	0.054	0.43	0.040	0.43	0.055	0.43	0.055
TOR	Toravere	0.43	0.058	0.42	0.041	0.43	0.057	0.43	0.058
PAY	Payenne	0.44	0.060	0.46	0.036	0.47	0.052	0.47	0.052
Mean		0.46	0.054	0.44	0.039	0.45	0.054	0.45	0.054
STD		0.05	0.003	0.04	0.003	0.04	0.004	0.04	0.004
LER	Lerwick	0.37	0.052	0.39	0.042	0.40	0.057		
SBO	Sede Boger	0.64	0.022	0.59	0.013	0.62	0.023		

3.3 Assessment of COSMO-REA6 GHI

The ability of COSMO-REA6 to provide the realistic variability of GHI is qualitatively demonstrated by an arbitrarily selected time-series of GHI on June 23, 2008 at the BSRN station Lindenberg, Germany (Fig. 3.2). The large scatter of the one minute resolution data indicates broken cloudiness with alternating cloudy and clear sky periods in the first half of the day while the smooth shape of the GHI during the rest of the day points to clear sky conditions. When the BSRN measurements are averaged to 10 min the variability due to changing cloud conditions is still visible and similar to the one of COSMO-REA6 for the corresponding grid box. MERRA-2 represents the observed GHI measurements well in the clear sky period, but cloud induced variability in the morning seems to be too smooth. With its three hour averages ERA-Interim is not capable to represent cloud induced short-term variations at all.

In order to quantitatively assess the quality of the COSMO-REA6 GHI the 10 min average measurements for all BSRN station between 1995 and 2014 are compared with the corresponding reanalysis data. The scatter density plot (Fig. 3.3) of more than 1.6 million matching pairs shows that most samples are clustered along the main diagonal indicating a good overall agreement with a mean difference between the reanalyses and measurements (bias) of -10 Wm^{-2} and a correlation coefficient of 0.86. The scatter density plot shows two distinct features: (1) Small observed GHI values are quite often overestimated by COSMO-REA6 and (2) GHI values higher than approx. 1000 Wm^{-2} do not occur at all in COSMO-REA6 although these are represented in the measurements. Because such high values are related to cloud free situations with high solar elevation angle the underestimation in COSMO-REA6 indicates a too strong extinction of solar radiation likely caused by aerosols. This effect is even visible in the time-series of a single day (Fig. 3.2). Given the small bias of -10 Wm^{-2} (averaged over the whole data), we hypothesize compensation effects of the two listed characteristics.

Tab. 3.1 provides a statistical comparison between instantaneous COSMO-REA6 GHI and measurements (10 min averages) for each BSRN site in terms of bias, RMSE, and the correlation coefficient. In order to support the following discussion of Tab. 3.1 in terms of cloud characteristics, transmissivity mean values and its variance are given in Tab. 3.2. The mean difference between the reanalyses and measurements (i.e., the bias) varies between -49.7 Wm^{-2} and 12.6 Wm^{-2} among the sites (Tab. 3.1). The root mean square error (RMSE) values between 100 and 145 Wm^{-2} might appear high but are related to the high resolution providing realistic variations in GHI from COSMO-REA6 (Fig. 3.1 and Fig. 3.2). Therefore a slight misplacement of clouds in time or space will lead to strong differences compared with measurements. In order to compare the RMSE with those from global reanalysis daily GHI is assessed later on in Sec. 3.5.

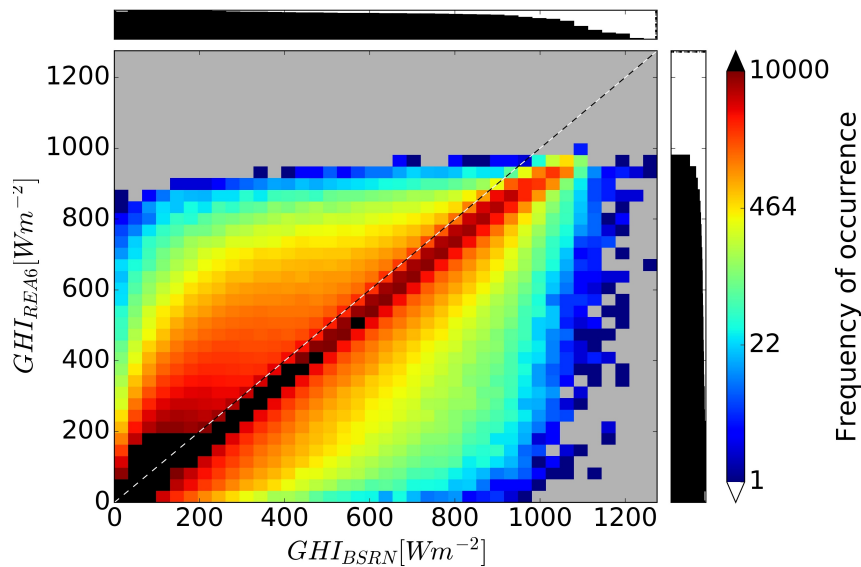


Figure 3.3: Scatter density plot of GHI between measurements from all ten BSRN sites (10 min averages) and corresponding values from COSMO-REA6 (instantaneous). The time frame is 1995-2014.

From the list of stations, Sede Boqer (Israel) stands out, as it has a large negative bias ($-49.7 Wm^{-2}$) but shows the highest correlation with COSMO-REA6 of all sites. The high correlation and low RMSE is probably caused by the low average cloudiness at Sede Boqer (see Tab. 3.2, Sede Boqer has on average high transmissivity and low variance). As already discussed above the high cloud variability on small scales leads to a poor performance of the reanalysis when a slight shift of a cloud in time or space occurs. With respect to the negative bias, there are probably two causes: (1) Sede Boqer's proximity to the border of the COSMO-REA6 domain with the resulting boundary effects, and (2) the low prevalence of clouds. The latter is consistent with the use of an optically too thick aerosol climatology in COSMO-REA6 (see Sec. 2) that results in a negative bias in clear sky situations due to too strong radiation attenuation by aerosols. At the site Lerwick, the largest positive bias of GHI ($12.6 Wm^{-2}$) occurs in combination with the smallest correlation coefficient (0.75). In contrast to Sede Boqer, Lerwick (Scotland) which shows the highest positive bias ($12.6 Wm^{-2}$) is situated close to the North Sea with high cloudiness i.e. the averaged transmissivity values are low (Tab. 3.2).

The apparent dependency of the bias on the cloud climatology motivates a refined analysis in respect to the effect of clouds on the extinction of solar radiation. For this purpose we look at the discrete probability density function for transmissivity T (Fig. 3.4) as defined in Sec. 3.2.1. For all BSRN stations the measurements reveal a bimodal distribution with local transmissivity maxima around 0.2 and 0.7. The high transmissivity maximum around 0.7 shows a more pronounced peak whose amplitude strongly varies between stations. As high transmissivity is typically associated with clear sky the amplitude of this peak likely reflects the differences in clear sky occurrence at the different sites. The broader low transmissivity peak around 0.2 is

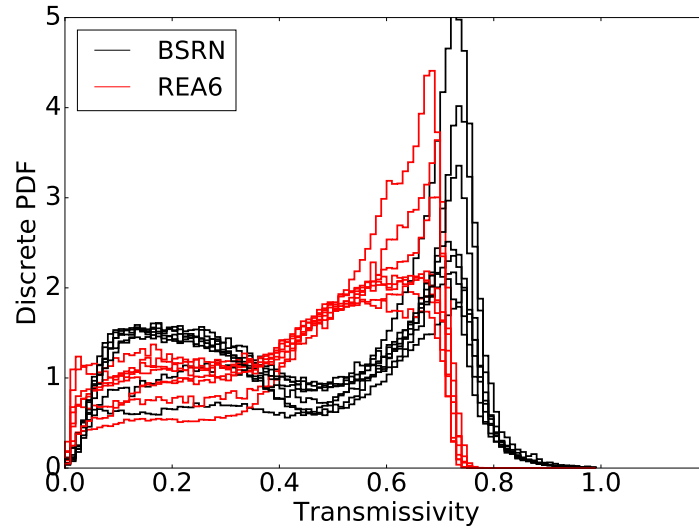


Figure 3.4: Discrete Probability Density Functions (PDF) for transmissivity from BSRN measurements (black) and COSMO-REA6 (red). Each individual line represents a BSRN station. Lerwick and Sede Boqer are omitted here. The bin sizes are 0.01.

likely connected with cloudy conditions. Thus, we hypothesize that the local minimum around 0.5 separates cloudy from clear sky conditions which differs from the value of 0.7 given by Boilley and Wald [2015] for daily mean values.

In order to test our hypotheses the SYNOP data set (Sec. 3.2.4) with corresponding GHI and ceilometer measurements for Germany is used. When looking at the observed Probability Density Function (PDF) of transmissivity (Fig. 3.5) a similar bimodal distribution as for the BSRN station appears. The ceilometer measurements allow to stratify the data into different cloud conditions which confirms that the majority of high transmissivity cases originates from clear sky conditions. Also high clouds defined as clouds with a base of 5 km and higher are mostly associated with high transmissivities. These are commonly composed of ice particles and show a much lower average optical depth explaining their high transmissivity. Lower transmissivities mostly comprise cases with low (cloud base below 2 km) and medium high (cloud base between 2 and 5 km) clouds. Only a few high transmissivity cases with low or medium CBH exist. These can be explained by the fact that even the appearance of one 15 s cloudy sample within 10 min will still lead to the measurement of a CBH although the majority of time is cloud free. Furthermore, the ceilometer measures only vertically while GHI measurements are influenced by the whole hemisphere. The difference in sampling may lead to the determination of clear sky conditions from ceilometer measurements in a nearly overcast sky and vice versa.

The frequency distribution of COSMO-REA6 transmissivity (Fig. 3.4) shows some differences compared to the measurements. As already seen in the scatter density plot (Fig. 3.3) highly transparent scenes with transmissivities higher than 0.8 do not appear and the whole distribution seems to be squeezed towards lower transmissivities compared to the measurements.

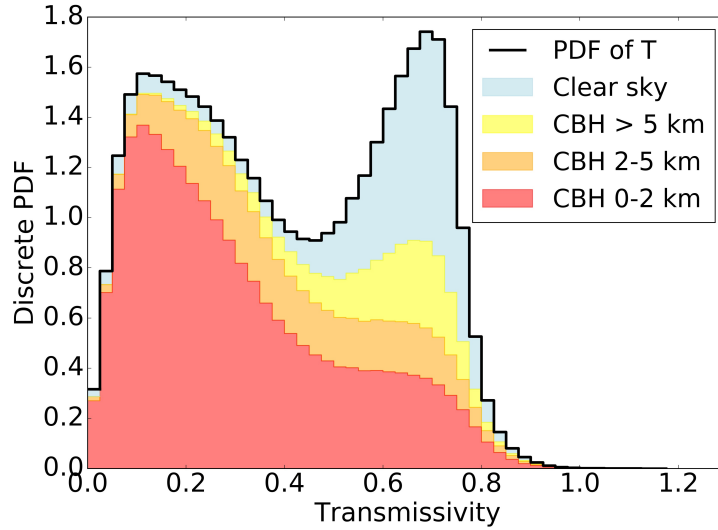


Figure 3.5: Discrete probability density function for transmissivity measured at 87 German SYNOP stations with corresponding ceilometer measurements. Colors indicate the cloud situation as given by the ceilometer measurements: Clear sky conditions (blue), high clouds (yellow), medium altitudes (orange) and low level clouds (red). See text for definitions.

Nevertheless, the strong variability in amplitude of the high transmissivity peak is reproduced indicating that the reanalysis is able to represent the cloud climatology (true/false events) at the different sites. For transmissivities in the medium range many more cases compared to measurements occur indicating that clouds are optically relatively thin in COSMO-REA6. The narrower transmissivity distribution is in accordance with the systematic underestimation of transmissivity variance by COSMO-REA6 as shown in Tab. 3.2. In summary, two different characteristics in COSMO-REA6 appear: (1) GHI is underestimated in clear sky conditions due to the use of the Tanré aerosol climatology which is known to exhibit unrealistically high values of aerosol optical thickness [Zubler et al., 2011] and (2) on average, clouds are optically too thin causing an overestimation of GHI.

3.4 GHI post-processing

Given the under- and overestimation of GHI as described in the previous section we developed a post-processing using reanalysis data only to correct the systematic differences for the clear sky and the cloudy regime, separately. The proposed post-processing is based on the determination of scaling factors for GHI from COSMO-REA6 through orthogonal distance regression [ODR, described in detail by Markovsky and Huffel, 2007, under the name total least-squares method] using different scaling factors for either cloudy or clear sky situations. A transmissivity threshold T_{th} is used to distinguish both regimes. $T \geq T_{th}$ refers to clear sky and $T < T_{th}$ refers to cloudy sky (see Sec. 3.3). Furthermore, we consider the annual cycle and the solar elevation angle

which describes the length of the light path in the atmosphere as potential influence factors for the under- or overestimation of GHI. Therefore, the scaling factor a generally depends on the predictor T as well as on the month of year m and the solar elevation angle θ :

$$a(T, m, \theta) = \begin{cases} a_{\text{clear},\theta} & \text{for } T \geq T_{\text{th}} \\ a_{\text{cloud},m} & \text{for } T < T_{\text{th}} \end{cases}$$

with $a_{\text{clear},\theta}$, $a_{\text{cloud},m}$ the scaling factors for clear sky and cloudy conditions, respectively. The post-processed GHI (Q_{GHIpp}) is then defined as

$$Q_{GHIpp} = Q_{GHI} \cdot a(T, m, \theta) \quad (3.3)$$

with Q_{GHI} being the global horizontal irradiance of the reanalysis. Using the TOA radiation Q_{TOA} , equation 3.3 can be easily transformed to the transmissivity space ($T = \frac{Q_{GHI}}{Q_{TOA}}$) as:

$$T_{pp} = T \cdot a(T, m, \theta) \quad (3.4)$$

with T_{pp} the post-processed transmissivity and $a(T, m, \theta)$ the invariant scaling factors from Eq. 3.3.

The scaling factor $a(T, m, \theta)$ is determined as the slope of the linear ODR between the BSRN- and the COSMO-REA6 transmissivity. The ODR has the advantage to consider uncertainties in both, measurements and reanalyses. The best case ODR would have a slope equal to the angle bisector ($a = 1$), thus no adjustment would take place. It should be mentioned that the ODR regression is forced to cross the coordinate origin to keep very small radiation values unchanged, otherwise the ODR would in some cases generate negative radiation values. For cloudy situations twelve scaling factors are estimated, one for each month. For clear sky situations six scaling factors are estimated, one for each solar elevation regime: $10^\circ - 20^\circ$, $20^\circ - 30^\circ$, $30^\circ - 40^\circ$, $40^\circ - 50^\circ$, $50^\circ - 60^\circ$ and $60^\circ - 90^\circ$.

In general, the scaling factors are determined by the annual cycle of the cloud- and aerosol climatologies as well as by the solar elevation angle. In both regimes (clear and cloudy) all of these dependencies are directly or indirectly considered. For simplicity we only consider the seasonal variation under cloudy sky conditions ($a_{\text{cloud},\theta}$) due to the dominance of diffuse radiation over direct radiation. Under clear sky conditions ($a_{\text{clear},m}$) the sun position is more important since aerosol (and water vapor) extinction, which depends mainly on the path of direct solar radiation, dominates.

The scaling factors $a(T, m, \theta)$ are determined from all available matches of reanalyses data and measurements from eight BSRN sites in Central and Western Europe (Tab. 3.1). The two stations with the minimum and maximum bias, i.e., Sede Boqer and Lerwick, are excluded. The transmissivity threshold distinguishing the clear sky and cloudy sky regimes has been set ad

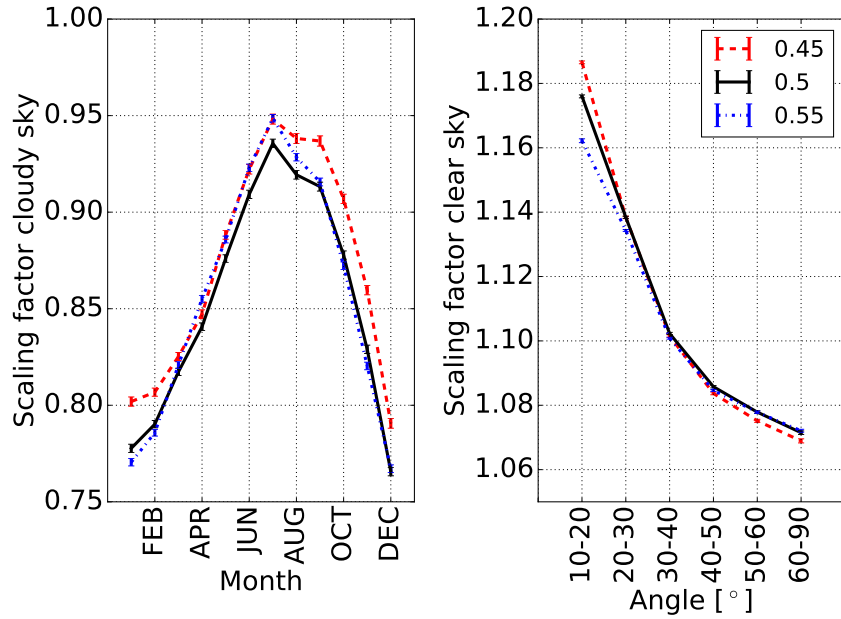


Figure 3.6: Sensitivity of the estimated scaling factors to transmissivity thresholds T_{th} for the cloudy regime with low transmissivity values ($T < T_{th}$, left) and the clear sky regime with high transmissivity values ($T > T_{th}$, right). Different colors represent the scaling factors estimated with $T_{th} = 0.45$ (red), $T_{th} = 0.5$ (black), and $T_{th} = 0.55$ (blue). Vertical lines illustrates the uncertainties of the ODR fit.

hoc to $T_{th} = 0.5$. Therefore the sensitivity of the estimated scaling factors to this threshold is investigated in more detail (Fig. 3.6). In the cloudy sky regime ($T < T_{th}$) the estimated scaling factors are smaller than one because COSMO-REA6 overestimates the GHI compared to the measurements, i.e. the clouds are optically too thin. This effect can be seen during the whole year, but the effect is stronger for winter months with scaling factors around 0.8 than for summer with scaling factors around 0.93. When varying $T_{th} = 0.5$ by $\pm 10\%$ the scaling factor only changes by roughly $\pm 2\%$. Note: The scaling factors from March till September are smallest (largest adaptations necessary) for $T_{th} = 0.5$. Thus, the threshold $T_{th} = 0.5$ is well chosen because an increase of T_{th} seems to include cases which need positive adjustments (cases of the clear sky regime), and a decrease of T_{th} seems to exclude cases which need negative adjustments (cases of cloudy sky regime). For clear sky conditions ($T > T_{th}$) the scaling factor varies with the solar elevation angle between 1.19 for low and 1.07 for high solar elevation angles. A scaling factor larger than one indicates a general underestimation of the GHI by the reanalysis for these situations as already discussed in Sec. 3.3. The sensitivity of the scaling factor to the transmissivity threshold in this regime is highest for low elevation angles ($< 20^\circ$) with values varying between 1.16 and 1.19 and nearly diminishes for medium elevation angles. In summary, the sensitivity to the transmissivity threshold seems to be marginal. Therefore, the chosen threshold value of $T_{th} = 0.5$ is used for the post-processing approach.

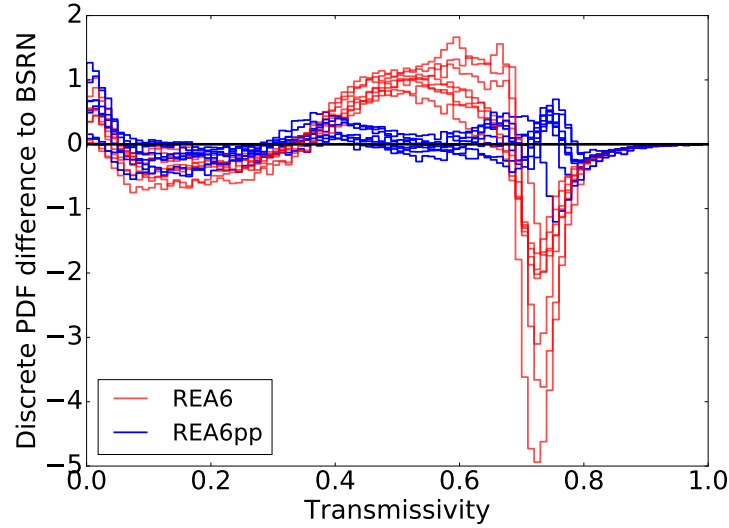


Figure 3.7: Difference between the transmissivity distribution from measurements and the one from COSMO-REA6 (red) and COSMO-REA6pp (blue). Sites used for estimating the scaling factors are considered only. Positive values indicate an overestimation of COSMO-REA6 while negative values show an underestimation.

In order to combine the clear sky and cloud regime, post-processing such that a continuously distributed transmissivity without a discontinuity at the transmissivity threshold T_{th} is achieved, a weight function is applied. A sigmoid function is chosen as weighting function, which is defined as

$$f = \frac{1}{1 + \exp(-\frac{1}{c}(x - b))} \quad (3.5)$$

with the coefficient b shifting the function on the x-axis and the coefficient c defining the slope of the sigmoid function. In our application, the coefficient b is set to the transmissivity threshold which distinguishes between the two regimes ($b = T_{th} = 0.5$). The slope of the sigmoid function c is estimated in order to minimize the distance between the observed and post-processed discrete PDF over all eight BSRN stations. The quantity measuring the distance between two probability distributions is known as Earth Mover's Distance [EMD, Rabin et al., 2008]. By minimizing EMD an optimum slope of $c = 0.03$ is derived which results in an EMD improvement of factor 4 compared to the EMD before post-processing (not shown).

3.5 Evaluation of the new GHI data set

The post-processing described in Sec. 3.4 is applied to the COSMO-REA6 reanalysis. To reduce computational costs, the solar position was calculated for every third grid point and was afterwards linearly interpolated to the complete model grid. The post-processed GHI data set covers the time period from January 1, 1995 to December 31, 2014 with a temporal resolution

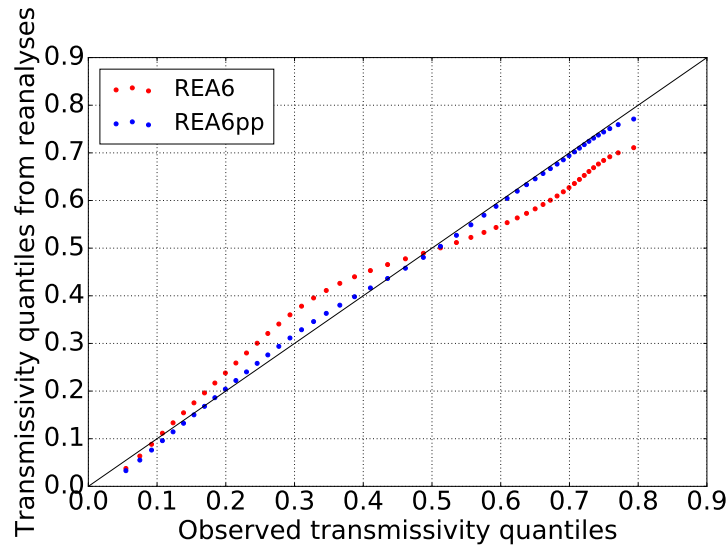


Figure 3.8: Quantile-quantile plot comparing the transmissivity distribution from measurements and the one from COSMO-REA6 and COSMO-REA6pp. Considered observations are from the eight BSRN stations listed in Tab. 3.1.

of 15 minutes for 848×824 grid points in the European domain (Fig. 3.1). The resulting post-processed product of COSMO-REA6 GHI is from now on referred to as COSMO-REA6pp.

3.5.1 Marginal distribution

In order to test the quality of the post-processing, Fig. 3.7 shows the deviation of the transmissivity distribution to the measured one for both COSMO-REA6 and COSMO-REA6pp. The figure clearly shows that the under- and overestimation identified in Fig. 3.4 have been significantly reduced for all transmissivities: (i) The clear sky peak of COSMO-REA6 as a consequence of the strong aerosol extinction has now been shifted to transmissivities around 0.8 much closer to the observed values. (ii) The underestimation of transmissivities below 0.4 associated with too thin clouds has been eliminated. An equivalent illustration of the bias reduction depending on transmissivity is given by Fig. 3.8.

3.5.1.1 Separate evaluation for clear sky and cloudy conditions

The post-processing has mainly been developed in order to reduce the systematic bias in "clear sky" ($T > T_{th}$) and "cloudy sky" ($T < T_{th}$) situations. Since the method is not designed to handle the problem of misrepresented clouds in COSMO-REA6, only situations where both transmissivity values - observed and reanalyzed - simultaneously lie above or under the threshold, are considered in the evaluation of GHI (Fig. 3.9).

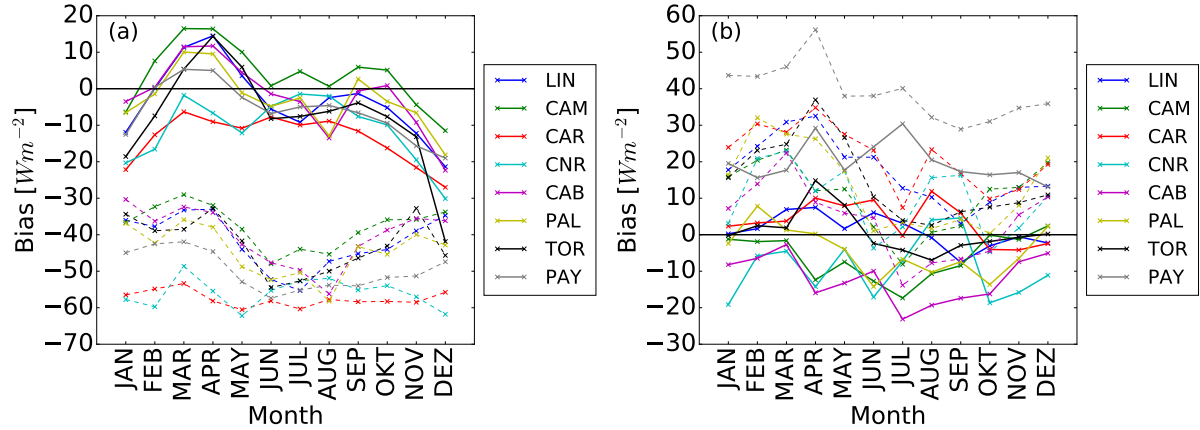


Figure 3.9: Monthly mean bias for COSMO-REA6 (dashed) and COSMO-REA6pp (solid lines) for (a) clear sky situations and (b) cloudy sky situations. To calculate the monthly averages, we considered only situations where the observed transmissivity and the COSMO-REA6 transmissivity simultaneously exceeds 0.5 (a) or is below 0.5 (b).

For each BSRN site the monthly mean bias in COSMO-REA6 (dashed) and COSMO-REA6pp (solid) is evaluated. In case of clear sky situations, an improvement is evident for all individual sites (Fig. 3.9a). The general underestimation of GHI in COSMO-REA6 with bias values between -62 and -30 Wm^{-2} depending mainly on the site has disappeared in COSMO-REA6pp with most monthly mean values between -20 and 20 Wm^{-2} . Nevertheless, a systematic (but reduced) underestimation remains during the winter months, particularly in December. This is probably caused by the annual cycle of clear sky ($T \geq T_{\text{th}}$) and cloudy sky ($T < T_{\text{th}}$) situations with $\sim 32\%$ ($\sim 55\%$) of cases being clear sky situations in winter (summer) months. Local effects could also be responsible for the worst bias of -40 Wm^{-2} in Toravere, Estland, in December.

The bias has also been improved in COSMO-REA6pp for cloudy sky situations (Fig. 3.9b). While the bias before the post-processing ranges from -18 Wm^{-2} to 59 Wm^{-2} , afterwards it is reduced to values ranging from -22 Wm^{-2} to 38 Wm^{-2} . Nevertheless, some sites still exhibit a systematic positive or negative bias which are caused by local effects.

3.5.2 Joint distribution

To assess the improvements of the post-processing at individual times and locations, Tab. 3.1 compares bias, RMSE, bias corrected RMSE (BC_RMSE), and mean absolute error at individual stations before and after post-processing (COSMO-REA6pp). The usage of the two sites that have not been used in the estimation of the post-processing parameters (Sede Boqer and Lerwick colored in red) allows for a performance assessment of the post-processing method for independent measurements. After post-processing, the large bias at most stations including Sede Boqer is significantly reduced, e.g. the bias is reduced from -29.8 to -7.8 at Carpentras,

France, and from -19.6 to -2.8 Wm^{-2} at Cener, Spain. This reduction is expected as sites with large biases are mostly effected by one of the two regimes. The RMSE and the BC_RMSE, which are sensitive to departures in the tails of the distribution, show slightly increased values. Considering that the post-processing increases the number of low as well as high radiation cases, it broadens the distribution function of the GHI. Since the largest deviations of the reanalysis from the measurements are caused by misrepresented clouds, the number of cases with large transmissivity deviations is increased. Thus, the RMSE and the BC_RMSE, which weight deviations quadratically increase. In comparison, the MAE which weights all deviations to measurements equally shows an improvement (in seven of ten cases) of the post-processed radiation. The post-processing is derived from eight BSRN stations but applied to the full COSMO-REA6 domain. Therefore the application of the post-processing to the two independent test sites is most interesting. Here the MAE improves strongly from 83.2 to 59.4 Wm^{-2} for Sede Boqer and becomes slightly worse (97.9 to 105.2 Wm^{-2}) for Lerwick.

As mentioned before, the post-processing leads to a broadening of the GHI/Transmissivity distribution. In order to check if that results in a more realistic distribution, the variance of observations, COSMO-REA6, and COSMO-REA6pp (after post-processing) are shown in Tab. 3.2. While COSMO-REA6 significantly underestimates the observed transmissivity variance, it is well represented by COSMO-REA6pp, even at the sites with different climatic conditions (Lerwick and Sede Boqer). Note that the mean values are more or less unchanged by the post-processing.

So far, the previous tables only showed the statistical results for all data, i.e. they do not show the individual improvement for the cloudy and clear sky cases, separately. In order to investigate the improvement of the post-processing without bias compensation effects from the two cloud regimes, Tab. 3.3 and Tab. 3.4 show the statistical results for clear and cloudy cases separately. The separation of "clear" and "cloudy sky" is done with the same criteria used for Fig. 3.9. In clear sky cases, there is an improvement in each individual score. The post-processing reduces the systematic biases of -39 till -67.8 Wm^{-2} to a range of -17.9 till 6.1 Wm^{-2} . The MAE improves by at least 6.9 up to 61.6 Wm^{-2} . Also the RMSE improved for each individual site (not shown). In cloudy sky cases the bias improves at 7 of 10 BSRN stations. At the other 3 stations an over-adjustment took place. Nevertheless, the MAE improves at 9 of 10 stations, and the RMSE at all considered stations (not shown).

3.5.3 Cross-validation of the new GHI data set

Cross-validation is a common method to investigate the potential to generalize the application of a statistical method. The principle of cross-validation is to (1) divide the data into a training and verification data set, (2) estimate the statistical model using the training data, and (3) test the model with the verification data set [for more details see von Storch and Zwiers, 2003; Stone,

Table 3.3: Same as Tab. 3.1 but for clear sky situations only (both transmissivity values - observed and reanalyzed - are simultaneously above the threshold $T_{th} = 0.5$). Results are given in Wm^{-2} .

			COSMO-REA6		COSMO-REA6pp		Cross-validation results	
	Station name	Years	Bias	MAE	Bias	MAE	Bias	MAE
LIN	Lindenberg	63805	-43.8	59.0	-0.1	45.8	0.4	45.9
CAM	Camborne	54025	-39.0	62.6	6.1	54.9	7.2	55.2
CAR	Carpentras	140587	-57.9	65.8	-11.7	34.5	-14.6	35.6
CNR	Cener	34097	-54.9	67.4	-7.7	42.8	-8.0	42.9
CAB	Cabauw	36861	-42.2	58.7	0.8	49.1	0.9	49.3
PAL	Palaiseau	39336	-45.8	62.3	-1.1	48.1	-0.9	48.2
TOR	Toravere	54313	-44.5	53.2	-0.3	39.5	0.3	39.6
PAY	Payerne	76618	-50.9	59.9	-3.6	37.3	-3.3	37.2
Mean	Mean	499642	-47.4	61.1	-2.2	44.0	-2.2	44.2
STD	STD	499642	6.1	4.2	5.1	6.3	6.1	6.2
LER	Lerwick	155356	-40.2	63.8	2.9	56.9		
SBO	Sede Boqer	131584	-67.8	75.2	-17.9	37.4		

Table 3.4: Same as Tab. 3.1 but for cloudy sky situations only (both transmissivity values - observed and reanalyzed - are simultaneously below the threshold $T_{th} = 0.5$). Results are given in Wm^{-2} .

			COSMO-REA6		COSMO-REA6pp		Cross-validation results	
	Station name	Years	Bias	MAE	Bias	MAE	Bias	MAE
LIN	Lindenberg	93451	17.6	63.0	1.4	58.6	1.3	58.6
CAM	Camborne	82716	8.8	73.3	-7.2	69.7	-7.5	69.7
CAR	Carpentras	59152	21.6	69.7	3.5	64.5	3.2	64.3
CNR	Cener	24411	9.2	75.8	-9.8	72.1	-10.1	72.1
CAB	Cabauw	64600	2.7	68.8	-12.9	66.4	-14.2	66.3
PAL	Palaiseau	53867	12.5	73.2	-5.0	68.9	-5.5	68.9
TOR	Toravere	75083	14.6	60.2	0.6	56.2	0.9	56.3
PAY	Payerne	85265	39.1	73.5	20.0	64.9	22.6	66.0
Mean	Mean	538545	15.8	69.7	-1.2	65.2	-1.1	65.3
STD	STD	538545	10.3	5.2	9.6	5.1	10.6	5.1
LER	Lerwick	155356	13.5	66.6	-0.1	63.1		
SBO	Sede Boqer	131584	8.1	44.1	-10.9	45.6		

1974; Michaelsen, 1987; Kohavi, 1995]. In order to test the potential to spatially generalize the post-processing, cross-validation is applied by removing one observational site at time from the training data set while applying the approach. The last columns in Tab. 3.1 show the bias, BC_RMSE and the MAE for the individual sites, by omitting the site while estimating the scaling factors. In comparison to the post-processed results using the full data set, the bias is slightly increased by 0.2 till 1.5 Wm^{-2} for all stations except for Palaiseau where the bias actually becomes smaller. However, all changes lie below the measurement uncertainty of 5 Wm^{-2} and no considerable changes can be found for BC_RMSE and MAE. Also, when applying cross-validation to the clear and cloudy sky cases separately, the resulting scores are not significantly reduced compared to the COSMO-REA6pp scores (see Tab. 3.3 and Tab. 3.4). Additionally, also the transmissivity variances changes just slightly comparing the cross-validation results with the

dependent COSMO-REA6pp results (Tab. 3.2). Thus, it is expected that the developed post-processing produces improved radiation fields for the whole COSMO-REA6 model domain.

3.5.4 Daily mean values

Up to now we only considered instantaneous GHI values which are available at 15 min resolution from COSMO-REA6. Because of the coarser resolution of other reanalyses products, most previous studies [e.g. Boilley and Wald, 2015; Posselt et al., 2012] have been concerned with daily mean values of GHI. In order to relate the performance of COSMO-REA6 to these studies in the following we compare the daily average GHI from COSMO-REA6 and COSMO-REA6pp to the global, coarser resolution ERA-Interim reanalysis using BSRN measurements as a reference. Note, that due to the quality control of BSRN measurements (Sec. 3.2.4) only the GHI values associated with solar angles greater than 10 degree are used to calculate the daily averages. For consistency COSMO-REA6 and COSMO-REA6pp have been treated similarly. However, the ERA-Interim 3-hourly data comprise also the radiation values of solar angles below 10 degrees, thus causing a systematic error in the evaluation. This systematic difference in daily GHI due to the limitation in solar angles is estimated with the help of the continuous COSMO-REA6 data. Neglecting the low elevation angles leads to an underestimation of the daily average GHI of about 2.9 Wm^{-2} which needs to be kept in mind when interpreting the following results.

The statistical comparison of daily mean GHI from reanalysis with the ten BSRN stations is provided in the form of box-whisker diagrams in Fig. 3.10. The results indicate that COSMO-REA6 as well as COSMO-REA6pp are in better agreement with the observed GHI compared to ERA-Interim and MERRA-2, i.e. showing lower bias, RMSE and MAE as well as a higher correlation with measurements in the median of all stations. As to be expected COSMO-REA6pp performs better compared to COSMO-REA6 in terms of bias and the MAE. For the latter the median improved from 20.3 Wm^{-2} to 16.8 Wm^{-2} . The benefit of the post-processing is most pronounced in the reduced length of whiskers for bias and MAE of COSMO-REA6pp meaning that systematic deficits at some of the stations could be cured without compromising the quality at other stations.

3.5.4.1 Comparison to previous studies

Boilley and Wald [2015] evaluated two global reanalyses, i.e. ERA-Interim and MERRA as well as the HelioClim [Blanc et al., 2011] satellite product to GHI surface observations in different regions of the globe. They find a lower uncertainty in the satellite product and conclude that this should be preferred over the global reanalyses. Thus, the question arises whether COSMO-REA6pp which has shown improved performance compared to ERA-Interim has a similar quality as satellite products.

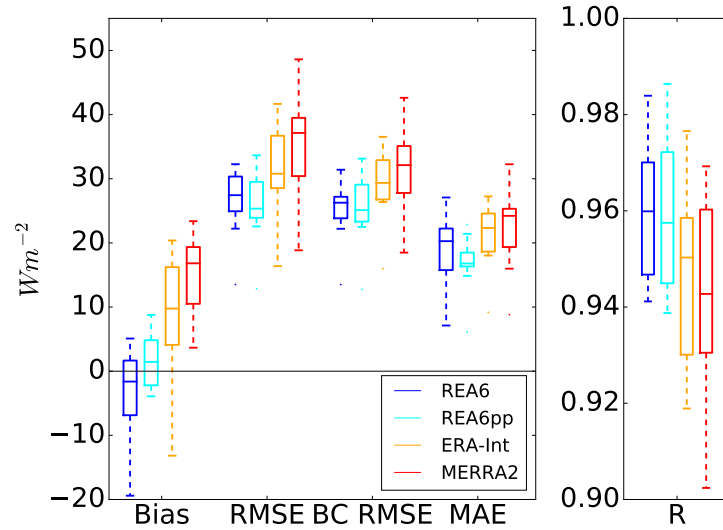


Figure 3.10: Statistical assessment of daily mean GHI from COSMO-REA6, COSMO-REA6pp, ERA-Interim, and MERRA-2 over the years 1995-2014. The reference GHI is provided by the ten BSRN stations listed in Tab. 3.1. Each boxplot is created by 10 values, one for each BSRN site. The box extends from the first to the third quartile (interquartile range IQR) with a line at the median. The whiskers have the maximum length of 1.5 times IQR. All points beyond the whiskers (flyers) are shown as dots. Note that due to the consideration of sun elevation angles below 10 degrees ERA-Interim is about 2.6 Wm^{-2} higher than all other data sets.

Posselt et al. [2012] investigated the performance of a variety of satellite and reanalysis GHI products using BSRN stations as reference. Because they included five additional BSRN stations outside the COSMO-REA6 domain their results are expected to be slightly different than ours. For ERA-Interim they found a daily mean bias of 5.6 Wm^{-2} and a MAE of 26.9 Wm^{-2} which are quite similar to our findings, i.e. 6.6 Wm^{-2} (bias) and 20.8 Wm^{-2} (MAE) where a correction for the solar elevation angle cutoff has been applied to the data from Fig. 3.10. This similarity for ERA-Interim encourages us to indirectly relate the performance of COSMO-REA6pp to the other products investigated by Posselt et al. [2012]. Their best product, i.e. the satellite based product SARAH [Müller et al., 2015], reveals a similar performance (bias= 4.6 Wm^{-2} , MAE= 15.5 Wm^{-2}) compared to COSMO-REA6pp in our study (bias= 1.8 Wm^{-2} , MAE= 16.8 Wm^{-2}). All other products including HelioClim show a worse performance in representing measured daily GHI than COSMO-REA6pp.

3.5.5 Spatio-temporal representation

One expected advantage of COSMO-REA6 compared to global reanalysis is the enhanced representation of observed GHI spatio-temporal variability. In order to confirm this, we apply the evaluation method proposed by Cannon et al. [2014] developed to assess the ability of a reanalysis to represent wind speed on different spatial scales. They calculate the linear correlation

between measurements and reanalysis for wind speed differences at two geographically distant sites. By looking at the correlation as a function of site-to-site distance they evaluate on which scales the wind speed variability given by reanalysis is similar to the observed one. Here we apply the same method to GHI which has to our best knowledge not been done before. The method includes the following steps:

- Calculate the difference in GHI δQ between two sites i and j for measurements and reanalysis data, respectively

$$\delta \mathbf{Q}_{obs} = \mathbf{Q}_{obs,i} - \mathbf{Q}_{obs,j} \quad (3.6)$$

$$\delta \mathbf{Q}_{rea} = \mathbf{Q}_{rea,i} - \mathbf{Q}_{rea,j} \quad (3.7)$$

with $\mathbf{Q} = (Q_{t1}, \dots, Q_{tn})^T$

- Calculate the correlation: $r(\delta \mathbf{Q}_{rea}, \delta \mathbf{Q}_{obs})$
- Do this calculation for every site combination
- Plot the results as function of distance between the observation sites

The linear correlation is derived for a data set from 119 German SYNOP stations available from 2007-2013 and is shown as a function of distance between stations in Fig. 3.11. We restrict the evaluation to the 9-12 UTC averages (1) to avoid issues with respect to the daily cycle inducing a positive correlation and (2) to match the ERA-Interim output interval. In general the correlation increases steadily with increasing distance and starts to level off around 300 to 500 km distance. The general evolution from smaller to larger correlation with increasing distance is caused by the better representation of large scales, e.g. frontal systems, compared to small scale phenomena in numerical weather prediction models. For COSMO-REA6, the low correlation of less than 0.3 for scales below 50 km is due to small scale clouds. These are frequently related to convection at sub-grid scales making it very difficult to simulate clouds exactly at the correct spatio-temporal location. By averaging over larger areas or time intervals this uncertainty is effectively reduced as can be seen in the strong reduction of the MAE from roughly 100 Wm^{-2} (Tab. 3.1) for instantaneous GHI compared to 20 Wm^{-2} (Fig. 3.10) for daily means.

While ERA-Interim, MERRA-2, and COSMO-REA6 show a similar shape of the linear correlation as a function of distance COSMO-REA6 outperforms both global reanalyses with a higher correlation at all scales (Fig. 3.10). Comparing the two global reanalyses, ERA-Interim performs slightly better on scales above 270 km. The maximum correlation is 0.7 for both global reanalyses and 0.8 for COSMO-REA6. As expected the post-processing does not influence the resolved variability and COSMO-REA6pp is nearly identical to COSMO-REA6. The advantage of the high resolution reanalysis is especially visible at shorter scale, i.e at 100 km the correlation is about 0.3 for both global reanalyses while it is 0.42 for COSMO-REA6. To investigate whether

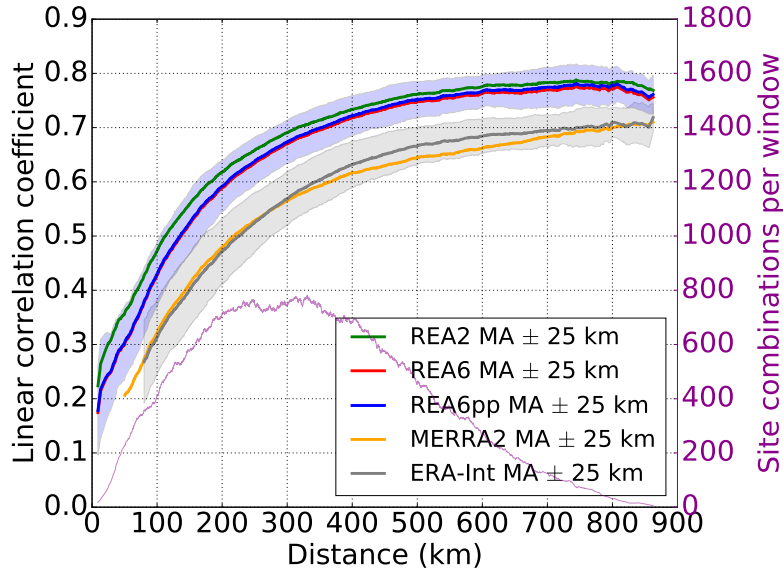


Figure 3.11: Linear correlation of site to site GHI differences in model and corresponding differences in measurements as function of distance. The correlations between measurements and model are done for the models ERA-Interim (grey), MERRA-2 (orange), COSMO-REA6 (red), COSMO-REA6pp (blue), and COSMO-REA2 (green). The correlations are shown as moving averages about ± 25 km. Shaded is the standard deviations of all correlations in the considered moving window (shown for ERA-Interim and COSMO-REA6pp). The magenta line shows the number of correlation values per moving average window.

an even higher resolution improves the representation of small scale clouds even further, we also investigate the performance of the convection-permitting 2 km reanalysis COSMO-REA2 available only for Germany. The comparison (Fig. 3.10) clearly shows that COSMO-REA2 represents the observed GHI variability best for all scales and especially at small scales reaching a correlation of 0.47 at 100 km distance. In summary, both COSMO reanalyses are able to represent spatio-temporal distributions of GHI significantly better than ERA-INTERIM and MERRA-2. Thus, also cloud distributions and the connected atmospheric processes are more realistically represented in the high resolution reanalyses.

3.5.6 Ramp rates

Ramp rates, i.e. the temporal variability of transmissivity, are most important for the solar energy sector. Extreme ramp rates cause fast changes of power production and might be critical for grid stability. Thus, we want to investigate whether ramp rates obtained from COSMO-REA6 and COSMO-REA2 are statistically consistent with the observed ones.

NWP models and reanalyses are known to have deficits in representing clouds at the exact spatio-temporal location. Furthermore, the coarse spatial resolution smoothes the representation

of short term characteristics. Nevertheless, the statistics of the variability should match at least on the temporal scales greater than the effective resolution of the reanalyses. To test the performance of representing ramps, we use the cumulative distribution function (CDF) of transmissivity ramp rates (ΔT). Using CDFs is reasonable, as the ramps do not need to occur at the same spatio-temporal location. Nevertheless, it shows whether ramps are statistically represented with the correct intensity.

The CDFs of ΔT are generated for temporal resolutions (a) 3 h, (b) 1 h, and (c) 30 min (Fig. 3.12). The ramp rates in case (a) are the differences of the 3 h average from 9-12 and 12-15 UTC. In case (b) and (c) the ramp rates are based on the hourly and 30 minute averages of each day in 2007-2013 between 11 and 14 UTC, respectively. Average values from the COSMO reanalyses are approximated by averaging instantaneous values given all 15 min i.e. four instantaneous values represent one hour. In case of MERRA-2 instantaneous values given all 60 min are used to calculate the aimed averaging interval. From Fig. 3.12 it is evident that observed ramps on a three hour scale are best represented by COSMO-REA6pp. ERA-INT, MERRA-2, COSMO-REA6, and COSMO-REA2 underestimate extreme ramp rates, i.e. the most extreme upper 10% of observed ramp rates are underestimated by about 50%. MERRA-2 performs best when comparing with the other original reanalysis products. The CDFs for the higher temporal resolutions show in general the expected reduction of the reanalyses' ability to represent extreme ramp rates (smoothing effect). Considering one hour ramp rates, the regional reanalyses perform better than MERRA-2, indicating a more pronounced smoothing effect for the global product. While the COSMO-REA6pp CDF is still close to the observed one for a time scale of one hour, the ramp rates are underestimated considerably for time scales of 30 min i.e. the upper 10% of observed ramp rates are underestimated by about 1% and 30%, respectively.

3.6 Summary

We present a novel post-processed radiation data set based on the high resolution reanalysis COSMO-REA6 that covers Europe over two decades (1995-2014) with 15 min temporal and 6 km horizontal resolution. A first evaluation of the original reanalysis data set using quality-controlled measurements of the Baseline Surface Radiation Network (BSRN) revealed systematic underestimation under clear sky conditions and overestimation during cloudy conditions. The reasons for these discrepancies originate from the aerosol climatology which causes too strong solar extinction and the underestimation of the optical depth of clouds, respectively.

A post-processing scheme was developed to correct for these systematic deficits in COSMO-REA6. In order to separate clear sky and cloudy conditions a transmissivity threshold of 0.5 is used that has been identified with the help of simultaneous GHI and ceilometer observations. As part of the post-processing, scaling factors were estimated by linear orthogonal distance

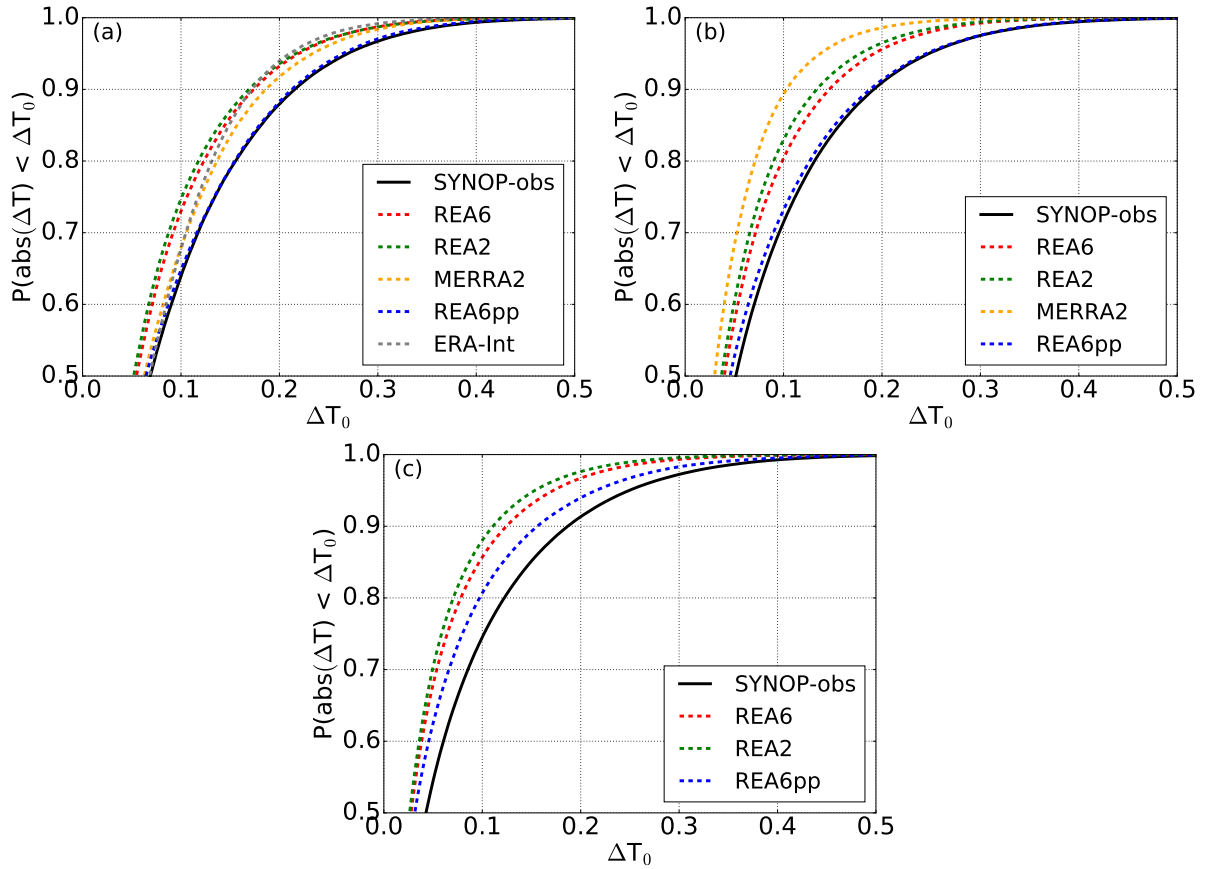


Figure 3.12: Cumulative distribution functions of ramp rates in transmissivity. Ramp rates are shown for (a) 3 hour averages to compare with ERA-INT, (b) 1 hour averages, and (c) 30 min averages.

regressions between COSMO-REA6 and BSRN transmissivities. To account for the annual cycle as well as different solar elevation angles, scaling factors were derived for different seasons and solar angles. An optimized weighting function was determined to ensure a smooth transition between clear and cloudy conditions.

The post-processing coefficients are based on observations at eight BSRN stations fulfilling the highest quality requirements and covering all major European climate zones. While a further improvement of the developed post-processing approach might be achieved by using a larger number of observation sites, we decided to only use the eight BSRN sites which come with high quality standards as recommended by Gueymard and Myers [2009]. The scaling factors are estimated by using a joint data set of all available BSRN sites. Although this procedure reduces the individual site performance in the post-processing, the approach is supposed to minimize local effects and therefore enhances the overall spatial performance of the post-processing. Cross-validation results show the potential of the deduced post-processed data set with a general reduction of systematic biases and a better representation of measured variance for independent

locations. This is also valid for independent verification sites exhibiting strongly deviating climate regimes compared to the measurements in the training data set.

As most other GHI products are available on coarser temporal resolution, the relative performance of COSMO-REA6 is analyzed in terms of daily mean GHI. The novel data set COSMO-REA6pp clearly outperforms the global reanalyses ERA-Interim and MERRA-2 with a lower bias and mean absolute error (MAE), i.e. bias of 1.8 Wm^{-2} and MAE of 16.8 Wm^{-2} . When comparing the performance of COSMO-REA6pp for daily mean GHI with those from other studies, i.e. Posselt et al. [2012], Boilley and Wald [2015], the COSMO-REA6pp performance seems to be superior to most satellite and global reanalysis products with the exception of the SARA satellite data set [Müller et al., 2015]. The highest benefit of COSMO-REA6pp compared to global reanalyses is its ability to resolve smaller cloud systems and therefore better represent the spatio-temporal GHI variability. By using measurements from independent German observation sites a higher correlation for spatial GHI difference compared to ERA-Interim was demonstrated.

A ramp rate analysis was done to show the potential of reanalyses to represent small scale variability. The post-processing improves the representation of GHI changes at different time-scales compared to COSMO-REA6 and outperforms ERA-Interim and MERRA-2. The observed ramp rate statistics are well represented by COSMO-REA6pp up to a temporal resolution of 1 hour. On smaller time-scales the performance decreases and ramp rates are underestimated by all reanalyses.

In summary, we found a superior performance of COSMO-REA6 in representing observed GHI compared to global reanalyses ERA-Interim and MERRA-2. Further, the post-processed product COSMO-REA6pp was found to represent the observed GHI distribution more realistically. In particular, clear sky radiation amounts are improved.

3.7 Conclusion

The new COSMO-REA6pp GHI is recommended for all applications considering absolute values of GHI. In particular, not or only slightly aggregated value investigations (intra-day) will profit from the post-processed GHI, because of the significantly improved clear sky radiation (particularly important for solar energy production studies) and the better representation of GHI ramp rates. However, since many renewable energy studies are using the individual radiation components, direct and diffuse radiation, we will investigate the individual components in one of our next studies.

With respect to renewable energy applications, the regional reanalysis COSMO-REA6 provides not only GHI but also the necessary meteorological parameters, e.g., wind speed at various

heights, temperature, precipitation, in a spatio-temporally consistent fashion covering a time period of 20 years. With the new post-processed radiation fields accounting for the shortcomings in the original COSMO-REA6 radiation representation, the overall data set represents a valuable source of information to scientific, governmental as well as commercial users. COSMO-REA6 as well as the post-processed radiation data is available for download via the COSMO Regional Reanalysis website³.

³<http://reanalysis.meteo.uni-bonn.de>

4 The added value of high resolution regional reanalyses for wind power applications

This chapter is based on: Frank, C. W., S. Wahl, J.D. Keller, B. Pospichal, A. Hense, S. Crewell: The added value of high resolution regional reanalyses for wind power applications, submitted to Renewable Energy, accepted 29. September 2019

Atmospheric reanalyses are the only source of spatial and temporal gridded wind information at wind turbine height providing data over several decades in the past. The application potential of reanalyses in the renewable energy sector depends strongly on the quality of the meteorological quantities. While global reanalyses have a resolution of typically 50 km, new regional reanalyses COSMO-REA6 and COSMO-REA2 have about 6 km and 2 km horizontal grid spacing, respectively. Here, we investigate the added value of the new regional reanalyses for the renewable energy sector, especially their application potential for site assessment. Four well established wind towers in Europe are used as reference for this purpose. We find regional reanalyses performing significantly better or at least similar to global reanalyses. Especially marginal distributions show significant improvements e.g. the most extreme temporal wind changes (ramp rates) at typical hub-heights are underrepresented by global reanalyses between -80 to -43% while COSMO-REA2 represents them with relative errors between -14 to +9%. Considering biases, mean absolute errors, and correlations most significant improvements occur close to ground and in areas with complex terrain. Moreover, vertically extrapolated wind measurements which are commonly used for site assessment show a stronger site dependency in their performance than reanalyses.

4.1 Introduction

Atmospheric reanalyses - best guesses of the atmospheric state in the past derived by combining numerical weather prediction models and observations - become increasingly important in the field of wind and solar energy applications [e.g. Rose and Apt, 2015; Kubik et al., 2013; Cannon et al., 2014; Staffell and Pfenninger, 2016; Pfenninger and Staffell, 2016]. The importance of atmospheric reanalyses in the energy sector is driven by the need of highly resolved long-term information of atmospheric variables on an uniform grid. In this way, area resolved power simulations become possible including all variability scales of the local weather conditions - from short-term (\sim hourly) up to inter-annual variability. These simulations are expected to play a key role to answer many current research questions related to topics such as e.g. (1) spatial compensation potential of power production [Henckes et al., 2018], (2) planning of a sustainable power system, and closely related (3) the dimensioning of necessary storage capacities in a renewable energy dominated electricity grid [Nelson et al., 2012]. These questions are currently only approachable by the use of atmospheric reanalyses, either with global reanalyses, covering the whole Earth with relatively coarse resolution, or with regional reanalyses, covering a part of the globe with finer resolution.

The main advantage of reanalyses is the provision of spatially resolved wind information on any desired height (e.g. hub-height) from hourly up to climatological scales. Therefore, in the renewable energy sector reanalyses are sometimes applied in so-called measure-correlate-predict (MCP) methods where short-term measurements are related to some long-term products (e.g. reanalyses) to estimate climatological wind characteristics at a target site [Carta et al., 2013]. A more general application of reanalyses provided weather data can be found in so-called re-forecasts. Here, reanalysis data are used as input to numerical weather prediction models without data assimilation. With the given reanalysis as reference, re-forecasts are a typical tool for model validation and subsequent improvements, also in terms of renewable energy related variables [Dabernig et al., 2015].

A further advantage of reanalyses in the renewable energy sector is that they provide both wind and solar radiation in a physically consistent way. This is not the case when using different sources (e.g. observations) for the quantities wind and solar radiation. Thus, reanalyses are the only way to make use of the weather dependent spatio-temporal correlations between different types of renewable energy production.

High potential of regional reanalyses lies in the field of wind power site assessment where up to now tower measurements are vertically extrapolated to get local wind information at potential sites. Typical vertical extrapolation as for example evaluated by Gualtieri and Secci [2011] can introduce uncertainties in the derived hub-height wind speed characteristics. Nevertheless, the extrapolated wind speed information is typically used in site assessment. Thus, the resulting

extrapolated wind speed quality represents a benchmark for possible alternative hub-height wind speed sources which might be provided by new high resolution regional reanalyses. Note, for Germany those towers are prescribed to have a minimum height of $2/3$ (e.g. 66 m) of the target height (e.g. 99 m) and need to operate for at least one year [Fördergesellschaft Windenergie und andere Erneuerbare Energien, 2011]. Those measurement requirements are an expensive part of site assessment studies which might be avoided if reanalyses were accurate enough. If so, reanalyses might also solve the problem of the limited measurement periods, as they typically provide climatological information.

Up to now, most applications still use global reanalyses which cover the whole Earth with horizontal resolutions of tens of kilometers. Recently, new high resolution regional reanalyses with much finer horizontal resolutions were developed (COSMO-REA6 [Bollmeyer et al., 2015] and COSMO-REA2 [Wahl et al., 2017] with 6 km and 2 km horizontal resolution, respectively). One of the central questions of this work is to what extent the field of renewable energy can benefit from these new regional reanalyses.

The evaluation of the regional reanalyses COSMO-REA6 concerning hub-height wind speed has up to now only been performed based on long-term averages. Borsche et al. [2016] studied the monthly wind speed variability between 10 and 116 m height from COSMO-REA6 and tower measurements. They showed that COSMO-REA6 mean winds are realistic and at least as close to the measurements as the global reanalyses ERA20C [Poli et al., 2013] and ERA-Interim [Dee et al., 2011]. Considering close to ground wind validation, Kaiser-Weiss et al. [2015] compared the regional reanalyses COSMO-REA6 with global reanalyses and near-surface winds in Germany. They showed that for the majority of stations the Weibull parameters of the daily mean wind speed frequency distribution match well with the ones derived from the reanalyses fields. Furthermore, Camargo et al. [2018] performed a close to ground wind assessment of the two regional reanalyses for the Czech Republic and in close cross-border regions.

However, there is a lack of investigations concerning the advantages of regional reanalyses - also compared to global reanalyses - to represent the actual wind speed at hub-height at hourly resolution. Moreover, to the best of our knowledge, there is no literature accessing new high resolution reanalyses in terms of their site assessment potentials.

The main goal of this study is to provide a comprehensive assessment of the new regional reanalyses COSMO-REA based on tower observations and its competitive performance to global reanalyses. In this way, the study investigates how reanalyses reproduce different wind characteristics relevant for the renewable energy sector. Here, the focus is put on biases, temporal wind speed changes, vertical gradients and low wind persistencies at different heights. The added value of regional reanalyses is worked out by additionally considering global reanalyses in all validation steps. Moreover, in order to judge the application potential of regional reanalyses for site assessment studies, we additionally compare the uncertainty of reanalyses with that of

vertically extrapolated wind measurements. In a last step we investigate how biases and uncertainties of wind simulations propagate through conversion models to the final product of wind power estimates. As reference for validation, measurements of four tall towers (>100 m) located in different environments of central Europe are used.

The structure of this paper is as follows: Section 4.2 describes the reanalyses and observational data sets. Vertical wind extrapolation methods and the applied method to estimate the uncertainties of later results are provided in section 4.3. The main part of section 4.4 provides a comprehensive evaluation of the different products to represent tower measurements up to 280 m, while a last part assesses the reanalyses potential to simulate power production. Section 4.5 concludes with a discussion of the results and relates them to other findings in literature.

4.2 Reanalyses and observations

4.2.1 High resolution regional reanalyses

The two reanalyses COSMO-REA6 (REA6) [Bollmeyer et al., 2015] and COSMO-REA2 (REA2) [Wahl et al., 2017] have been developed within the Climate Monitoring Branch of the Hans-Ertel-Centre for Weather Research⁴. Both, REA6 and REA2 are based on the COntortium for Small-Scale Modelling limited-area model (COSMO 4.25.2 and COSMO 5.00.2, respectively), which is part of the operational Numerical Weather Prediction (NWP) model chain of the German Meteorological Service (DWD). The output frequency of all variables of both reanalyses is 1 hour for 3D variables (e.g. wind profiles) and 15 minutes for 2D variables.

COSMO-REA6 covers the European domain CORDEX EUR-11 [Jacob et al., 2014] with a horizontal resolution of about 6 km and 40 vertical layers. Currently, COSMO-REA6 is available for the period 1995-2017. The production of later periods is ongoing. COSMO-REA2 covers Germany and parts of the neighbouring countries with a horizontal resolution of about 2 km and 50 vertical layers. The reanalysis is currently available from 2007-2013 (which determines the time period for the present study). At the tower sites, where the comparison of reanalyses and measurements is performed, COSMO-REA6 and COSMO-REA2 cover the lowest 350 m above ground with about seven vertical layers (Fig. 4.1).

The boundary conditions for the limited area reanalysis COSMO-REA6 is provided by the global reanalysis ERA-Interim [Dee et al., 2011], COSMO-REA2 is driven by COSMO-REA6. The data assimilation scheme to adjust the model state to the observations is the nudging scheme, which is a stepwise adaptation of prognostic variables towards observed values. An overview of the assimilated wind observations close to the measurement towers will be shown in section 4.2.4.

⁴<https://www.herz-tb4.uni-bonn.de>

The main differences between the two COSMO-reanalyses are (1) the spatial resolution, (2) the explicit resolution of deep convection in COSMO-REA2, and (3) the additional assimilation of weather radar data in COSMO-REA2 [Bollmeyer et al., 2015; Stephan et al., 2008].

4.2.2 Global reanalyses

The Modern-Era Retrospective Analysis for Research and Applications, Version 2 [MERRA-2, Gelaro et al., 2017], is the latest global reanalysis produced by the NASA Global Modeling and Assimilation Office [GMAO, Molod et al., 2015]. MERRA-2 is based on the Goddard Earth Observing System Model, Version 5. Observation assimilation is performed by a three-dimensional variational data assimilation scheme (3DVAR). The MERRA-2 product is available from 1980 to present with a horizontal grid resolution of about $0.5^\circ \times 0.625^\circ$ (latitude x longitude). The vertical wind profiles are available every 3 h. In the lowest 350 m above ground the output is provided at four different heights (Fig. 4.1). When using reanalyses for wind energy related studies MERRA-2 is most commonly used [e.g. Cannon et al., 2014; Kubik et al., 2013]. This qualifies MERRA-2 to be the benchmark reanalysis in the wind energy sector.

ERA-Interim [Dee et al., 2011] is the second global reanalysis used in this study. ERA-Interim provides meteorological fields from 1979 to present. The numerical weather prediction model used to produce ERA-Interim is the Integrated Forecasting System (IFS) of the European Centre for Medium-Range Weather Forecasts (ECMWF) in the operational version of 2006 (IFS release Cy31r2). The horizontal resolution of ERA-Interim is approximately 80 km. The applied data assimilation scheme is a four dimensional variational assimilation scheme. The stored output frequency of 3D variables is 3 hourly whereby the 0, 6, 12, and 18 UTC fields are analyzed and 3, 9, 15, and 21 UTC are forecast fields.

4.2.3 Tower measurements

Tower measurements are the only available in-situ observations at hub-height with high quality and high temporal resolution. However, publicly accessible tower measurements of high quality over long time periods are limited to a very small number of locations. Here, we make use of four well established meteorological towers located in central Europe (joint region of all reanalyses) with maximum measuring heights between 98 m and 280 m. All towers used are onshore, since the added value of regional reanalyses is expected to be more prominent in complex environments. The four towers are located in rather different wind climate conditions. The median wind speed at 100 m above ground varies between 4 ms^{-1} in Karlsruhe and 7 ms^{-1} in Cabauw (see Fig. 4.2).

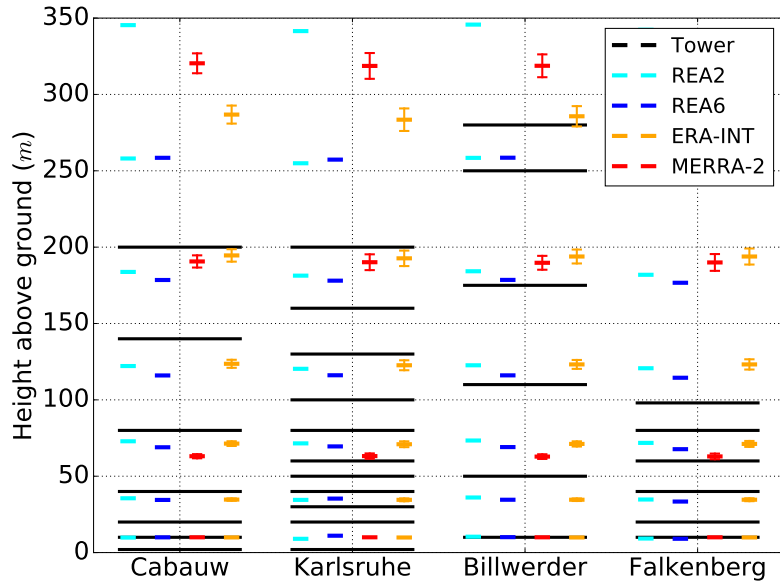


Figure 4.1: Vertical levels of reanalyses products and wind measurements at the different tower sites. Measurement heights are depicted as black horizontal lines. Model height levels are drawn as short lines. ERA-Interim and MERRA-2 levels are shown with standard deviations, since their model level heights depend on pressure.

The Cabauw tower is part of the Cabauw Experimental site for atmospheric research (CESAR) observatory located in the western part of the Netherlands in flat grass land [Van Ulden and Wieringa, 1996]. The weather tower Hamburg is the observation site of the University of Hamburg and the Max-Planck-Institute for Meteorology [Brümmer et al., 2012]. The tower is located in a surrounding of agricultural fields, close to flat suburban buildings, and to industry in the west. The Lindenberg tower is operated by the Meteorological Observatory Lindenberg (Richard Aßmann Observatory) of the DWD in a region of grass, fields and forest (in the surrounding area of <10 km) [Beyrich and Adam, 2007]. The fourth tower operated by the Karlsruhe Institute for Technologie (KIT) is located directly within a 40 m high forest [Kohler et al., 2018]. For the measurements in Lindenberg, Cabauw, and Hamburg comprehensive quality control was performed by Petrik et al. [2019]. The quality control applied to measurements in Karlsruhe is described in Kohler et al. [2018].

Each site provides wind speed and direction at individual heights and for individual time periods. At all sites cup-anemometers are installed to measure the wind speed. For our study 10 minute averages are taken. We only use time steps for which measurements are available at all measurement heights. For reasons of temporal matching we use a frequency of 3 hours which is the output interval of the global reanalyses. The general data availability per site in the evaluation period 2007-2013 is 5-7 years. An overview on data availability of the towers and site specific characteristics is given in Tab. 4.1 and figure 4.1. Note, that for Hamburg measurements at 280 m are less frequent (7266 data points \sim 2.5 years), since measurements at that level only

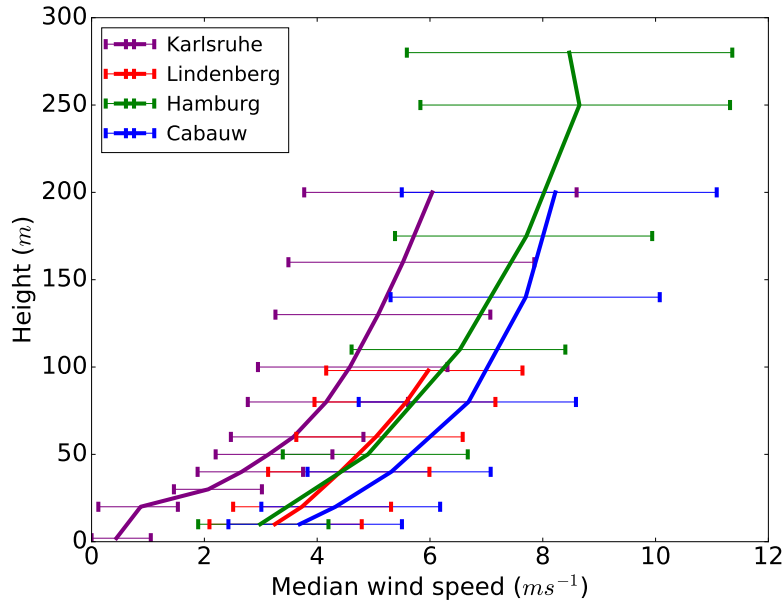


Figure 4.2: Measured wind speed at the different tower locations and heights. Shown are the 25, 50, and 75th percentiles.

Table 4.1: Meteorological tower locations and number of considered data points (time steps). Only time steps with measurements on all tower heights available are considered. The evaluation time span in total is 7 years from 2007-2013. Beside the number of data, the year equivalent indicates the data availability in terms of years.

Tower	Latitude	Longitude	Height a.s.l (m)	# Data	Year equivalent
Cabauw, Netherlands	51.970	4.926	-0.7	20455	7.0
Hamburg, Germany	53.519	10.103	0.3	15366	5.3
Karlsruhe, Germany	49.093	8.426	110.4	18465	6.3
Lindenberg, Germany	52.166	14.122	73	19914	6.8

started in 2010. To avoid disturbances by the tower itself the lowest measurements are often performed at small separate towers. The 10 and 20 m measurements in Cabauw for example are performed on two separate small towers in the north and the south of the main tower. In Karlsruhe and Hamburg towers in a distance of 50 m (outside the forest) and 30 m, respectively, are used to measure close to ground variables.

For a later classification of the data into different stability regimes, additional measurements of temperature and global radiation are used (see Sec. 4.3).

4.2.4 Assimilated observations

To guarantee a fair comparison between the different reanalyses it is important to know if wind measurements from the reference towers or any other wind related observations close to the

Table 4.2: Assimilated wind observations close to the reference towers in Cabauw, Hamburg, Karlruhe, and Lindenberg. The abbreviation REA denotes both, COSMO-REA6 and COSMO-REA2.

Reanalysis	Site name	Instrument/Product	Location	Temporal frequency
All	Cabauw	Wind profiler above ~ 500 m	300 m south	Hourly or 30 min
All	Lindenberg	Wind profiler above ~ 500 m	5 km	Hourly or 30 min
MERRA-2, ERA-Int	All	Satellite derived cloud motion vectors	-	-
MERRA-2, REA	Lindenberg	10 m wind	5 km	-
MERRA-2, REA	Hamburg	10 m wind	~ 10 km	-
MERRA-2, REA	Cabauw	10 m wind	20 km, De Bilt	-
All	Lindenberg	Radiosonde	5 km	4/day at 0,6... UTC
All	Cabauw	Radiosonde	20 km, De Bilt	1/day at 0 UTC

towers were used in the assimilation process. If specific observations are assimilated into one, but not another reanalysis, a different performance is expected. Generally, none of the tower measurements themselves were assimilated into any of the reanalyses.

However, since most of the towers are located close to meteorological observatories, other data were used for assimilation. An overview of assimilated wind observations close to the tower sites is given in Tab. 4.2. In Cabauw and in Lindenberg wind profiler observations in heights above about 500 m are assimilated. Thus, although the assimilation height is larger than the maximum tower measurement height it should be taken care when interpreting the performance of the reanalyses at those sites, since reanalyses data are spatially coupled. Moreover, at those two sites, Cabauw and Lindenberg, also radiosonde measurements are assimilated which is not the case at the other sites. Thus, at this sites the tower measurements are expected to be more accurate represented by the reanalyses products. Although the minimum distance between towers and the next 10 m wind measurement is 5 km, it is worth mention that only ERA-Interim does not assimilate 10 m wind at all. Thus, one could expect that all other reanalyses perform a bit better in representing the tower measurements.

4.3 Methods

4.3.1 Matching of model and measurements

All reanalyses have different vertical grids (Fig. 4.1). In order to compare the wind speed from reanalyses with tower measurements a linear interpolation from model levels to the tower heights (Fig. 4.1) is applied. In cases of nonlinear vertical profiles this approach induces errors whose magnitude depends on the specific wind profile and the vertical resolution of the model. Since

the vertical model resolution close to ground is relatively high (between 30 and 80 m for REA2, REA6, and ERA-Interim and between 50 and 150 m for MERRA-2, see Fig. 4.1) this issue is ignored here.

The horizontal matching of gridded reanalyses data with point measurements is done by the nearest neighbour approach. On the temporal scale, the different data products are analysed every 3 h, determined by the output interval of the global reanalyses. In contrast to reanalyses which provide domain representative values, tower measurements are point values. The matching of spatially representative values with point values is not exactly possible, but the differences can be reduced by temporal averaging of the point values under consideration of meteorological processes and associated scales. Considering a typical horizontal wind speed of $U = 10 \text{ ms}^{-1}$ in a $L = 6 \text{ km}$ grid box it would need $T = L/U = 600 \text{ s}$ to cross the whole spatial length of the grid box [Stull, 1988a]. Thus, the 10 min averages of point measurements compare best with instantaneous values of a reanalysis with 6 km horizontal grid spacing. This seems to be an advantage for the regional reanalyses because global reanalyses are not expected to resolve phenomena close to the 6 km scale. Nevertheless, many renewable energy applications benefit from higher resolution.

4.3.2 Uncertainty estimates

When comparing statistical parameters, such as median or RMSE, a confidence level is calculated. The confidence intervals are derived by the use of the Block-Jackknife method [Kaigh, 1983]. Similar to the Bootstrap method, the Jackknife method is a resampling technique to estimate confidence intervals of a statistical parameter $\theta(x)$ derived from one sample x with unknown underlying distribution (non-parametric estimator) [von Storch and Zwiers, 2003]. The confidence intervals of the arbitrary statistical parameter θ are estimated based on the statistical parameter distribution $F(\theta(x^*))$ derived from n_J sub-samples (x^*) from x . It has been found that the distribution constructed by the n_J values $\theta(x^*)$ reasonably represents the sampling distribution of $\theta(x)$ [Kaigh, 1983].

The difference of the Bootstrap and the Jackknife methods is the technique of sub-sampling. While in the Bootstrap approach the sub-samples are chosen by random sampling with replacement, Jackknifing is based on the leave-one-out idea [Efron and Tibshirani, 1994]. For a sample x consisting of independent and identically distributed entries the bootstrap method was found to work well. For the case of correlated data (entries of sample x are not independently distributed) the Jackknife sampling method is preferable. By leaving-one-out the sub-samples remain in the correct temporal order. Since temporal correlations often last longer than one time step the leaving-one-out method does not result in independent sub-samples. To solve that problem we apply the Block-Jackknifing where temporal blocks are skipped in each sub-sample.

Applying the Block-Jackknifing to temporally correlated data, in our case the time-series of wind speed, we still need to consider the remaining problem of temporally correlated entries within each sub-sample. This problem leads to an underestimation of variance in the individual sub-samples (caused by the violation of the independency assumption). In accordance to von Storch and Zwiers [2003] this issue can be statistically corrected by the use of the equivalent sample size n_e

$$n_e = n/D \quad (4.1)$$

with n the length of the sample and D the variance inflation factor, also known as decorrelation length, which is the time between effectively independent sample-entries. The decorrelation length D is defined as

$$D = 1 + 2 \sum_{k=1}^{n-1} (1 - k/n) r_k \quad (4.2)$$

with r_k being estimates of the autocorrelation of wind speed at lags k .

The central argument for non-parametric methods as Jackknifing can be found in the mathematical expression of the variance of estimators [von Storch and Zwiers, 2003] which is defined as

$$Var(\theta) = \frac{1}{n} \sigma(\theta)^2 \quad (4.3)$$

with θ the statistical parameter to be estimated and its variance σ . As stated above the statistical parameter θ is reasonably represented by the distribution of $\theta(x^*)$. Thus, the left site of equation 4.3 can be substituted by e.g. the median minus the 5th percentile of $\theta(x^*)$ for the left hand uncertainty and the 95th percentile minus the median of $\theta(x^*)$ for the right hand uncertainty. Thus, the confidence interval is estimated by the calculation of a left hand and right hand $\sigma_{l,r}$ calculated with

$$\sigma_{l,r}(\theta) = (Var(\theta)_{l,r} n_e)^{0.5}. \quad (4.4)$$

Decorrelation lengths used in this study are derived by applying eq. 4.2 for each tower wind time-series individually. Using measurements between 50 m and 280 m we found the derived decorrelation length just slightly varying with height ($\pm 2 - 14\%$). Thus, for simplicity we use one averaged decorrelation length per site. This simplification leads to an underestimation of the uncertainty intervals close to the ground and to an overestimation in the highest heights with errors up to 7%. The estimated decorrelation lengths are 4, 3, 2.5, and 3 days for Cabauw, Karlsruhe, Hamburg, and Lindenberg, respectively. The block length used in the Block-Jackknife procedure is set to 5 days. For each sub-sample (in total 200) the number of blocks ignored is determined by the condition to retain 95% of the original data in each sub-sample.

4.3.3 Vertical extrapolation of measurements

Practical and financial reasons motivate measurements on rather small towers which need subsequent vertical extrapolation to estimate hub-height wind speed. In order to extrapolate measured wind speed to hub-height sundry mathematical expressions exist. Among these are the logarithmic law, log-linear law (also known as Monin-Obukhov relation) and the power law [Irwin, 1979; Stull, 1988b].

As the logarithmic laws are "difficult to use for engineering studies" [Bañuelos-Ruedas et al., 2010], the more simple power law is widely used. Although being the only method without physical basis [Gualtieri and Secci, 2011], it seems to give a better fit to most of the data over a greater height range and for higher wind conditions [Hadi, 2015]. The general power law may be written as:

$$v_2 = v_1 \left(\frac{z_2}{z_1} \right)^\alpha \quad (4.5)$$

with v_1 and v_2 being the wind speed in measuring height z_1 and target height z_2 , respectively. The power law exponent α is known as Hellmann (or friction) exponent. It is found to be a function of atmospheric stability, wind speed, surface features (roughness length), and the extrapolation height interval [e.g. Irwin, 1979; Gualtieri and Secci, 2011]. For practical use lookup tables of α as function of terrain type were collected e.g. by Masters [2004]. The values vary between 0.4 in urban areas with high buildings and 0.1 over smooth ground or water. Further studies reveal a high diurnal variability changing from less than 1/7 (~ 0.14) during daytime to more than 1/5 (~ 0.2) at night over the same terrain [Spera, 1994]. The Hellmann exponent α can also be directly determined if measurements of v_1 and v_2 are available:

$$\alpha = \frac{\ln v_2 - \ln v_1}{\ln z_2 - \ln z_1} \quad (4.6)$$

The high variability of α led to the development of various methods to estimate an appropriate exponent based on surface measurements. Gualtieri and Secci [2011] performed a comprehensive evaluation of some of the most commonly used methods to extrapolate 10 m wind to 50 m wind at one location close to the coastline and one industrial location in Southern Italy. They compared the logarithmic approaches with four different power law approaches (meaning 4 different approaches to estimate the exponent α). They found the power law approach of Smedman-Högström and Högström [1978] (PL_SH) performing best compared to all other methods. Here, we chose three different methods for α with increasing level of complexity:

PL_const: This approach assumes a constant value for the Hellmann exponent. According to the international standards for wind turbine design provided by the International Electrotech-

nical Commission (IEC) the constant Hellmann exponent α is set to 0.2 [IEC, 2005].

PL_2L: This two level measurement based extrapolation method uses a temporal adapted Hellmann exponent. Using wind measurements at two height levels in eq. 4.6 the Hellmann exponent is estimated for each time step and subsequently applied to extrapolate to higher levels.

PL_SH: The Smedman-Högström and Högström [1978] approach estimates the Hellmann exponent by the use of an empirical relation using both surface roughness and atmospheric stability. The relation was derived from wind measurements from three 100 m masts in Southern Sweden:

$$\alpha = c_0 + c_1 \log(z_0) + c_2 [\log(z_0)]^2 \quad (4.7)$$

where coefficients c_0 , c_1 and c_2 are stability dependent coefficients as defined by Smedman-Högström and Högström [1978] and z_0 is the roughness length. In order to find appropriate coefficients c_0 , c_1 and c_2 we estimate the Pasquill-Gifford stability category for each time step by applying the short wave radiation and temperature gradient (SRDT) method [EPA, 1994; Bowen et al., 1983]. Similar as [Mohan and Siddiqui, 1998], we chose a slight modification of the proposed SRDT method by adding an extra category beyond the most stable Pasquill-Gifford class. This additional class corresponds to a stable nighttime situation with wind speeds lower than 0.5 ms^{-1} (the adopted categorization scheme can be found in the supplementary material in Tab. 4.4).

4.3.3.1 Wind extrapolation set-up

The vertical wind speed extrapolation methods (Sec. 4.3.3) are based on wind speed measurements at reference height(s) and additional information to specify atmospheric stability. In general, the reference height used is 10 m. Only in Karlsruhe a height of 40 m is used, as this tower is located in a forest with an approximately height of 40 m.

In case of the PL_2L extrapolation a second reference height is necessary to estimate the Hellmann exponent. This second height is in general set to 40 m motivated by the standard height of tilt-up towers [Lubitz, 2006]. For Hamburg the second height is set to 50 m because in 40 m no measurements are available. For Karlsruhe the 60 m measurements are chosen as second height, as it is the height of large tilt-up towers.

For the PL_SH extrapolation method the roughness length is used to consider local surface conditions. We roughly estimated the roughness length according to pictures and the suggestions of the WMO guide to 0.1 except for Karlsruhe with 0.25 [WMO, 2008, Chap. I.5-13]. For an overview of these set-up parameters see Tab. 4.3.

Table 4.3: Reference heights (h_1 and h_2) and roughness lengths (z_0) used for the different vertical extrapolation methods per site.

Site	h_1 (m)	h_2 (m)	z_0 (m)
Cabauw	10	40	0.1
Karlsruhe	40	60	0.25
Hamburg	10	50	0.1
Lindenberg	10	40	0.1

4.4 Results

This section addresses the central questions (1) if regional reanalyses perform better in representing measured wind speed compared to global reanalyses and (2) whether reanalyses are advantageous in representing the wind speed on hub-height compared to extrapolated wind speed (both based on 10 m extrapolations for PL_const and PL_SH and measurements from two different heights for PL_2L, respectively). The quality of different reanalyses and extrapolation methods, together called products later on, is assessed by ranking.

The section is structured in three parts: Firstly, the marginal distributions (time-independent statistics) are compared in order to assess whether the products are able to represent realistic frequency distributions of typical wind metrics on hub-height. Secondly, the joint distributions are compared in order to assess the temporal and spatial representation of measurements and products, combined. The third part provides an outlook on the performance of the products after conversion into theoretical power yields.

4.4.1 Marginal distributions

Marginal distributions provide the frequency occurrence of a quantity by ignoring temporal similarity of the different data products. In the context of site assessment for wind power plants marginal distributions are of particular importance, since they provide the information of wind speed frequency distribution at a site.

4.4.1.1 Wind speed

The realistic representation of absolute wind speed values is vital for wind assessment studies. A relative frequency histogram (Fig. 4.3) shows the capability of the different data products to match the general occurrence of specific wind speed values. Due to the height dependence of the wind speed the marginal distributions are shown on different height levels. For a quantitative comparison of the distribution differences the Earth Mover's Distance [EMD, Rabin et al., 2008] is calculated. The EMD score describes the number of values which need to be rearranged

to match the measured distribution perfectly and is given in percent. The smaller the EMD the better the agreement. The uncertainty estimates of the EMD scores are the 5th and 95th percentiles derived by Block-Jackknifing (see Sec. 4.3.2).

In general, the reanalyses distributions follow the measured ones better in higher levels where local conditions become less important (Fig. 4.3). As reanalyses products represent grid cells they are per definition not able to resolve and represent sub-grid influences to the wind field. An evident feature is the overestimation of wind speed by MERRA-2 which was also found for 10 m wind in the UK, especially for high wind speeds above 20 ms^{-1} [Cannon et al., 2014].

The extrapolation methods PL_const and PL_SH tend to underestimate the broadening of the wind speed distribution with height at all considered measurement sites. Thus, a systematic underestimation of wind speed occurs with increasing extrapolation height. The extrapolation method PL_2L represents the measured distributions better than the other two methods but overestimates wind speed significantly in Karlsruhe. This overestimation in Karlsruhe is likely to be caused by the influence of the surrounding forest.

In order to rank the performance of different products to represent the measured frequency histogram Fig. 4.3 is complemented by the quantitative EMD scores. COSMO-REA6 performs most often significantly better in representing the measured distribution. Only in Hamburg at 175 and 280 m height, ERA-Interim performs better. Here, the REA6 distribution is slightly too broad with a slight shift to higher wind speed values. Thus, the wind speed seems to be overestimated by REA6 (in accordance with bias scores derived later in section 4.4.2.1). Furthermore, the EMD ranking shows REA2 being frequently ranked between the two global reanalyses which might be caused by the slight shift of the REA2 distribution towards higher wind speeds. In general, regional reanalyses outperform the global ones as demonstrated with their persistent occurrence among the first three ranks when comparing just the four reanalysis products.

Comparing the reanalyses with extrapolations, only PL_2L which requires a second wind speed measurement is able to represent the measured wind speed distributions for all heights with similar quality like the reanalyses. With the exception of Karlsruhe where the PL_2L method shows deficits.

4.4.1.2 Temporal wind speed changes

Wind speed changes per time interval, often called ramp rates, cause wind power generation change. Since supply and demand in a power system always have to be balanced, weather-induced generation changes cause compensation costs, i.e. flexible power plants need to be turned on/off or electricity storage is needed [Graabak and Korpås, 2016]. As ramp rates are

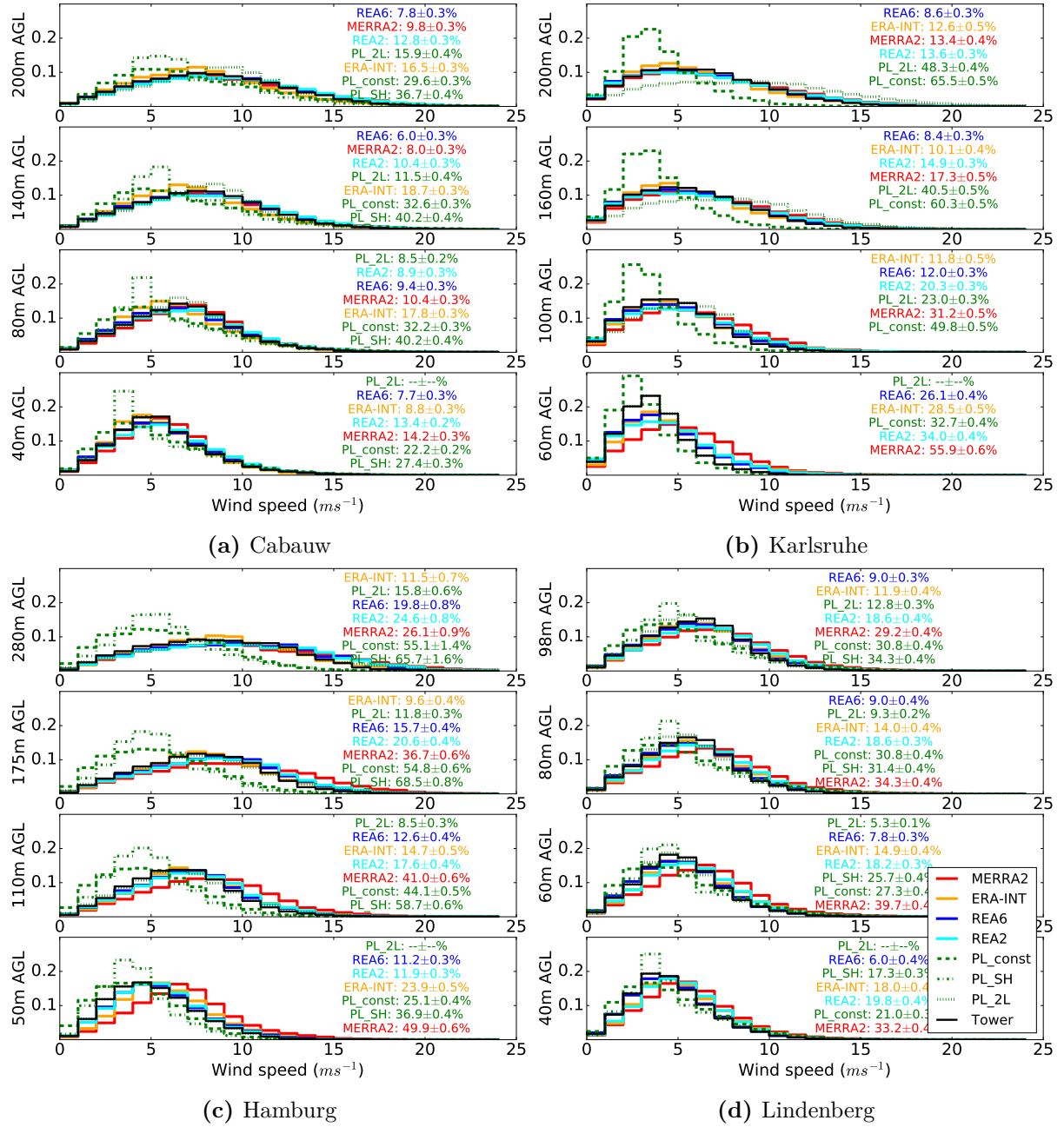


Figure 4.3: Marginal distribution of wind speed at different tower heights from measurements, extrapolation methods and reanalyses. The EMD scores, quantifying the distribution difference relative to the measured distribution, are ranked with best performance listed first (Best score: EMD = 0%). Reanalyses data are vertically linearly interpolated to the tower levels. The number of considered data per tower is shown in Tab. 4.1.

the driving process for balancing efforts it is important to know their statistical characteristics as accurately as possible.

In order to quantify the ability of the different products to represent the ramp rates, their marginal distributions are shown relative to the measured ramp rates (Fig. 4.4). The global reanalyses systematically underestimate the occurrence of more intense ramp rates and overestimate that of weak ramp rates. These problems are significantly reduced in the regional reanalyses as their marginal distributions are much closer to the measured ones. The slightly different result close to ground in Karlsruhe is probably caused by the general overestimation of the wind speed in the reanalyses at this location causing probably more intense ramp rates.

Considering the most extreme measured ramp rates (lowest 5% + highest 5%) at levels above 98 m, global reanalyses underrepresent these extremes by -80 to -43%. The regional reanalyses COSMO-REA6 and COSMO-REA2 show significant improved extreme ramp rate representation with relative errors between -28 to +2%, and between -14 and +9%, respectively.

The performance of the vertical extrapolation methods varies strongly with site, height and the method applied. Only the PL_2L method performs more robust with a strong overestimation of extreme ramp rates for all heights and sites except for Hamburg at 10 m above reference height.

4.4.1.3 Vertical wind speed gradients

The vertical wind speed gradient is important when considering shear stress on wind-blades [Fernandez et al., 2018]. In order to investigate which reanalyses accurately represent vertical gradients on typical hub-heights, the frequency distribution of wind speed differences from one tower level to the next are investigated (Fig. 4.5). As already used in Fig. 4.3, the EMD is used to get a quantitative measure for the difference of the distributions. According to the EMD score the regional reanalyses perform about twice better than the global reanalyses in representing the distributions of vertical wind gradients. With more narrow distributions global reanalyses and especially the vertical extrapolation methods underestimate the occurrence of high wind speed gradients. This effect is significantly reduced in the regional reanalyses.

Applying the analysis for different thermal stability conditions we found that the improvement in the regional reanalyses is caused by a better representation of vertical wind speed gradients especially during stable atmospheric conditions (not shown). For all well-mixed and neutral conditions regional and global reanalyses perform more or less similarly.

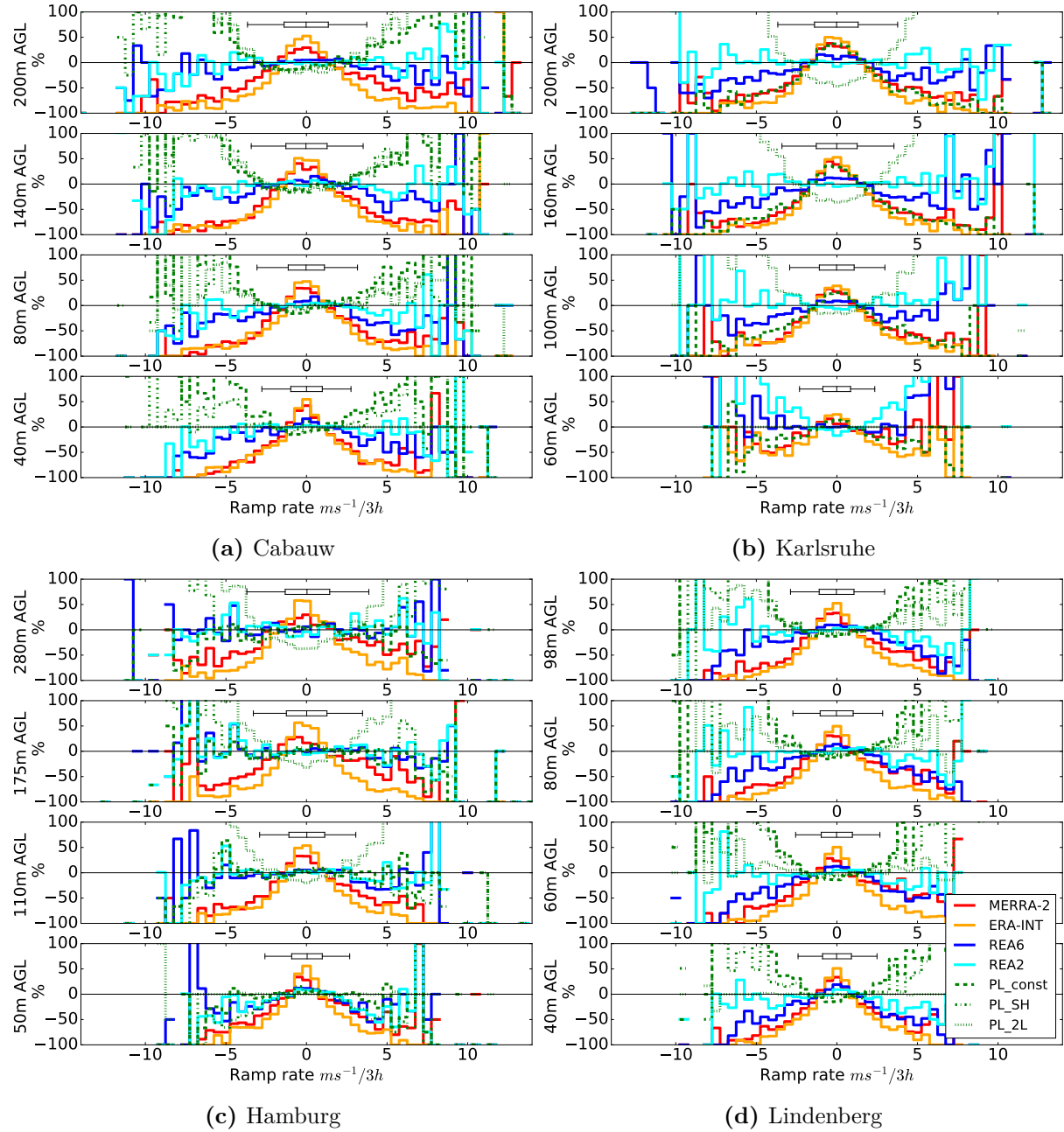


Figure 4.4: Relative deviation of ramp rate occurrence from reanalyses and extrapolation methods with respect to tower measurements for different tower heights. The reference distribution is derived from the 10 min tower measurements considered every 3 hours. Ramp rates of the reanalyses are based on the instantaneous wind speed values every 3 hours. The horizontal box plots show the 5, 25, 50, 75, 95th percentiles of the reference distributions. The number of considered data per tower is given in Tab. 4.1.

4.4.1.4 Low wind persistence

Statistics of weak wind situations and especially persistent low wind situations are of great importance for the energy sector, as electricity production shortages can occur during these times. Thus, persistent situations should be represented as accurately as possible.

In our study (Fig. 4.6) the weak wind persistence is determined by the number of successive time steps with a wind speed below 3.5 ms^{-1} . The considered time steps are 3 hourly, as it is the resolution of the global reanalyses. In order to get similar results in model and measurements only the 10 min averages of the measurements around the considered 3 hourly interval are used to determine the measured persistence. In case of the reanalyses the instantaneous 3 hourly values are checked if they meet the low wind criteria (lower than 3.5 ms^{-1}).

The longest persistencies of weak wind situations (up to 21 hours) occur in Karlsruhe which is in accordance with the general weaker wind speed at this location compared to the other sites (see also Fig. 4.2).

The relative error of persistent low wind events derived from reanalyses varies in general between -80% and +80%. In most cases, especially in the lower heights, MERRA-2 underestimates the number of persistent low wind events, which is consistent with the general overestimation of the wind speed by MERRA-2 (see bias in Fig. 4.7). Although MERRA-2 also shows positive wind speed biases at the higher tower levels this does not necessarily lead to underestimations of low wind persistence at these levels. This is in accordance with the marginal distributions of MERRA-2 which show an increasing agreement with the measurements with increasing height. At the upper tower levels the regional reanalyses show typically a slight underestimation of the 3 h persistence turning to overestimation for longer persistence.

The relative error of persistent low wind events derived from extrapolated wind speed varies strongly. While relative errors from reanalyses typically remain below 80%, the relative errors of extrapolated wind speed often exceed this value. Thus, reanalyses clearly outperform the extrapolation methods in representing the number of persistent low wind events.

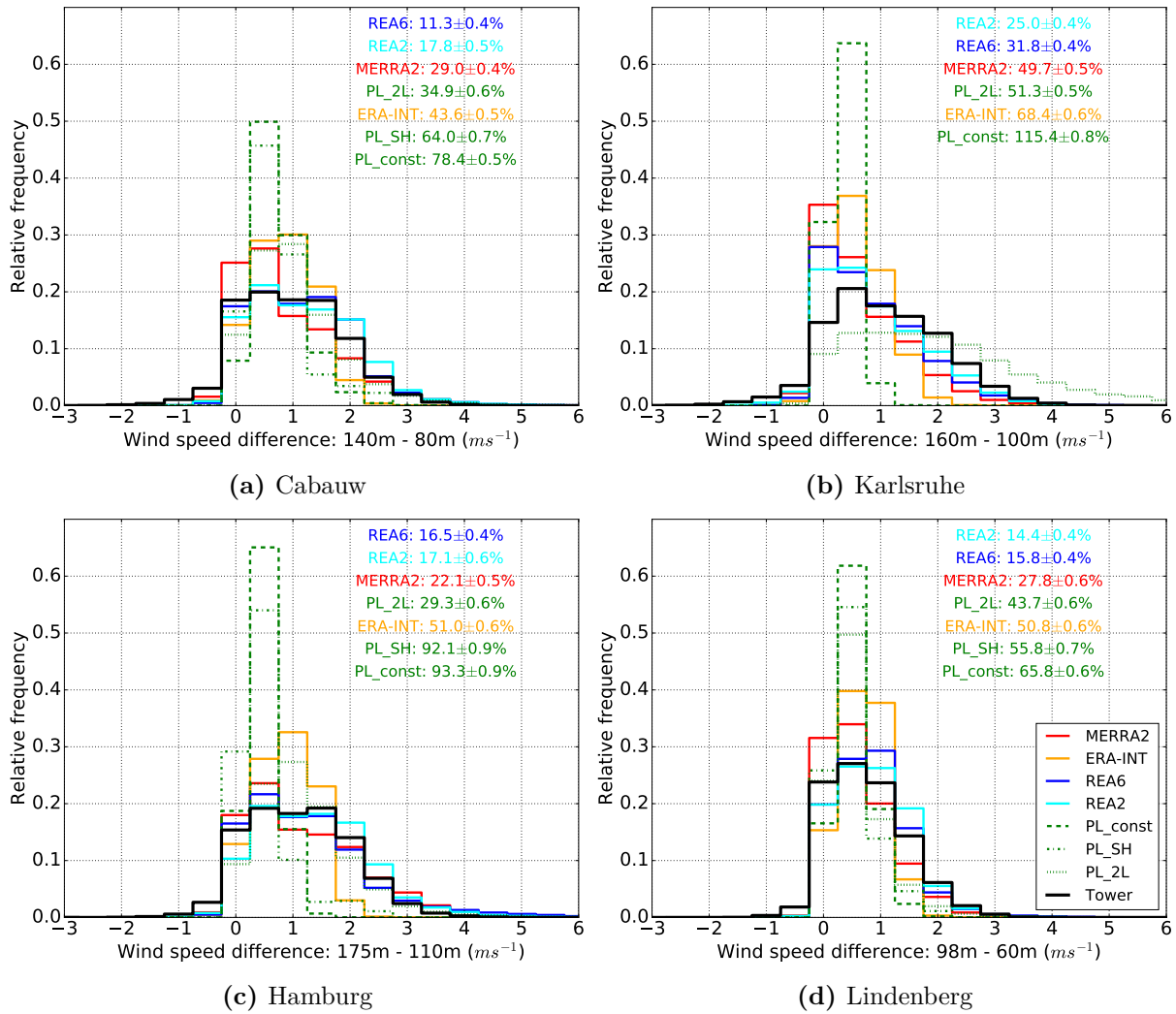


Figure 4.5: Vertical wind speed gradient between site specific measurement heights from measurements, extrapolation methods and reanalyses. The EMD scores, quantifying the distribution difference relative to the measured distribution, are ranked with best performance listed first (Best score: EMD = 0%).

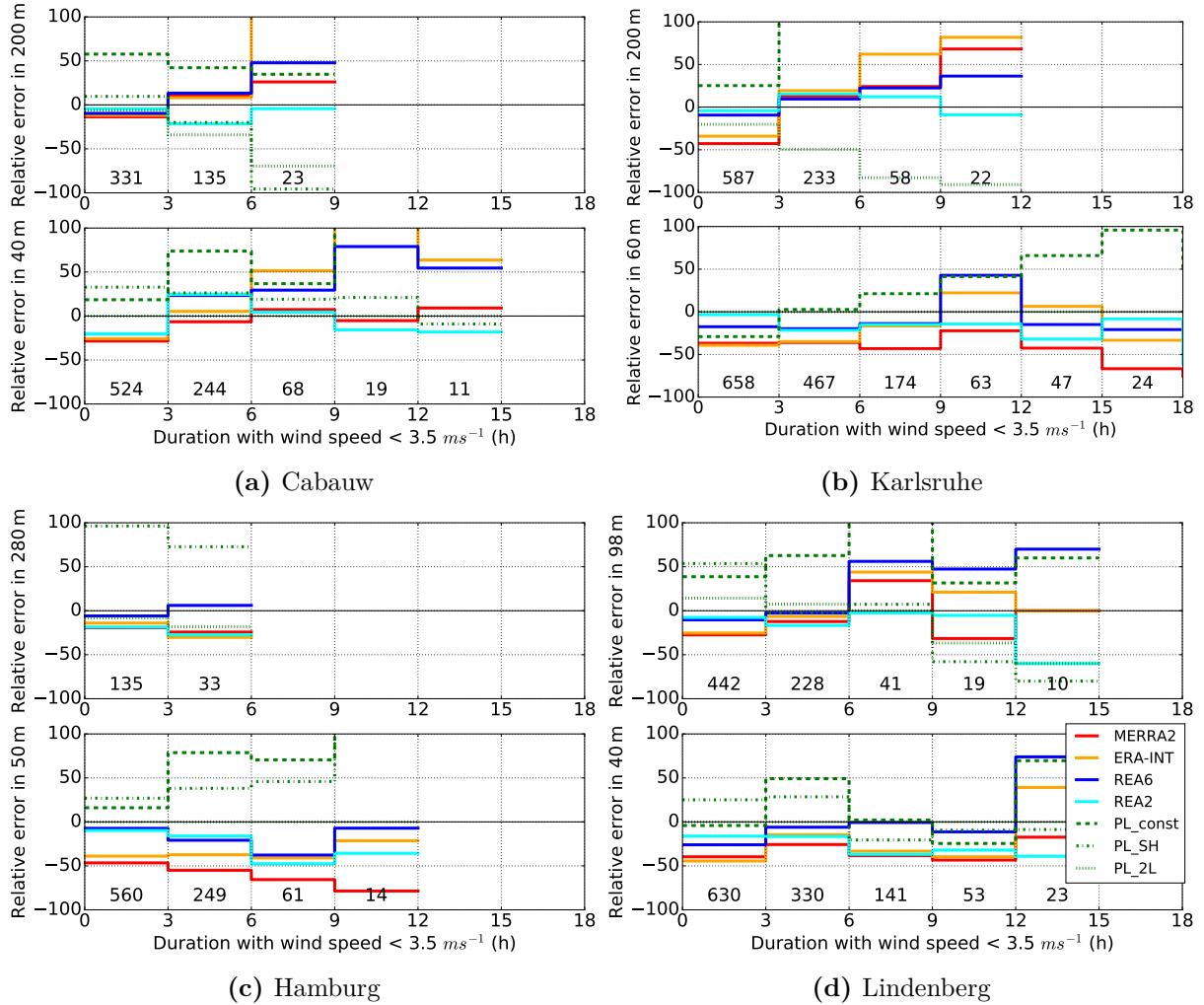


Figure 4.6: Relative error of low wind persistence at different heights between reanalyses, extrapolation methods and tower measurements. The numbers provide the total occurrence of measured persistencies per class (3 hourly binned classes). The lines show the relative error of the different products in representing the measured number per class. Direct site-to-site comparisons are not possible since the number of measurements varies with site (Tab. 4.1).

4.4.2 Joint distributions

In order to assess the ability of wind products to represent measurements in space and time, joint distributions scores, such as bias, mean absolute errors (MAE) and correlations are analyzed. Related to site assessment studies, these joint distributions are important, since MCP methods often rely on them [Carta et al., 2013].

4.4.2.1 Bias and bias corrected MAE

Regional reanalyses turn out to be the best products for representing the local wind speed by looking at profiles of wind speed bias and mean absolute error (Fig. 4.7). While the bias shows systematic under- or overestimation of the different products, the bias corrected mean absolute error (BC_MAE) depicts whether the products vary coherently in phase and amplitude with the measurements. Comparing the reanalyses products in terms of bias and BC_MAE, most values are lowest for the regional reanalyses, especially for REA6. The only exception can be found at Hamburg where the bias of ERA-Interim is lowest with less than 0.5 ms^{-1} in heights above 150 m.

Largest bias values occur close to the ground in Karlsruhe. The domain averaging reanalysis products are not able to represent the strong influence of the local forests. Thus, all reanalyses overestimate the wind speed at this location. Especially at sites like Karlsruhe, where local small-scale conditions predominate the wind characteristics, regional reanalyses are expected to outperform the global ones. This improvement is confirmed by significantly reduced bias as well as BC_MAE scores in the regional reanalyses (e.g. in 40 m height the bias reduced from $1.5 \pm 0.3 \text{ ms}^{-1}$ to about 1 ms^{-1}).

PL_const and PL_SH are based on 10 m wind measurements. Evidently, their performance decreases with increasing extrapolation height. The height of equal performance of the extrapolated wind speed and the reanalyses is 50-100 m above reference height. Above that height the reanalyses perform better. Except for Karlsruhe, the PL_2L MAE is comparable to that of the reanalyses in a height of about 100 m above reference height which is roughly 2-3 times the upper measurement height. PL_2L seems to be more dependent on local conditions compared to the other extrapolation methods (best performance in flat regions).

4.4.2.2 Correlations

The correlation shows the ability of the different products to follow measured temporal tendencies. The wind speed correlation of the different products with the towers are in general quite similar from one to the other tower location (Fig. 4.8). As expected the correlation increases

slightly with height for the reanalyses, as local effects decrease with height and large scale processes become the driving factor. In contrast, the correlation of the extrapolation methods decreases with increasing distance to the measurement height.

Among the reanalyses COSMO-REA6 and COSMO-REA2 generally outperform the global reanalyses. Significant improvement can be found in Karlsruhe where the spatial resolution becomes more important in order to represent the inhomogeneous local conditions. The correlation of extrapolated wind speed and reanalyses wind speed become similar in a height range between 80 to 150 m above the measurement height. The exact height depends on the tower location, the reanalyses, and on the used extrapolation method. One main exception can be found for Karlsruhe, where the PL_2L extrapolation method leads to drastically decreasing correlation scores with height. Here, reanalyses outperform the extrapolations in just a few meters above reference height. Similar to the bias also the correlation score indicates the PL_2L extrapolation method to be the one most dependent on local conditions.

4.4.2.3 Stability dependent validation

The vertical wind speed profile strongly depends on the thermal stability of the atmosphere. Thus, the performance of the different extrapolation methods and reanalyses are studied under different atmospheric stability conditions. The thermal conditions are determined by the use of temperature differences between top of the tower (except Hamburg where we chose 175 m) and 10 m (except Karlsruhe with 30 m). Cases with temperature decrease with height of more than 1 K per 100 m are assigned to unstable conditions. A gradient of less than 0.5 K per 100 m is classified as stable. The representation of the different stability conditions by COSMO-REA6 was validated in detail by Petrik et al. [2019].

Both, reanalyses and extrapolation methods perform better under unstable conditions, especially above 50 m (see Fig. 4.9 and for all sites Fig. 4.11 in the annex chapter 4.7). This behaviour is also found considering diurnal cycle investigations where stable conditions mostly prevail during night and unstable conditions during daytime (not shown here). The weaker performance during stable conditions is closely connected to more intense vertical wind speed gradients (often caused by thermal inversions) which increase extrapolation uncertainties Gualtieri and Secci [2011].

Comparing the different reanalyses in terms of the bias we found for both stability conditions that the regional reanalyses have a smaller or equal bias than the global reanalyses. Thus, the largest bias values can always be found in global reanalyses.

Considering the BC_MAE under stable conditions we found similar or better performance of regional reanalyses compared to global reanalyses for all sites. However, a significant improvement can only be seen in Karlsruhe. Although we find the same for COSMO-REA6 under unstable conditions this is not the case for COSMO-REA2. At two of the four sites the COSMO-REA2

BC_MAE scores are similar or significantly better than that of the global reanalyses, but at the other two locations we find significant degradation compared to the global reanalyses and COSMO-REA6.

Considering the extrapolation methods under stable conditions the quality decreases rapidly with height. All sites show that when extrapolating wind characteristics based on 10 m measurements, reanalyses outperform the extrapolated ones in heights above 70 m. Using two measurement levels for extrapolations, reanalyses outperform the extrapolated wind in heights above 3 times the upper measurement level.

Under unstable conditions it is always one of the extrapolation methods that produces the best wind speed estimates at all height levels. But considering the MAE (combining the effects of bias and BC_MAE) at least one of the extrapolation methods produces worse estimates as the reanalyses in heights above 80 m above ground. The method which performs worse is different from site-to-site. Thus, we can not find the one extrapolation method being superior to all reanalyses for all sites. Again we can note that reanalyses perform less site dependent.

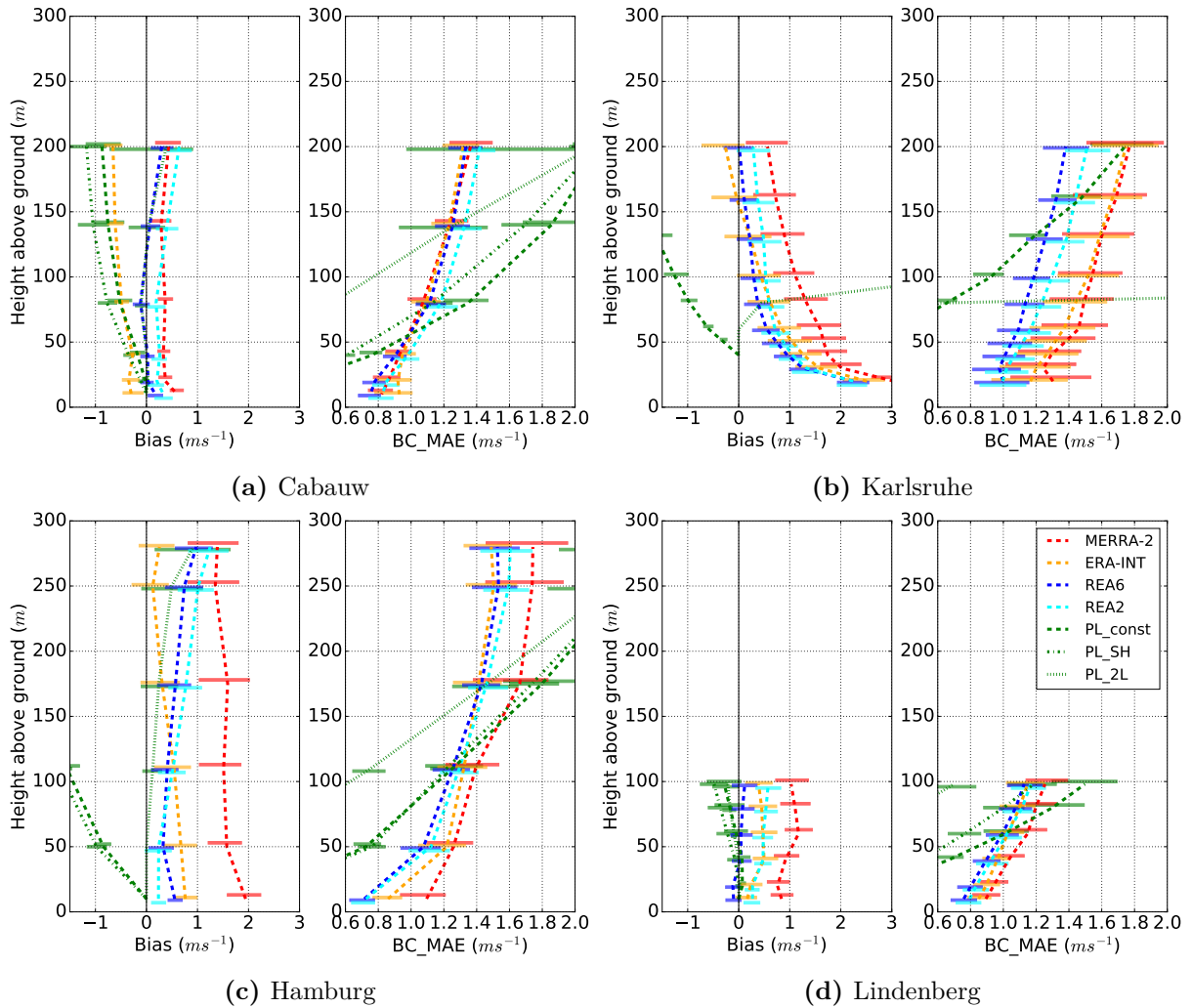


Figure 4.7: Bias and bias corrected mean absolute error (BC_MAE) profiles of instantaneous wind speed from reanalyses and extrapolation methods compared to 10 min averaged tower measurements. The vertical matching is done by linear interpolation of all products to the tower heights. The number of considered data per tower can be seen in Tab. 4.1.

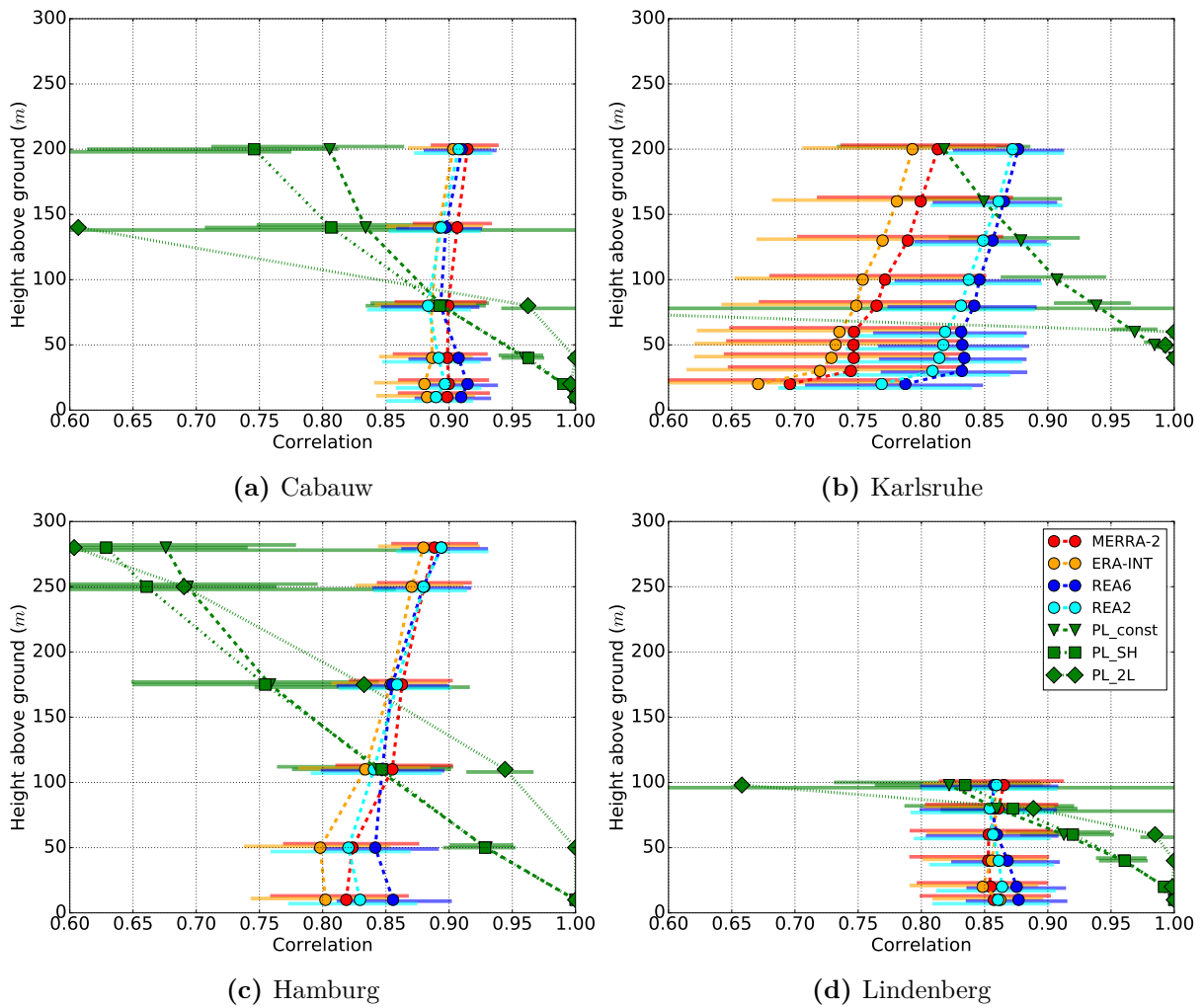


Figure 4.8: Pearson correlations between tower measurements and reanalyses as well as extrapolation methods, based on 3 hourly values. 10 min averaged measurements are used as reference. The number of considered data per tower can be seen in Tab. 4.1.

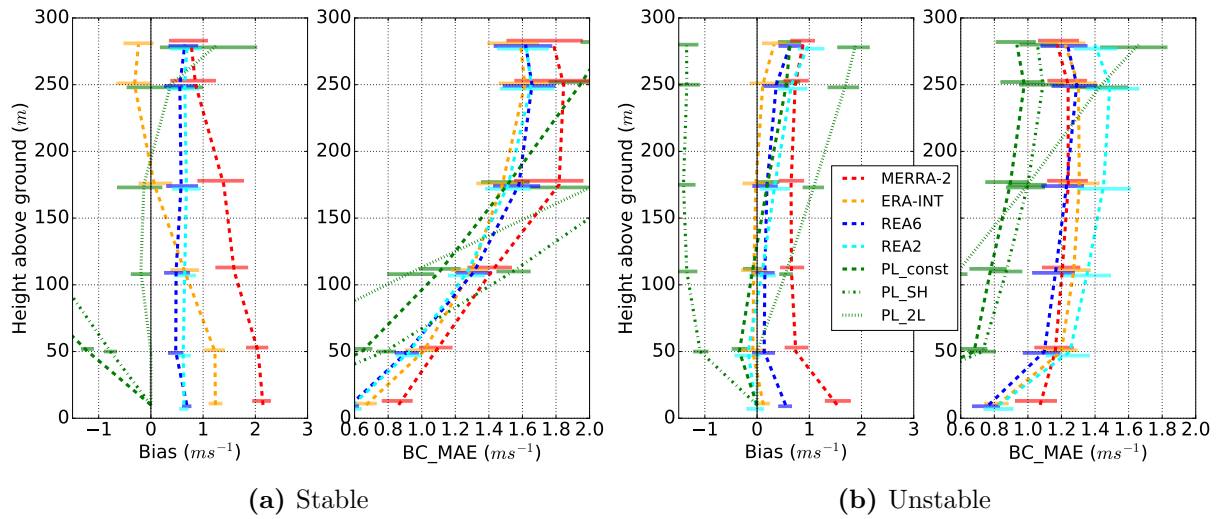


Figure 4.9: Bias and bias corrected mean absolute errors (BC_MAE) under stable (4.9a) and unstable (4.9b) thermal conditions for the example site Hamburg. The scores are based on 3 hourly values from reanalyses and extrapolation methods. 10 min averaged tower measurements considered every third hour are used as reference.

4.4.3 Accumulated relative power estimates

The ultimate product of interest from a practical point of view is the power yield of an installed wind power plant. Thus, a central question is if the products are able to represent realistic power estimates of theoretical wind turbines. In this study, we investigate the accumulated power generation of the considered seven years and compare the different reanalyses and extrapolation methods with measurement based power estimates.

The power generation estimates E_{out} are calculated by the use of turbine characteristics of a 2.5 MW wind turbine from General Electric (General Electric 2010⁵). The turbine does not generate electricity below cut-in velocity (3.0 ms^{-1}) and above the cut-out wind velocity (25 ms^{-1}). Between the cut-in and the rated wind speed (about 12.5 ms^{-1}) the estimated power is proportional to the wind speed:

$$E_{out} = \frac{1}{2} c_p \rho \pi R^2 v^3 \quad (4.8)$$

with a constant power coefficient c_p of 0.35 and a rotor diameter of 100 m. The air density is assumed to be a constant standard value of 1.225 kg m^{-3} . The maximum power production is constant between rated wind speed and cut-out wind speed.

In order to estimate comparable power estimates derived from measurements and reanalyses, only the 3 hourly values (10 min averages in case of measurements and instantaneous values in case of reanalyses) which are available for all products are used to derive the total power generation per site. The number of considered time steps is shown in Tab. 4.1.

The comparison of reanalyses based power estimates with those derived from tower measurements shows an overestimation by reanalyses of 10-50% for most heights and sites (Fig. 4.10). The only underestimations were found with REA6 in Lindenberg and ERA-Interim in Cabauw. While the relative errors of the regional reanalyses in 100 m AGL are usually lower than 25% the global reanalyses reach values of about 60%. Closely connected, we find the performance of the power estimates derived from regional reanalyses to be less variable from site-to-site than those derived from global reanalyses.

The performance of extrapolation methods varies strongly with site, method and height. The estimates based on the extrapolation methods PL_const and PL_SH lead after about 50 m extrapolation height to comparable uncertainties with the reanalyses products. Above that height reanalyses perform better than extrapolation based estimates of the power generation. In contrast, the PL_2L method provides for all sites (but Karlsruhe) and heights better or comparable power estimates compared to reanalyses.

⁵<https://wind-turbine.com/windkraftanlagen/9813/ge-2-5-100.html>

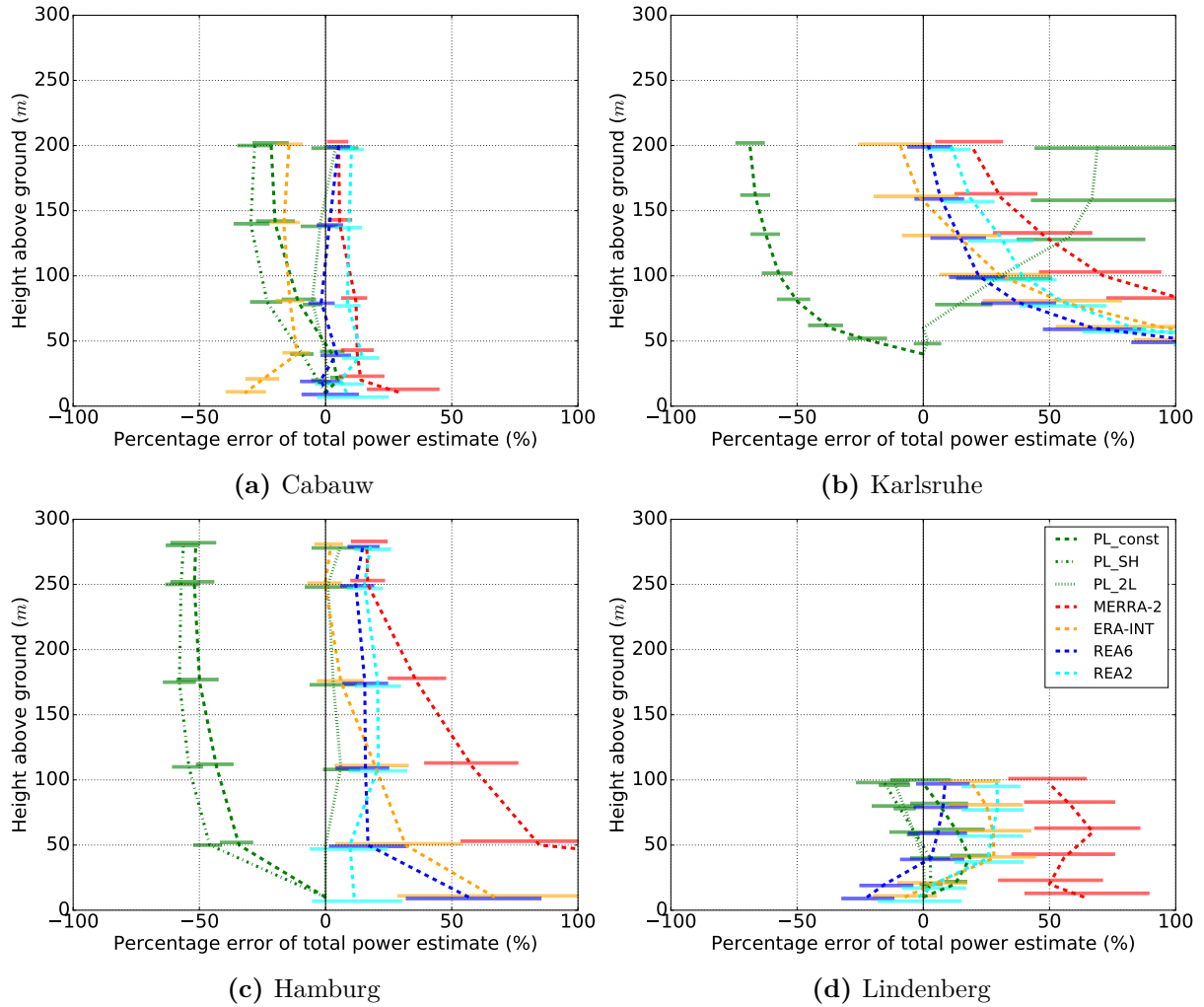


Figure 4.10: Mean relative error of estimated power generation from reanalyses and extrapolated wind products. The reference power estimates are derived from tower measurements (2007-2013). The number of considered data per tower can be seen in Tab. 4.1.

Considering the uncertainty estimates (derived by Jackknifing, see Sec. 4.3.2) of the power generation estimates we find increasing uncertainties with height for the estimates based on extrapolated wind speed and decreasing uncertainties with height for estimates based on reanalyses. The decrease with height in case of reanalyses based estimates might be a result of the non-linear conversion to power generation. While wind speeds above rated-velocity yield to a constant full power generation the low wind speed values (between cut-in and rated velocity) are expected to introduce more uncertainty to the estimates. Thus, the uncertainties close to ground appear higher as shown in Fig. 4.10. In contrast, in case of the extrapolation based estimates the general uncertainty increases with height. For instance, BC_MAE of the wind speed seems to dominate the compensating non-linearity effect of the power curve.

4.5 Discussion

We found that regional reanalyses often outperform global reanalyses in terms of their quality to represent measured wind speed. Especially marginal distributions of wind speed metrics are found to be significantly improved (see 4.4.1). Joint validation metrics e.g. the bias corrected mean absolute error revealed the added value of regional reanalyses predominantly in more complex terrains and close to ground, as expected. Nevertheless, in a few cases some metrics at specific heights and sites also show global reanalyses performing significantly better (e.g. the ERA-Interim bias above 250 m in Hamburg, Fig. 4.7c). This is not unexpected since the results can be influenced by coincidentally better guesses of the local conditions by the coarser resolution than by the finer which depends strongly on the exact location of the measurement. Moreover, joint distribution scores are sometimes degraded by finer resolutions caused by spatiotemporal mismatching combined with increased variance representation in the finer resolved models [Gilleland et al., 2009]. Nevertheless, most metrics show regional reanalyses outperforming the global reanalyses ERA-Interim and MERRA-2, which is consistent with the findings of Borsche et al. [2016] and Kaiser-Weiss et al. [2015] who investigated reanalysis performance on aggregated scales and/or close to ground.

Comparing two regional reanalyses the results imply COSMO-REA6 being slightly better in representing the real wind speed compared to COSMO-REA2 in terms of bias and mean absolute errors. A similar result is found by Steinke et al. [2019] who could not find an added value of the higher resolved COSMO-REA2 compared to COSMO-REA6 in terms of the integrated water vapor. These unexpected results might be explained by the slightly different underlying NWP models of the two regional reanalyses. One reason for model differences is e.g. an applied optimization of COSMO-REA2 with respect to precipitation [Wahl et al., 2017]. Thus, other model variables might be slightly degraded (e.g. the quality of wind speed) leading to compensation of the expected added value by increasing the resolution. Nevertheless, the temporal ramp rate study and vertical wind speed gradient study show better statistical representation of variability scores by COSMO-REA2 (see Fig. 4.4 and 4.5).

The comparison of reanalyses with vertically extrapolated wind observations revealed more realistic wind representation by extrapolation methods close to reference height and degradation with increasing height. The height where reanalyses and extrapolations perform similarly varies with site, method, and stability. Nevertheless, the height of equal performance is found in roughly 50-100 m above reference height if extrapolations are based on one level (see e.g. Figs. 4.7 and 4.8). For the two level based extrapolation method PL_2L the results show that the level of similar performance is slightly higher than 100 m above reference height (2-3 times the upper measurement height) but the method seems to be even more site-dependent than the other extrapolation methods.

In contrast to the general statement of Gualtieri and Secci [2011] who found the PL_SH to be the best extrapolation method (tested for two sites), we could not identify a single method which systematically outperforms the other approaches (see e.g. Fig. 4.7, 4.11).

Kubik et al. [2013] already showed that the global reanalysis MERRA provides comparable power estimates in 60 m height when comparing to power estimates based on vertically extrapolated 10 m measurements. Since Kubik et al. [2013] used the PL_const method with a calibration eliminating systematic errors, their derived results for Northern Ireland can be compared to our PL_const bias corrected MAE score in Fig. 4.7. For two of our sites, Cabauw and Lindenberg, we find exactly the same height (60 m) where reanalyses and extrapolation become more or less equal realistic. For Hamburg and Karlsruhe this height is slightly higher in about 100 m above reference height. Finding the reasons for the different heights of common quality is a difficult task, since many parameters influence the performance of the reanalyses and extrapolation methods as e.g. the different climatologies and different representation of stable, neutral and mixed situations etc.

Comparing the site-to-site performance of reanalyses and vertical extrapolation products we found extrapolated wind profiles to be more variable. Thus, reanalyses represent the real wind profiles spatially more robust than extrapolation methods, e.g. the bias corrected mean absolute error in 100 m of the regional reanalyses varies for all sites between 1.1 and 1.25 ms⁻¹ while the extrapolations varies between 0.6 and 1.5 ms⁻¹.

The extrapolation methods as well as the reanalyses show better performance under unstable conditions. In these situations, for each investigated site at least one extrapolation method outperforms the reanalyses products, but the best method varies from site-to-site significantly and the least performing extrapolation method (also more or less random from site-to-site) is typically outperformed by the reanalyses in heights above 50 m above reference height. Again, reanalyses and in particular the regional reanalyses come up with more site independent representativity scores.

4.6 Conclusion

The high resolution regional reanalyses COSMO-REA6 and COSMO-REA2 are evaluated in the context of wind energy applications to quantify their added value compared to established global reanalyses. Using in-situ tower measurements as reference, the reanalyses are also compared to extrapolated wind profiles based on small tower measurements (up to 60 m) which are commonly used as reference for site assessment studies.

Using wind measurements at four tall towers (up to 280 m) regional reanalyses are proven to better represent the measured wind speed or at least perform equally well (depending on the consid-

ered validation metric and site) compared to the global reanalyses ERA-Interim and MERRA-2. Especially close to ground wind speed is better represented by the regional reanalyses due to the enhanced horizontal resolution and better representation of land-surface interaction and orographic effects.

In particular the variability scores, namely for vertical wind gradients and temporal wind speed changes (ramp rates), are shown to be significantly improved in regional reanalyses. For example, global reanalyses underrepresent the extreme ramp rates (upper 10% in heights above 98 m) by up to 80%, while COSMO-REA2 represents them by $\pm 14\%$ (Fig. 4.4).

In economics, reanalyses are sometimes used in combination with short-term tower measurements in order to estimate climatological wind characteristics at a specific site [MCP methods, Carta et al., 2013]. For this task we highly recommend to move from the global reanalyses to the regional reanalyses especially due to their improved representation of marginal distributions (see Sec 4.4.1) which is particularly important when investigating occurrences of specific events as for example low wind situations or ramp rates. For this purpose, COSMO-REA6 already provides 23 years for whole Europe on a 6 km grid and is continuously extended in time.

However, the new regional reanalyses are still not accurate enough to completely replace costly tower measurements for site assessment studies. Instead of reaching the extrapolation accuracy in heights of $3/2$ above the measurement height (minimum prescribed height by site assessment guidelines in Germany) reanalyses perform only equally or better in heights of roughly 2-3 times above the upper reference height, at least for three out of four considered towers.

At this point we would like to remind the reader that all results are based on the finite number of considered validation metrics and on just four tower sites in central Europe. The site-to-site variability already indicates the local dependency which can reduce the general validity of results. For the future we recommend to use a larger number of reference towers to get more robust results. The collection of uniform tower measurements within e.g. the INDECIS project of the European Research Area for Climate Services (ERA4CS) will provide opportunities for validation across a wider geographical region and with more towers.

Despite the uncertainties and shortcomings discussed above, the regional reanalyses COSMO-REA6 and COSMO-REA2 have demonstrated their improved skill to estimate wind energy compared to commonly used global reanalyses. Together with the post-processed radiation by Frank et al. [2018], COSMO-REA6 provides a solid data foundation of hybrid wind-solar assessments in terms of country-based smoothing and compensation potentials on a European scale.

4.7 Annex

Table 4.4: Insolation-based key to Pasquill-Gifford stability categories. The reference wind speed (v_{10}) is the average wind speed, measured at 10 m above ground level.

Daytime					Nighttime		
	Global radiation (Wm^{-2})					2-10m ΔT ($^{\circ}Cm^{-1}$)	
v_{10} (ms^{-1})	≥ 925	925-675	675-175	< 175	v_{10} (ms^{-1})	< 0	≥ 0
< 2	A	A	B	D	< 0.5	E	G
2-3	A	B	C	D	0.5-2.0	E	F
3-5	B	B	C	D	2.0-2.5	D	E
5-6	C	C	D	D	≥ 2.5	D	D
≥ 6	C	D	D	D			

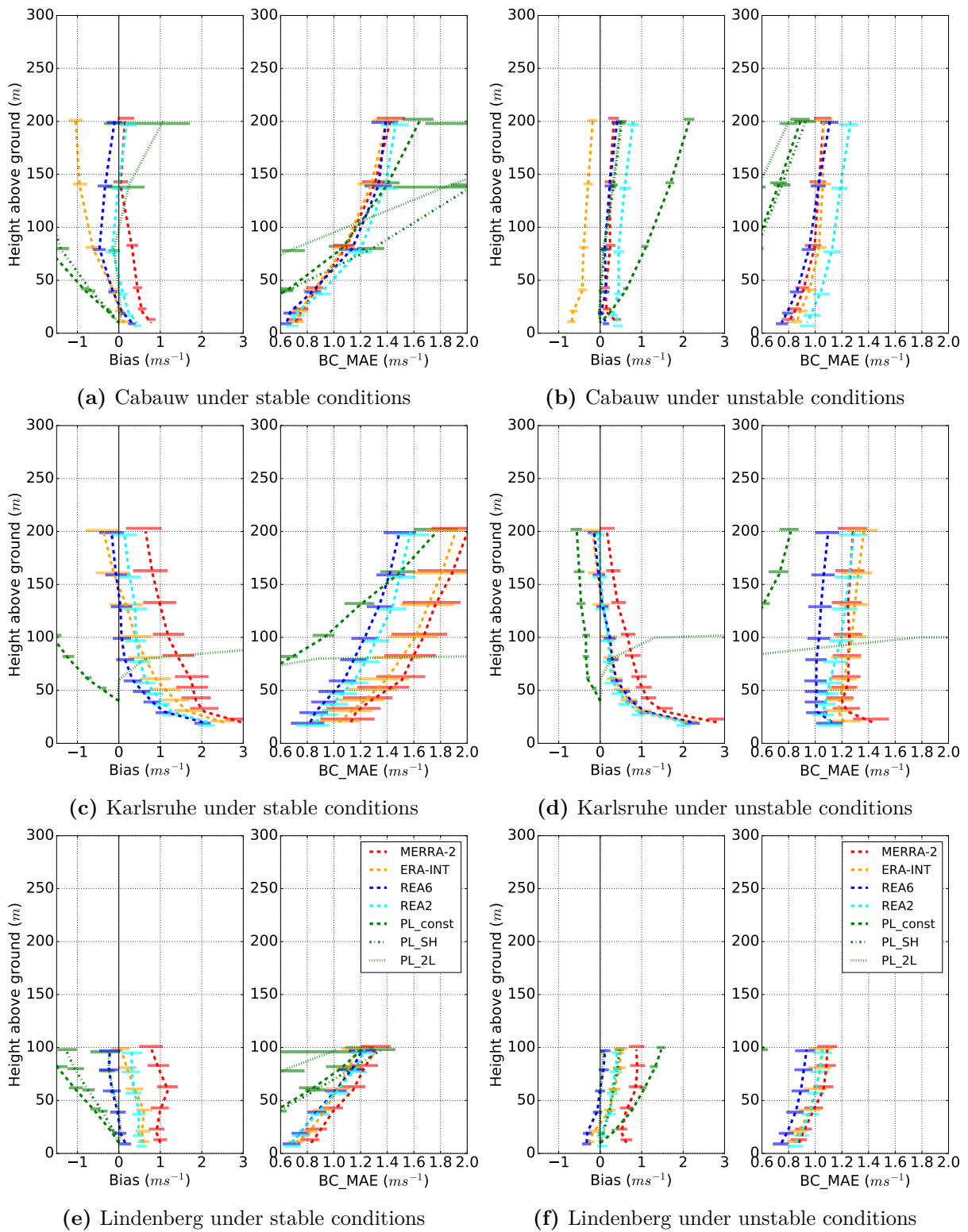


Figure 4.11: Bias and bias corrected mean absolute error (BC_MAE) of the different products under stable (left) and unstable (right) thermal conditions.

5 Hybrid wind-solar balancing effects: An European study using post-processed regional reanalysis

The increasing share of variable renewable energies requires the need for balancing interventions. One option to reduce the costly interventions is to exploit the natural decorrelations of wind and radiation. This study focuses on the characterisation of natural balancing potentials by either considering (1) optimized hybrid wind-solar installation ratios or (2) spatial compensation effects on an European scale. Therefore, multi-decadal and highly resolved meteorological data from the regional reanalysis COSMO-REA6 are used. In order to reduce systematic biases in the radiation components of COSMO-REA6, a post-processing is applied and its added value for derived photovoltaic (PV) estimates shown. Based on these post-processed and original COSMO-REA6 data power time-series for 12 European countries covering 20 years with daily resolution are generated. In order to consider only weather induced power variabilities only one constant power fleet distribution for wind and PV is used. Further, an additional scaling of the installed capacities to optimize the balancing effects of wind and PV is performed. The results show variability reduction potentials due to decorrelations between wind and PV power varying between 29% and 42%. The corresponding installation ratios for this optimized scenario are found to vary from country to country between 58% (42%) and 68% (32%) for solar (wind) energy. A further study to analyze cross-border balancing potentials shows the probability of occurrence for simultaneous extremes of PV in the one and wind in the other country being with 10% rather low. Thus, there is a high potential of cross-technology balancing of wind and PV between all European countries.

5.1 Introduction

The IPCC special report "*Global warming of 1.5°C*" scientifically substantiates the connection between man-made greenhouse gases and climate change [Allen et al., 2018]. The report states: "Ambitious mitigation actions are indispensable to limit warming". An essential step is the reduction of greenhouse gas emissions. CO_2 is found to be the most prominent greenhouse gas contributing to anthropogenic global warming. With a share of approx. 45% of total CO_2 emissions, the energy industry is the largest emitter of CO_2 , at least in Germany [UBA, 2018]. An ongoing approach to reduce greenhouse gas emissions is the transition from fossil based energy sources to non-fossil renewable ones.

While conventional power plants are steerable, important renewable energy sources, i.e. wind and solar radiation, vary naturally in time and space. Thus, adding renewable energy to the

electricity grid leads to increasing variability in the electricity production. Consequently, the physical electricity grid constraint of balanced energy production and demand can only be ensured with fast steerable conventional power plants or with some kind of storage. With today's technology, variations are balanced by 80% with conventional fossil based power [Bundesnetzagentur, 2018]. Without new types of storage, if production variability increases due to higher renewable power production more installed conventional reserve capacity is needed. With the aim to reduce necessary conventional power plants, production variability of renewable energy should be kept as low as possible.

In addition to the climate-related motivation, there are also economic reasons for keeping the variability of renewable energy feed-in as low as possible. In order to ensure grid stability, steerable power plants have to be powered up or run down, causing so called redispatch costs. For example, redispatch costs in Germany increased from 133 to 392 million Euro from 2013 to 2017 [Bundesnetzagentur, 2014, 2018]. In this respect also curtailment costs, indemnity costs for curtailed renewable power plants in order to secure grid stability, were reported to increase from 43.7 to 610 million Euro. A further economical problem is that renewable power plants have very low marginal (running) costs, leading to situations with low or even negative electricity prices. Thus, profitability for conventional flexible technologies will probably reduce [Graabak and Korpås, 2016] leading to in less installed capacities for balancing in the long run. With less flexible installations available for situations of low renewable energy generation other balancing options need to be considered (for an overview see Graabak and Korpås [2016]).

This study focuses on options to reduce the generation variability by renewables themselves. Given the spatial and temporal variability of wind and solar power, two types of natural balancing are possible: (1) Spatial compensation due to power production at different sites and (2) hybrid wind-solar balancing due to not perfect correlated (decorrelated) wind and radiation characteristics. Both balancing effects were already discussed in various publications.

Spatial compensation potentials have mainly been studied for the individual sources either PV or wind. In case of PV e.g. Perez and Fthenakis [2015] analyzed large-scale compensation potentials of distributed PV power plants by analyzing pair-decorrelation distances in terms of daily clearness indices. Their main finding is the more pronounced north-south balancing potential compared to east-west balancing. For short-term variations on the order of seconds to minutes Perez et al. [2012] found indications that the distance of decorrelation of two sites is a quasi linear function of the considered temporal variation scale. In the field of spatial compensations of wind power e.g. Henckes et al. [2018] investigated the compensation potential for European countries using a 20 year simulation with a focus on Germany. Here, several European countries are found to be particularly suited to compensate German low wind situations. Grams et al. [2017] investigated the relation of balancing potentials with general weather regimes in Europe. Caused by weather regimes they found for Scandinavia, Iberia and the Balkans a high potential for enhanced wind electricity generation during low wind extremes in the North Sea.

In the field of hybrid wind-solar balancing potentials most studies are concerned with future scenarios in order to find an optimal energy mix and best investment strategies [e.g. Child et al., 2019; Heide et al., 2010; Henckes et al., 2019; Vasilj et al., 2016]. Due to uncertainties of the applied future scenarios as well as computational limits of the meteorological input, these kind of investigations are often strongly simplified (see e.g. Pfenninger [2017]). Moreover with the focus on optimal investments in the whole energy system and not on the subtopic of renewable energy balancing potentials results concerned with this subtopic are typically rarely or subject to great uncertainty.

Only a few studies in the literature directly focus on the investigation of hybrid wind-solar balancing potentials but all of them focus on individual countries only or on Europe as a whole [Kaspar et al., 2019; Heide et al., 2010; Roques et al., 2010; Bett and Thornton, 2016; Zhang et al., 2018]. Since potential studies need to simulate the theoretical power at specific sites or areas on climatological scales (several decades) most of these studies have in common to use reanalyses products, at least for the wind power estimates. The advantage of reanalyses - being a synthesis of weather observations with a recent numerical weather prediction (NWP) model - is that they provide the best guess of historical spatial and temporal gridded weather information. Thus, power simulations at all potential sites become possible. On European scale, Heide et al. [2010] investigates optimal ratios of wind and PV installations including electricity storage devices under consideration of electricity demand curves. By focusing on a high-renewable scenario their main findings are that even with optimal ratios of installed wind and PV power large amounts of storage are necessary to meet the demand and that the derived optimal relationships strongly depend on the considered temporal variability (hourly or daily). With combined high resolution regional reanalysis and satellite observations Kaspar et al. [2019] investigate the reduction of low generation extremes when increasing the aggregation area (e.g. Europe compared to Germany). The main finding is the distinct reduction of the number of low production events when aggregating to larger areas or when switching from only one source (wind or solar) to hybrid generation. However, all these studies have been conducted for either individual countries or Europe as a whole.

Thus, to the authors best knowledge a study concerning a comprehensive balancing potential study of wind and PV power for as many European countries as possible based on one consistent meteorological data set is missing. Also Graabak and Korpås [2016] who wrote a comprehensive review on the state of the art knowledge of balancing effects in Europe concluded that "there are indications about possibilities for considerable reductions in variability" but up to know studies concerned with natural balancing potentials in Europe are limited. Thus, the study on hand aims to shed light on this topic by investigating balancing potentials between wind and PV power within and across European countries when adding PV production to wind production only.

For the simulation of PV and wind power the high resolution regional reanalysis COSMO-REA6 is used. With a horizontal resolution of 6 km, COSMO-REA6 [Bollmeyer et al., 2015] is currently the highest resolved regional reanalysis of the European domain providing all necessary meteorological input variables for renewable power estimates of the last 23 years (1995-2017). A variety of publications show COSMO-REA6 outperforming alternative coarser resolved global reanalyses as ERA-Interim, HIRLAM, and MERRA [Frank et al., 2019; Henckes et al., 2018; Frank et al., 2018; Steinke et al., 2019]. Reanalyses are proposed to play a key role in hybrid balancing investigations, as they are the only source of physically consistent wind and radiation information in time and space. They provide the opportunity to simulate consistent wind-solar long-term production time-series of fixed power plant fleet distributions. To our best knowledge, no hybrid balancing investigations based on reanalyses only have been published yet.

In order to reduce systematic biases of power estimates derived from reanalyses calibration methods are used. Staffell and Pfenninger [2016] proposed a country based calibration method. Here, wind speed values provided by reanalyses are systematically adapted in order to represent observed power estimates on country scale most realistically. Considering COSMO-REA6, the proposed calibration method is already applied to wind power estimates by Henckes et al. [2018]. Concerning solar radiation biases of COSMO-REA6 systematic GHI overestimations in high transmissivity cases and compensating underestimations in low transmissivity situations have been found (Sec. 3). By applying a transmissivity dependent post-processing, significant reductions of the compensating systematic effects are achieved. In order to derive most reliable PV estimates in this study an additional post-processing for the direct and diffuse radiation components in order to fit to the post-processed GHI values is developed. Additionally, similar to Henckes et al. [2018] and Pfenninger and Staffell [2016], a country based PV calibration triggered by historical PV time-series is applied.

Based on COSMO-REA6 derived power estimates for fixed installed capacities - in order to avoid installation induced variabilities - over 20 years with daily resolution in this study the following central questions are addressed:

- What is the general balancing potential when adding PV- to wind power generation in each individual European country?
- How do extremes smooth out per country when considering hybrid wind-solar production compared to individual source productions?
- Do specific countries especially benefit from hybrid production of other countries?
- Which countries are particularly suited to balance the extremes of other countries?

The study on hand is structured as follows: First, triggered by the GHI adaptation by Frank et al. [2018] a post-processing of the individual direct and diffuse radiation components of COSMO-REA6 is developed and its added value for PV power estimates is assessed (Sec. 5.3.1). Second,

the derived PV power estimates are validated and calibrated with historical country based PV power time-series (Sec. 5.3.2). Third, combining the calibrated post-processed PV power estimates with the calibrated wind power estimates from Henckes et al. [2018] European hybrid wind-solar balancing potentials are investigated (Sec. 5.3.3).

5.2 Material and methods

5.2.1 Regional reanalysis for PV and wind power estimates

With a resolution of 6 km in horizontal dimension and at least hourly output fields COSMO-REA6 is currently the best resolved regional reanalysis for the European domain (CORDEX EUR-11). Currently available are 23 years from 1995 to 2017. COSMO-REA6 is based on the COntortium for Small-Scale Modelling (COSMO) limited area model of the German weather service. Boundary conditions, which are the weather information advected into the covered simulation domain, are provided by the global reanalyses ERA-Interim [Dee et al., 2011].

For the assimilation of various observations a nudging-scheme is used. Here, the prognostic variables wind, temperature, humidity, and pressure are continuously adapted towards measurements. The sources of wind speed measurements are in principle radiosondes, air crafts, wind profiler and in-situ measurements at ground stations with the mean number of assimilated reports per 6 hours roughly being 300, 14 500, 186, and 19 000, respectively (for detailed information see Bollmeyer [2015]). In contrast to the simulated wind speed which is directly adapted to measurements, irradiance estimates do only profit indirectly from assimilation due to the general adjustment of the model state. Irradiances are calculated by the COSMO-REA radiative transfer scheme from different model parameters.

In chapter 3, the GHI product of COSMO-REA6 was already extensively investigated and a post-processing developed. The main findings were that high radiation values in COSMO-REA6 are systematically underestimated and low radiation values are systematically overestimated in the original COSMO-REA6 product. As the post-processing reduced these effects significantly the GHIpp product is chosen to be a boundary condition for the direct and diffuse radiation post-processing developed in this study (Sec. 5.2.2) which in turn serves as input for subsequent PV estimates. The applied conversion model to estimate PV power based on meteorological parameter is described in detail in Sec. 2.2.

Wind power simulations based on COSMO-REA6 for this study are obtained from Henckes et al. [2018]. For wind balancing investigations Henckes et al. [2018] generated a long-term generation data set from 1995-2014 for 15 400 European wind parks installed end 2014 . For construction the authors developed a Renewable Energy Output Model (REOM). Input for REOM, which uses a power curve approach, are park characteristics and the meteorological parameter wind

speed and air density. In order to interpolate the gridded COSMO-REA6 output to the exact turbine height and location, horizontal as well as vertical interpolation methods were applied (for more information see Henckes et al. [2018]).

5.2.2 Post-processing of COSMO-REA6 direct and diffuse radiation components

The generated power of photovoltaic modules mainly depends on the incidental irradiance to the solar module. For modules mounted with an arbitrary orientation estimates of the tilted radiation becomes necessary. Therefore, not only the global horizontal irradiance (GHI), which is given as post-processed product from Frank et al. [2018], is necessary but also its decomposition in direct and diffuse radiation. The components allow a precise estimation of the radiation on inclined surfaces, taking into account their different propagation characteristics. Thus, a post-processing for the radiation components direct and diffuse radiation is developed and applied to COSMO-REA6.

In order to develop a method to adjust the direct and diffuse components for all individual time steps and grid cells the procedure relies on reanalyses data only. The post-processed GHI ($Q_{GHI,pp}$) derived in Chapter 3 pre-defines the aimed sum of the post-processed direct ($Q_{dir,pp}$) and diffuse ($Q_{dif,pp}$) radiation by the relation

$$Q_{dir,pp} + Q_{dif,pp} = a Q_{dir} + b Q_{dif} = Q_{GHI,pp} \quad (5.1)$$

with Q_{dir} , Q_{dif} the radiation components provided by the COSMO reanalysis, and a and b the unknown relation coefficients. With two unknowns and one equation a further relation is necessary to solve for a and b . This second relation needs to provide information of a realistic ratio r of the direct and diffuse radiation components after the post-processing. Therefore, I use the climatological ratio distributions derived from reanalysis for various GHI-classes and assume the percentile of the ratio being unchanged by the post-processing. The following describes the developed procedure in detail.

Defining the radiation component ratio r at each grid point and each time step as

$$r = \frac{T_{dir}}{T_{dir} + T_{dif}} \quad \text{with} \quad T_{dir} = \frac{Q_{dir}}{Q_{TOA}} \quad \text{and} \quad T_{dif} = \frac{Q_{dif}}{Q_{TOA}}. \quad (5.2)$$

Fig. 5.1 illustrates the derived ratio distributions from COSMO-REA6 alternating with distributions derived from baseline surface radiation network (BSRN) measurements in Lindenberg. Note, the BSRN measurements have highest quality standards with uncertainties of 2 and 5 W m^{-2} , respectively [Heimo et al., 1993]. The general behavior of increasing ratios with increasing transmissivity values between 0 and 0.7 is well represented by the reanalysis. Not

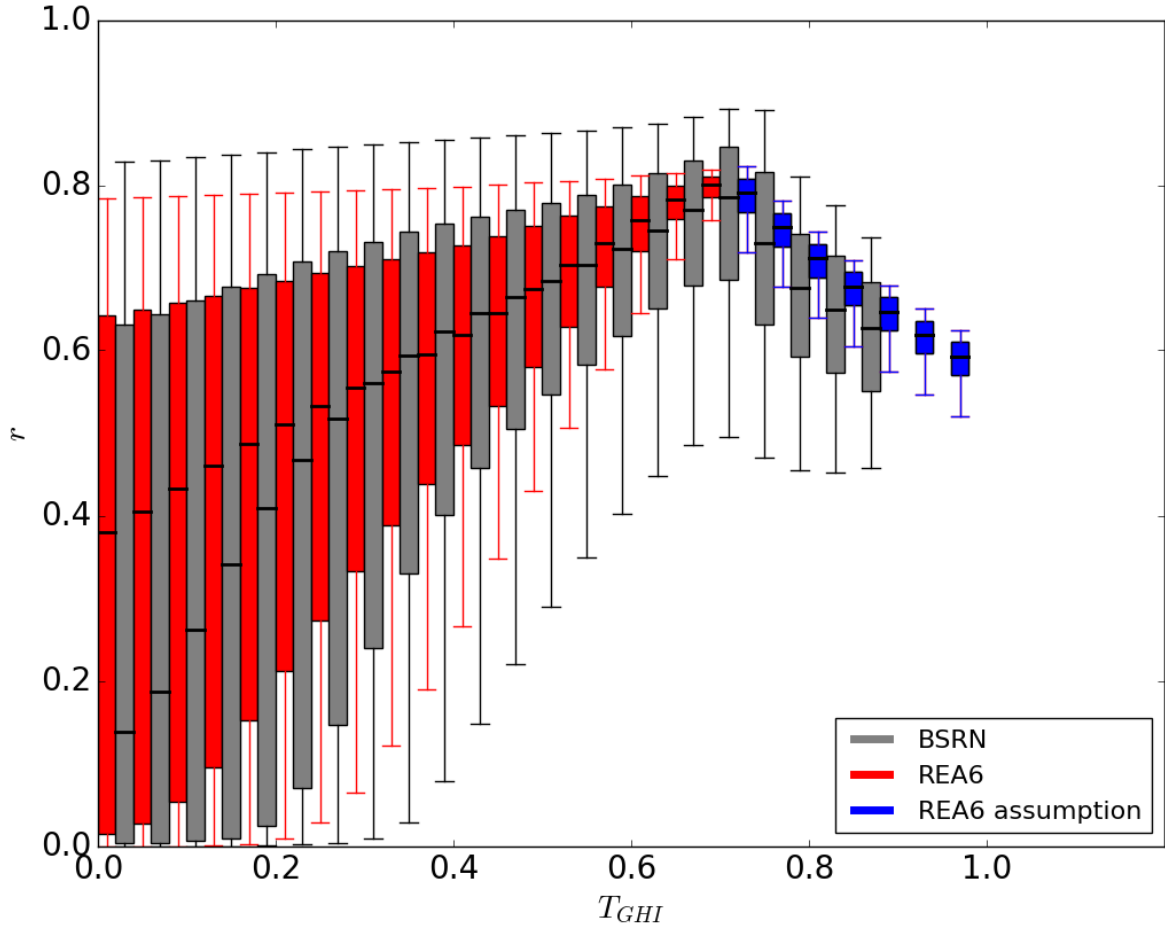


Figure 5.1: Distribution of the radiation component ratios r (direct component divided by GHI) as function of GHI transmissivity at the BSRN site Lindenberg. Grey boxplots represent the distributions derived from BSRN measurements (10 min averages), red ones from COSMO-REA6, and blue ones are artificially approximated using reanalysis radiation only. Percentiles shown are the 5, 25, 50, 75, and 95th.

represented at all is the observed decrease of the ratio for transmissivity values above ~ 0.7 . This is expected, since the high irradiance values are not simulated at all due to the use of the overestimated aerosol optical thickness in COSMO-REA6. However, the decreasing ratios indicate the physical limit of the direct radiation component in clear sky situations. Even higher transmissivities are only possible with increased diffuse radiation values. A typical effect leading to particularly high diffuse radiation is scattering at local cloud edges. Such effects can not be simulated by the COSMO-REA6 model which represents a grid cell mean. Consequently, based on COSMO-REA6 it is not possible to derive the climatological component ratio in situations of particularly high transmissivities (>0.7). However, since the climatological ratio distributions are intended to be used for a realistic adaptation of the individual radiation components an approximation of those is necessary.

Approximations of median ratios for the high transmissivity values are derived for each reanalysis pixel by assuming the direct radiation related to the median ratio of the highest transmissivity class ($median(r(T = max))$) in the reanalysis to be the maximum of physically possible direct radiation ($T_{dir,max}$). The maximum direct radiation per pixel can then be written as

$$T_{dir,max} = median(r(T = max)) T_{GHI,max} \quad (5.3)$$

with $T_{GHI,max}$ the mean value of the highest transmissivity bin in the reanalysis. Given the constant direct radiation the median ratios of the missing ratio distributions ($T > 0.7$) can then be estimated by

$$r(T_{GHI} > T_{GHI,max}) = \frac{T_{dir,max}}{T_{GHI}}. \quad (5.4)$$

This procedure provides the median values of r as a function of the transmissivity but not the corresponding distributions. As a pragmatic approach for all $T_{GHI} > T_{GHI,max}$ the frequency distribution of the T_{GHI} class 0.06 less than T_{max} is used. The resulting approximated ratio distributions are additionally drawn in Fig. 5.1. Testing the derived approach for ratio distribution approximations at eight BSRN sites shows that the site Lindenberg is a good representative for all ratio distribution plots. With the completed estimates of the ratio distributions for all grid points of COSMO-REA6 it is now possible to estimate the post-processed ratios. The only further assumption is that the percentile of the ratio in its ratio distribution is maintained.

The first step in the estimation of the post-processed radiation components is to calculate with the COSMO-REA6 provided radiation components the ratio r_{pre} before post-processing. In a second step its percentile in the ratio distribution in the related transmissivity class $T_{GHI,pre}$ can be calculated. Subsequently, the ratio of the post-processed radiation r_{pp} is determined by the calculated percentile in the target ratio distribution related to $T_{GHI,pp}$. This ratio information is the second condition necessary to determine the relation coefficients a and b . Based on the relations

$$r_{pp} = \frac{a T_{dir,pre}}{T_{GHI,pp}} \quad (5.5)$$

and

$$r_{pre} = \frac{T_{dir,pre}}{T_{dir,pre} + T_{dif,pre}} \quad (5.6)$$

the coefficient a can easily be derived by substituting $T_{dir,pre}$ in eq. 5.6 by the corresponding expression derived from eq. 5.5. After rearranging, a can be determined by:

$$a = \frac{T_{GHI,pp} r_{pp} - T_{GHI,pp} r_{pre} r_{pp}}{r_{pre} T_{dif,pre}}. \quad (5.7)$$

The coefficient b is then calculated from the relation given in Eq. 5.1. This post-processing has the advantage to adjust the individual radiation components in compliance with the post-processed GHI values from [Frank et al., 2018] and at the same time it maintains case individual

radiation component ratio discrepancies from the climatological median ratio given by the re-analysis. The post-processed radiation components are prerequisites for a realistic simulation of PV power based on COSMO-REA6.

5.2.3 PV reference data

For the assessment and calibration (Sec. 5.3.2) of derived PV estimates based on COSMO-REA6 real-world data of PV power are necessary. One provider of freely available wind- and PV power records is the Open Power System Data (OPSD) platform⁶. OPSD is funded by the German Federal Ministry for Economic Affairs and Energy in order to collect, check and uniform open data required by energy system models.

As the OPSD generation data is based on all currently installed capacities per country, while the simulated PV generation is only based on a subset of real installed capacity, generation data cannot be directly compared. An established detour to compare the production of two PV data sets with different installed capacities is to normalize the production in the respective data set with the theoretical production of the total installed capacity under standard test conditions (25° Celsius and 1000 Wm⁻²). To determine the resulting factor, which is also called the capacity factor CF, the installed capacities per country of the OPSD product are required.

Focusing on the whole European domain uniform generation and capacity data from OPSD are only available on country scale. The data packages made use of are the time-series data package version 2019-06-05 [OPSD, 2019b] and the national generation capacity package version 2019-02-22 [OPSD, 2019a]. The packages provide power generation as well as installed capacity since 2010 for a steadily increasing number of European countries. While the generation package encompasses hourly resolved power data the capacity package comprises yearly data only. Thus, in order to derive capacity factors (CFs), yearly capacity values are linearly interpolated to the hourly scale.

5.2.4 PV fleet information

A requirement for a realistic PV power simulation is a list which provides where and when which power plants have been operated. Especially, on European scale uniform collections with comprehensive information are difficult to access. The study on hand uses the solar power plant register purchased in January 2019 from Wiki-Solar (wiki-solar.org). Essentially, the PV power plant register comprises information on commissioning date, installed capacity and location of power plants with installed capacities exceeding 4 MW_{AC}. Smaller scaled PV power plants are not listed as there are no general reporting obligations especially for the private roof top

⁶<https://open-power-system-data.org/>

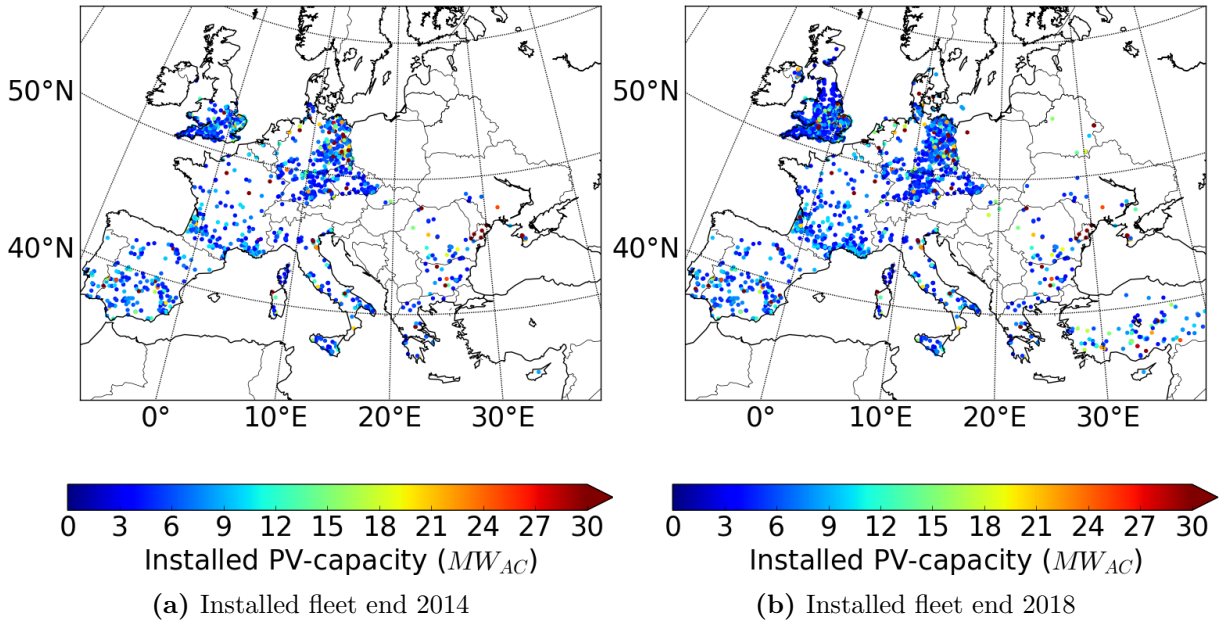


Figure 5.2: Spatial distribution of PV power plants listed by Wiki-Solar. (a) depicts all generating plants end 2014 and (b) end 2018. Caused by the high amount of private PV installations Wiki-Solar lists only power plants with capacities $> 4 MW_{AC}$.

installations. Fig. 5.2 illustrates the spatial distribution and the installed capacity of PV power plants in Europe for once at the end of 2014 and once end 2018. The PV fleet installed at the end of 2014 is of special interest, as it is that year with most OPSD reference data in a maximum number of countries in Europe. Thus, assessment and calibration of power estimates based on COSMO-REA6 is mainly performed with data from 2015. The recent fleet from end 2018 which contains significantly more installed PV capacity is used for a 20 year long-term simulation (evaluation run) to investigate variability characteristics of the current power plant fleet.

5.2.5 PV simulation set-ups

COSMO-REA6 based PV estimates are generated by applying the PV-simulation chain introduced in Sec. 2.2. Two different set-ups are implemented: (1) The *assessment run*, where PV-simulations are conducted under consideration of all PV fleet expansions over time and (2) the *evaluation run*, where only one fixed PV fleet installed at the end of 2018 is simulated for 20 years.

The assessment run is motivated by calibration and assessment issues of the PV power estimates based on the reanalysis. Power estimates simulated with the real-world operating PV fleet are directly comparable to the aggregated generation estimates provided by the OPSD platform.

The evaluation run is motivated by investigating long-term variability characteristics of the currently installed PV fleet and its balancing effects with wind power. Hence, with the long-term simulation of 20 years from 1995-2014 statistical evaluation of the generation variability and extremes becomes possible. Both simulations are conducted with the post-processed COSMO-REA6 radiation components as described in Sec. 5.2.2.

The two simulation runs are implemented upon a spatially gridded PV-atlas based on the COSMO-REA6 reanalysis. The PV-atlas is a theoretical PV-production data set on the assumption that polycrystalline PV modules operating with optimal orientation are regularly distributed in space. Thus, for the two fleet simulations the atlas just needs to be masked and scaled by the installed real fleet capacities. In order to reduce the computational generation effort of the PV-atlas the original COSMO-REA6 grid spacing (6x6 km) was reduced to a multiple of the COSMO-REA6 grid, namely 48x48 km. The chosen grid-spacing of the PV-atlas is motivated by the effective resolution of COSMO-REA6, meaning that scale on which the reanalysis is able to represent meteorological phenomena realistically. Wahl et al. [2017] showed the effective resolution of COSMO-REA6 being roughly the 48x48 km. Thus, the applied reduction of the horizontal grid spacing leads to almost no loss of information. With respect to the subsequent simulation of the installed fleets, no spatial averaging or distance weighting methods are applied in order to maintain the highest level of variability provided by COSMO-REA6. A graphical illustration of the two set-ups is shown in Fig. 5.3

5.3 Results

The result chapter is divided in three main parts. Firstly, improvements for PV estimates due to the post-processing of the COSMO-REA6 radiation components are investigated and quantified. Secondly, real fleet PV simulations are assessed and calibrated on country scale, and finally, European wind-solar balancing effects are assessed based on 20 year power simulations.

5.3.1 The added value of post-processed irradiance for PV power estimates

This chapter is concerned with the assessment of the post-processed COSMO-REA6 direct and diffuse radiation components. The main question to answer is whether the post-processed components add value to the original COSMO-REA6 data, especially for the subsequent application of PV estimates. In a first step comparisons to highly accurate BSRN site measurements are conducted. Here, marginal and joint distributions of the original COSMO-REA6-, the post-processed- and of the measured radiation components are discussed. In a second step the added value in the derived quantity PV estimates is investigated.

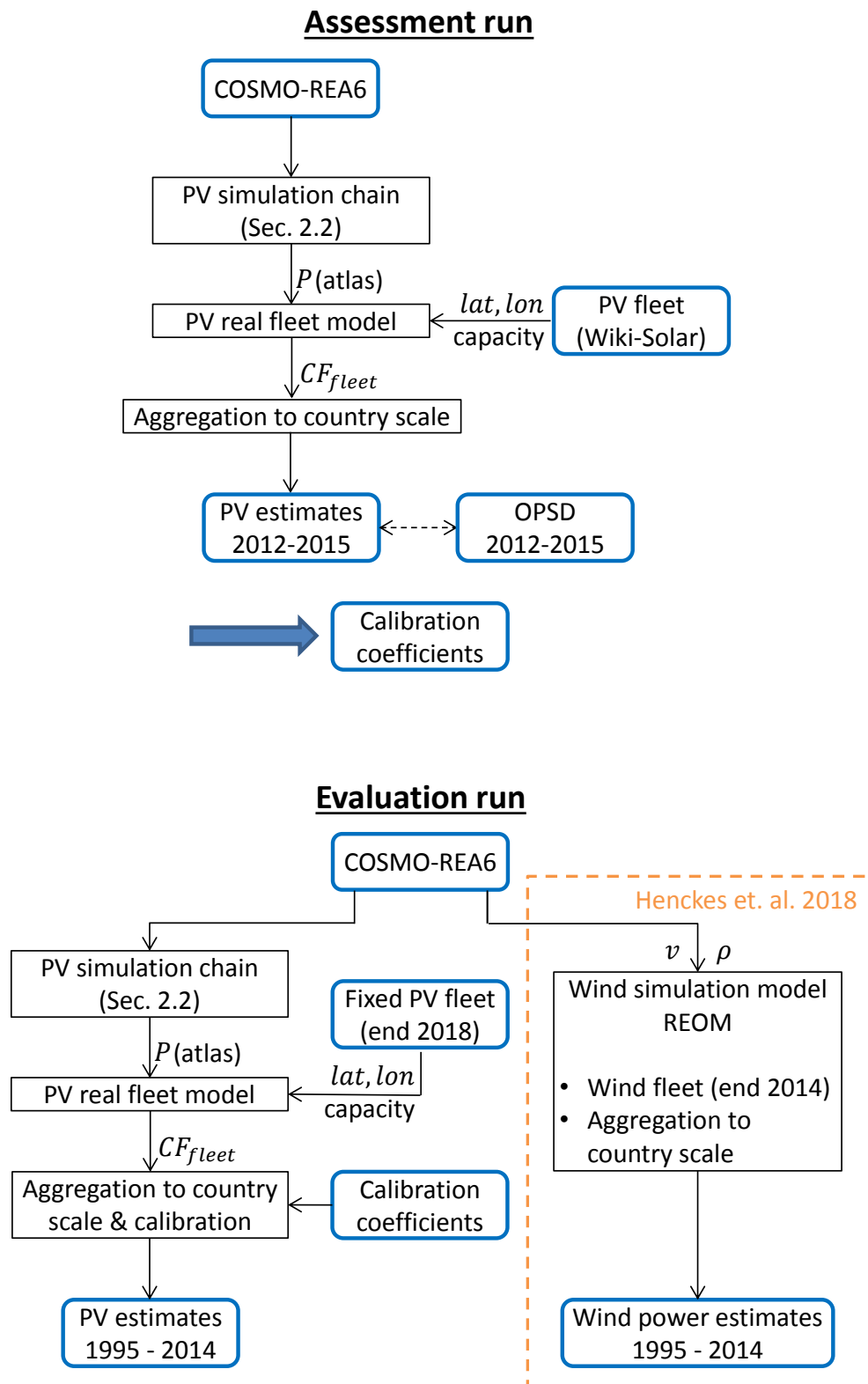


Figure 5.3: Illustration of the assessment and evaluation runs

5.3.1.1 Assessment of post-processed radiation components

For the assessment of the post-processed direct and diffuse radiation components measurements reported at the same eight BSRN sites as used in Sec. 3 are used. In a first step, marginal distributions - time independent comparisons - are considered in order to compare the general frequency distributions of modeled and measured radiation. In a second step, joint distributions are considered to find whether the post-processing adjusts the radiation in the correct situation and with an appropriate amplitude. Note, the reference measurements obtained from the BSRN sites can only be considered as semi-independent as their sum was already used to develop the GHI post-processing. Nevertheless, with the aim to assess the post-processed components on the European scale and to avoid miss-conclusions due to the use of measurements of lesser quality, here BSRN measurements are further used.

In order to assess the frequency distributions of the original (REA6) and the post-processed radiation (REA6pp) they are directly compared to the distributions derived from BSRN measurements (Fig. 5.4). Considering the direct radiation, Fig. 5.4a shows the frequency of occurrence in some intensity ranges improved and in some worsened due to the post-processing. Strong improvements of the frequency distribution due to the post-processing occur between 0 and 300 Wm^{-2} , as well as for radiation values above 700 Wm^{-2} . Between 300 and 700 Wm^{-2} the post-processing worsened the distribution slightly compared to the original COSMO-REA6 distribution. Considering the diffuse radiation, Fig. 5.4b shows the frequency of occurrence of the post-processed data set being slightly improved for low radiation values and slightly worsened for higher values. In summary, the frequency distribution does not show an overall improvement or worsening of the original frequency distribution of COSMO-REA6 when comparing to the measured distributions. Nevertheless, with no clear conclusion with respect to frequency distributions there still might be improvements in other metrics as will be seen in the following when considering joint distributions.

The scatter density plot between the measured radiation of the eight BSRN stations with (1) the COSMO-REA6 original direct radiation and (2) the post-processed COSMO-REA6 direct radiation (Fig. 5.5) shows qualitatively how the different COSMO-REA6 data sets match the 1.3 million BSRN measurements from 1995 - 2014.

Comparing the original COSMO-REA6 direct radiation with measurements shows a general underestimation by COSMO-REA6 above about 50 Wm^{-2} (Fig. 5.5a). The underestimation amplifies with increasing radiation. This effect is an expected and consistent consequence by using an aerosol climatology in COSMO-REA6 which significantly overestimates real-world aerosol optical thickness [Zubler et al., 2011]. Further, Fig. 5.5a shows a large number of pairs where either the REA6- or the BSRN radiation is very low or equal to 0 Wm^{-2} . These situations correspond to spatial mismatches of individual clouds in model and reality. Comparing the amount of pairs where COSMO-REA6 simulates 400 Wm^{-2} and BSRN are close to 0 Wm^{-2} with the

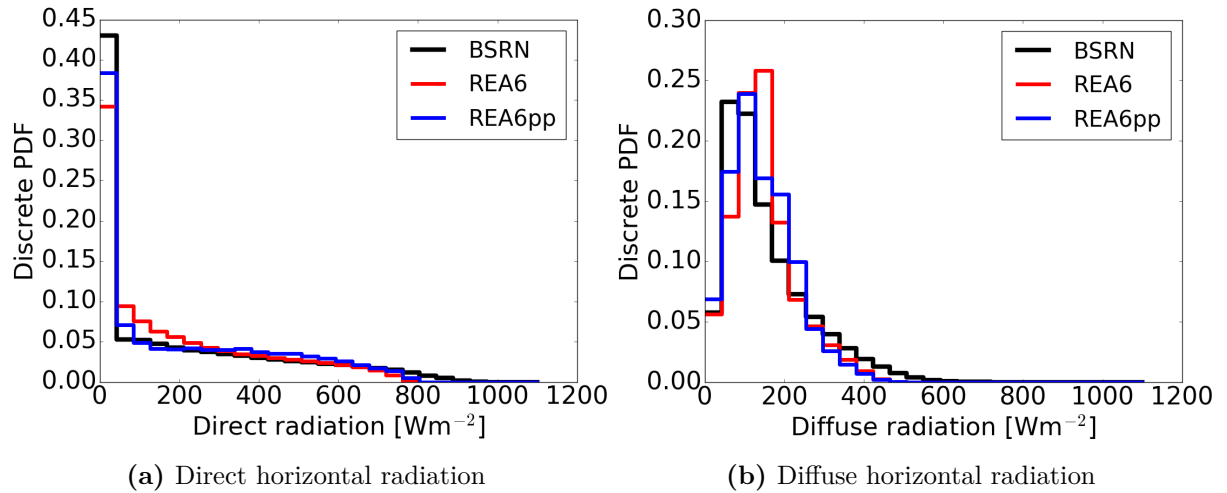


Figure 5.4: Frequency distributions of (a) direct horizontal radiation, and (b) diffuse horizontal radiation. Reanalyses distributions are based on instantaneous output and BSRN distributions on 10 min averages. Each distribution is based on 1.3 million radiation values estimated or measured between 1995-2014 and comprises values from eight BSRN sites.

vice versa situation more pairs are found where the COSMO-REA6 radiation is high and the BSRN measurement is low. Since this effect is obvious for all radiation amounts where either the one or the other source is close to 0 Wm^{-2} this effect suggests a positive bias. An obvious explanation for this bias is the general underestimation of the occurrence frequency of clouds in COSMO-REA6. Thus, in compliance with the conclusions of Ch. 3, this positive bias is expected to partly compensate the systematic negative bias evident for radiation where modeled and measured radiation values are simultaneously above 50 Wm^{-2} .

Comparing now the density plot constructed with the post-processed COSMO-REA6 direct radiation and measurements (5.5b) to that constructed with the original COSMO-REA6 values and measurements (5.5a) shows the post-processed radiation for some radiation ranges clearly improved and for some ranges at least similar good as the original COSMO-REA6 product. Especially, in the range from 100 to 500 Wm^{-2} improvements are evident. Also the radiation values above 500 Wm^{-2} are slightly improved. Nevertheless, the general problem of underestimating the highest radiation amounts remains. Similarly as the original COSMO-REA6 the post-processed radiation contains more cloud mismatch cases where COSMO-REA6 simulates high radiation values than vice versa. Thus, also for the post-processed direct radiation this effect is suggested to contribute with a positive bias.

When considering the scatter density of the diffuse radiation component instead of the direct component, no evident signals become visible (Fig. 5.16 and Fig. 5.17 in the annex chapter 5.5). Nevertheless, due to the post-processing the maximum possible diffuse radiation amounts are slightly increased and therefore improved. Moreover, there seems to be a slight increase of data pairs where the simulation is about 200 Wm^{-2} and the measurement about 100 Wm^{-2} . However,

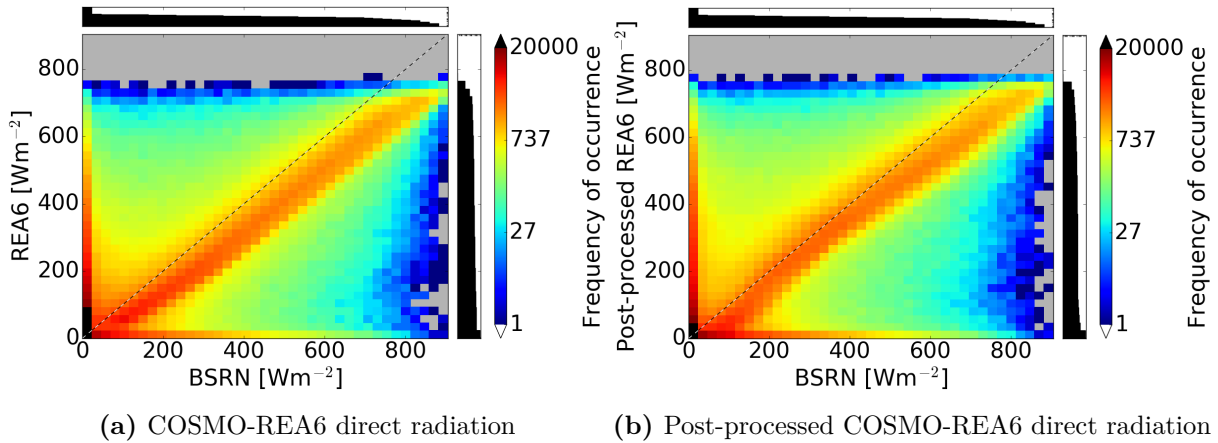


Figure 5.5: Joint distributions of measured direct radiation with (a) COSMO-REA6 direct radiation and (b) post-processed COSMO-REA6 direct radiation. Considered are measurements at eight BSRN sites. The contribution of the number of data from the individual stations is shown in Tab. 5.1.

since the effects are rather small, they are not further discussed. The figures are attached in the supplementary material.

Quantitative assessment of the direct and diffuse radiation before and after the post-processing is provided in terms of correlation, bias, and mean absolute error (MAE). First, the scores are calculated by considering all sky situations. Second, the statistics are determined for specific transmissivity ranges since they display how systematic optical thickness dependent biases are reduced due to the post-processing.

The assessment of the post-processed radiation for all sky situations shows on average slightly worsened correlation- and bias scores for both radiation components, and slightly improved MAE values at least for the direct component (Tab. 5.1 and 5.2). Note, an improved MAE by degraded bias score implies improved joint variation skills of the post-processed radiation. However, this improvement is only valid for the direct radiation part at four out of eight sites. An evident signal is the degraded bias, while for direct radiation it increases from -3.3 to 13.2 Wm^{-2} it decreases for diffuse radiation from -6.5 to -10.2 Wm^{-2} on average over all sites. As discussed for the scatter density plots (Fig. 5.5) the bias change of the direct radiation part due to the post-processing is mainly caused by two different effects: (1) the improvements where reanalysis and observed sky situations are similar (radiation values of both sources are simultaneously above 50 Wm^{-2}) and (2) the more or less unchanged positive bias where the sky situations are mismatched. Thus, the overall bias of the post-processed direct radiation is positive which is in accordance with the bias score results.

Since the post-processing is applied to reduce the clear sky positive and the cloudy sky negative bias (compensating effects) in the GHI product in the following clear and cloudy sky situations

Table 5.1: COSMO-REA6 scores of direct horizontal irradiance before (COSMO-REA6) and after applying the post-processing (COSMO-REA6pp). Compared are instantaneous values of COSMO-REA6 with 10 min averaged measurements of eight BSRN sites.

			COSMO-REA6 [Wm^{-2}]			COSMO-REA6pp [Wm^{-2}]		
	Station name	N values	R	BIAS	MAE	R	BIAS	MAE
LIN	Lindenberg	195879	0.76	12.9	80.0	0.75	26.2	81.9
CAM	Camborne	161475	0.70	30.1	92.4	0.68	47.7	98.9
CAR	Carpentras	251429	0.83	-37.2	105.7	0.82	-13.4	95.6
CNR	Cener	76127	0.79	-17.4	107.8	0.78	2.3	104.2
CAB	Cabauw	131674	0.72	3.9	81.0	0.71	16.4	84.4
PAL	Palaiseau	114046	0.73	9.0	91.8	0.71	24.2	94.0
TOR	Toravere	163573	0.78	-14.3	77.7	0.77	-3.8	75.9
PAY	Payerne	157096	0.81	-0.0	100.4	0.80	16.3	98.0
All	All sites	1251299	0.79	-3.3	91.9	0.77	13.2	90.8

are discriminated. Here, as in Ch. 3, the discrimination is conducted by the use of the GHI threshold of 0.5. Only if the transmissivity value is in both - reanalysis and observation - simultaneously smaller or higher than 0.5 the values are used for validation. This separate assessment for clear and cloudy sky situations avoids the consideration of strongly mismatched situations in the joint distributions. Thus, systematic errors intended to be reduced by the post-processing are expected to appear. In this way, systematic biases become visible which are reduced by the post-processing (Tab. 5.3). On average over all eight BSRN sites the direct radiation biases improve from -49.5 to -8.9 Wm^{-2} , and 17.4 to 10.4 Wm^{-2} for clear and cloudy conditions, respectively. Also the MAE values are significantly reduced for most sites and both sky situations. Slight worsening occurs for the diffuse radiation part. In cloudy conditions the bias and the MAE increased by about 5 Wm^{-2} . In clear sky conditions the bias decreased from -3.1 to -12.8 Wm^{-2} . With respect to the GHI the results show that the negative bias in clear sky GHI and positive bias in cloudy sky GHI are mainly caused by the direct radiation component provided by COSMO-REA6 and not by the diffuse radiation component. Considering the performance of the post-processing at individual sites significant differences from the averaged values can be found. The scores at the individual BSRN sites are additionally shown in the supplementary material (Tab. 5.7, 5.8, and 5.9, 5.10). However, with some significant improvements in the direct radiation and some degradation in the diffuse radiation the question arises whether the developed post-processing of the components improves or degrades the derived estimates of PV power. Therefore, the next section focuses on comparisons of simulated PV power estimates derived from post-processed radiation components, original COSMO-REA6 components, and BSRN measurements.

Table 5.2: COSMO-REA6 scores of diffuse horizontal irradiance before (COSMO-REA6) and after applying the post-processing (COSMO-REA6pp). Compared are instantaneous values of COSMO-REA6 with 10 min averaged measurements of eight BSRN sites.

			COSMO-REA6 [Wm^{-2}]			COSMO-REA6pp [Wm^{-2}]		
	Station name	N values	R	BIAS	MAE	R	BIAS	MAE
LIN	Lindenberg	195879	0.67	-13.9	54.3	0.67	-19.5	55.9
CAM	Camborne	161475	0.63	-25.8	65.6	0.61	-34.0	68.9
CAR	Carpentras	251429	0.58	10.7	58.0	0.53	8.9	61.1
CNR	Cener	76127	0.61	-3.1	62.6	0.56	-5.8	67.1
CAB	Cabauw	131674	0.66	-21.6	59.4	0.65	-29.1	62.3
PAL	Palaiseau	114046	0.66	-14.0	59.6	0.64	-20.8	61.9
TOR	Toravere	163573	0.63	8.7	49.4	0.59	7.9	52.5
PAY	Payerne	157096	0.61	-4.3	53.6	0.57	-2.1	57.9
All	All sites	1251299	0.63	-6.5	57.3	0.60	-10.2	60.3

Table 5.3: COSMO-REA6 direct and diffuse horizontal irradiance scores before (COSMO-REA6) and after applying the post-processing (COSMO-REA6pp). Compared are instantaneous values of COSMO-REA6 with 10 min averaged measurements of eight BSRN sites.

			COSMO-REA6		COSMO-REA6pp	
	Station name	N values	BIAS [Wm^{-2}]	MAE	BIAS [Wm^{-2}]	MAE
Direct clear	All sites	475258	-49.5	98.5	-8.9	84.9
Diffuse clear	All sites	475258	2.6	56.1	7.6	62.6
Direct cloudy	All sites	483489	17.4	25.2	10.4	19.7
Diffuse cloudy	All sites	483489	-3.1	52.7	-12.9	52.3

5.3.1.2 PV estimates with and without post-processed radiation components

For electricity related questions PV estimates are the final quantity of interest. Thus, a central question is whether the post-processing improves the PV power estimates.

For the conversion from meteorological quantities to power estimates the power model based on Huld et al. [2011] described in Chapter 2.2 is used. The model simulates the power generation of poly-crystalline PV modules as function of the incidental radiation on an optimally tilted module, the 2m temperature and the wind speed. The related capacity factor (CF) of the PV power estimates are calculated by dividing the instantaneous production by the theoretical production under standard test conditions ($Q_{STC} = 1000 Wm^{-2}$ and $T_{STC} = 25^{\circ}C$).

In order to quantify the added value of the radiation post-processing for derived PV estimates the power-conversion scheme is applied to (1) the original COSMO-REA6 values, (2) the post-processed values, and (3) the BSRN measurements. By using the same power-conversion scheme for the three setups the resulting differences in the PV estimates can be traced back to the

radiation input variables. Assuming additionally that the applied power-conversion scheme works perfectly provides the opportunity to consider the BSRN based estimates as reference.

Motivated by practicability and simulation speed, this study is only conducted for the year 2014 and with reduced temporal resolution. With the reduced temporal resolution from quarter hourly to hourly the final number of values used for this assessment is 19195. Therein, measurements from six BSRN sites contributing each with roughly 3000 values are considered together.

The first metric to analyse the added value of the post-processing in the power space is the quantile-quantile plot (qq-plot). The qq-plot provides the opportunity to compare the marginal distributions of two data sets. Given two similar distributions the qq-plot ends up in a straight line following the main diagonal. Two differing marginal distributions end up in discrepancies from the main diagonal.

Fig. 5.6 depicts the two qq-plot results when comparing the power estimates based on post-processed (blue) and original (red) COSMO-REA6 radiation with BSRN based ones. An evident difference in the distributions occurs for CF values above about 0.4. While the COSMO-REA6 radiation leads to a slight underestimation of the CF values above 0.4 the distribution derived from the post-processed COSMO-REA6 radiation fits the BSRN based CF distribution much better. Thus, the high production cases are statistically better represented when using the post-processed COSMO-REA6 radiation product.

The next metric, joint distributions (Fig. 5.7a), shows the COSMO-REA6 based CFs systematically too low for pairs above about 0.3. Thus, the underestimation of direct radiation shown in Fig. 5.5a seems to cause underestimations in the derived CF, too. This problem is significantly reduced when using the post-processed COSMO-REA6 components (Fig. 5.7b). The RMSE and the MAE of the original COSMO-REA6 derived CF are 0.163 and 0.113 while they are 0.171 and 0.112 for the post-processed COSMO-REA6 derived CF values, respectively. Again, the RMSE is slightly degraded while the MAE is roughly the same. Again, cloud mismatch related radiation pairs fan out further, while radiation pairs related to cloud-matches improve due to the post-processing. Closely connected is the improvement/increase of the variance due to the post-processing from 0.058 to 0.07. Which is much closer to the observed variance of 0.067. The increased variance can be traced back to the increased and improved GHI variance achieved with the post-processing in Ch. 3.

5.3.1.3 Summary and discussion

Due to the need for direct and diffuse radiation components as input for PV power conversion schemes and known systematic biases in the GHI product (see Ch. 3), here a post-processing of the direct and diffuse radiation components provided by COSMO-REA6 is developed (Sec. 5.2.2), applied, and evaluated. With the aim to develop a post-processed direct and diffuse

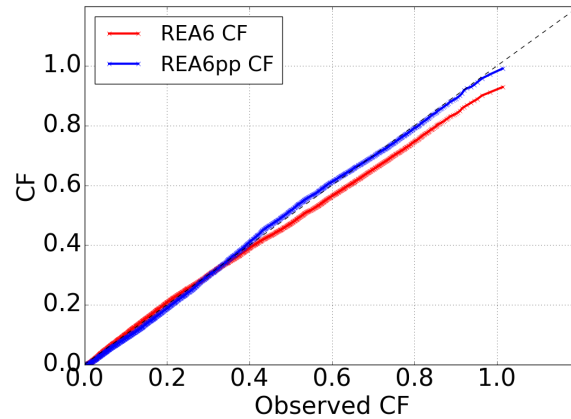


Figure 5.6: Quantile-Quantile plot of the CF derived from COSMO-REA6 and post-processed COSMO-REA6 with respect to the CF derived from BSRN measurements. Compared are instantaneous CF values of COSMO-REA6 with 10 min averaged values of eight BSRN sites.

radiation data set to simulate PV power all over Europe, the applied constrains are chosen in a way that the post-processing is finally applicable to the whole reanalysis domain. Main constrain for the adaptation of the radiation components is to achieve the post-processed GHI derived in Ch. 3.

From the evaluation one can summarize: Even though the representation of measured radiation components is slightly degraded due to the post-processing when considering all sky conditions, separated clear and cloudy sky evaluations show significant improvements of the post-processed radiation parts at least for the direct radiation component. Moreover, the investigation indicates that the systematic biases of the GHI in clear and cloudy sky situations are mainly caused by the direct radiation component and not by the diffuse component.

With the different improvements and worsening of the radiation components due to the post-processing subsequently the combined impact of the post-processed radiation components on the estimated PV power is studied. The derived power generation estimates are shown to be improved under similar cloud conditions and slightly decreased under mismatched cloud conditions in model and reality. Main improvements are achieved through the reduction of systematic underestimations of CF values above transmissivity values of 0.3 and a variance improvement of the simulated CF from 0.058 to 0.07 (reference: 0.067). As the main focus in the following balancing study is rather on statistical occurrence frequencies and on the variability of the derived CFs which show clear improvements due to the post-processing all following studies and sections will rely on the post-processed radiation components.

Strengths and weaknesses of the developed post-processing for the direct and diffuse radiation components are versatile. Strengths are the improved final sum by matching the post-processed GHI product and the significant improvement of the direct radiation component especially in

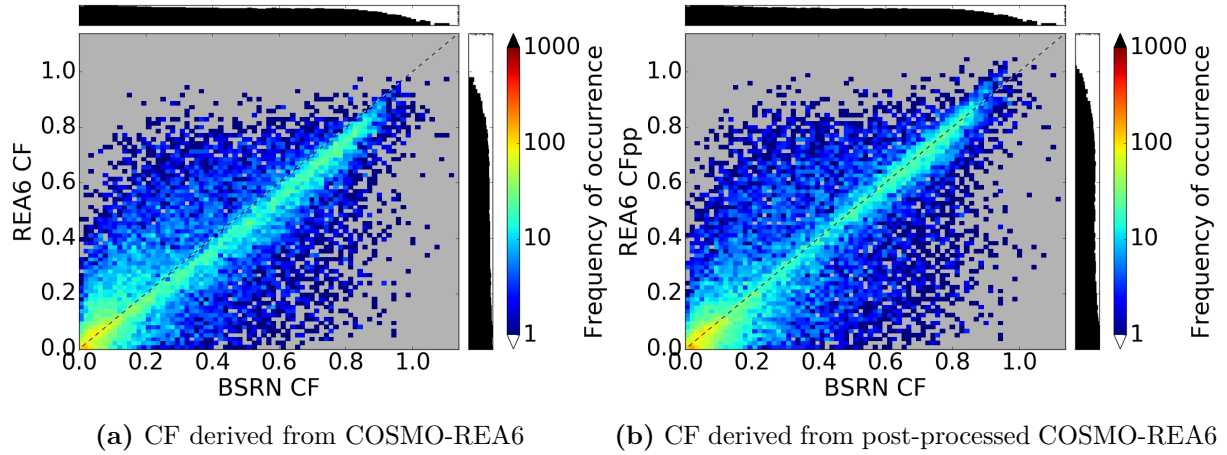


Figure 5.7: Joint distributions of measurement based CF with (a) COSMO-REA6 derived CF and (b) post-processed COSMO-REA6 derived CF. Considered are measurements at eight BSRN sites. Each distribution is based on 1.3 million radiation values estimated or measured between 1995-2014 and comprises values from eight BSRN sites.

the range between 100 and 500 Wm^{-2} . The remaining problem of underestimating the highest radiation values is related to the assumption that the maximum of direct radiation simulated by the reanalysis would be equal to the physically maximum possible direct radiation observed. This issue might be improved with a better guess of the real maximum value of the direct radiation component. A strength but also a weakness is that the procedure relies on reanalyses data only. Thus, it is possible to apply the post-processing to the whole reanalysis domain but radiation values of completely mismatched weather situations can be further degraded. This is due to the fact that radiation values are in principle increased when the reanalyses simulates clear sky and decreased when it simulates cloudy sky. Nevertheless, in a statistical manner, these situations can add a more realistic marginal distribution due to the broadening of the simulated radiation distributions which are generally underdispersive in the reanalysis model.

Applications expected to benefit most from the developed post-processing are those that require especially the direct radiation component. Thus, the most prominent field that might benefit from the post-processing is that of concentrating solar power (CSP).

5.3.2 Assessment and calibration of real fleet PV power simulations

Continuing with the derived PV estimates based on the post-processed reanalysis, here the derived product is evaluated using country aggregated PV reference data obtained from OPSD. Additionally, in order to correct for systematic remaining biases in the PV estimates on a country scale calibration coefficients are derived. Motivated by the comparison to real-world generation time-series, the simulation set-up used in this section is the *assessment run* (see Sec. 5.2.5).

5.3.2.1 Assessment with Open Power System Data

Open Power System Data (OPSD) provide the opportunity to validate the PV power simulations on a country scale. On European scale, 12 countries are found where simulations and observations are available simultaneously.

Crucial for a reliable statistic is that the whole PV fleet distribution within a country is well represented by the simulated large-scale power plants. Unfortunately, no complete list of PV fleet distributions does exist in order to validate whether the large-scale power plants are representatively distributed. Nevertheless, high numbers of installed large-scale power plants increase the likelihood to represent the whole PV fleet. Tab. 5.4 depicts the number of PV power plants with at least 4MW_{AC} per site per country at the beginning of 2015. With more than 100 PV power plants five countries, namely FR, DE, IT, ES, and GB do have a relatively high number of large-scale power plants. Here, the distribution is expected to represent the whole fleet distribution quite well. With 2 power plants BE and SK have the lowest number of large-scale power plants. Thus, statistics for those countries are expected to be rather weak. Nevertheless, not only the number of plants but also the number of small PV installations, the weather at the individual sites, and the size of the considered country determine the real representativity. Thus, a ranking of the representativity is hardly possible.

A further hint whether the listed power plants represent the spatial distribution of all power plants can be found in the spatial distribution of the listed large-scale PV installations (see Fig. 5.2a). The highest density of PV-plants usually occurs in the southern part of each country. In most countries there are obviously agglomerations for large-scale PV installations. In Germany, for example, these are located in the northeast and south. It is obvious that these agglomerations, in which large power plants are installed, are unlikely to coincide with the small installations on private roof tops. Especially in Germany, where a large number of private PV installations exists, this local mismatch might result in a spatial smoothing which can not be simulated with large-scale installations only.

In order to investigate systematic biases of the reanalysis derived PV power simulations Fig. 5.8 shows the annual mean CF and its deviation from OPSD observations in 2015. Generally, COSMO-REA6 represents the typical north-south gradient of increasing capacities due to higher sun elevation angles. While the capacity factors are roughly 12% in the northern countries they reach values of roughly 18% in the south. Highest average capacities occur for the southwestern countries Spain and Portugal with 17.5 and 17.3%, respectively, followed by France with 17.2%. Countries on the same latitude, but in Eastern Europe, show significantly lower CF averages with 13-16%. This superimposed east-west gradient leads to the general statement of increasing CF averages from northeast to southwest in Europe.

Table 5.4: Number of simulated PV power plants with a minimum installed capacity of $4 MW_{AC}$ at the beginning of 2015. Source: Solar power plant register purchased in January 2019 from Wiki-Solar (wiki-solar.org).

Country	ISO country codes	Number of plants
Belgium	BE	2
Bulgaria	BG	25
Czech Republic	CZ	71
France	FR	188
Germany	DE	420
Greece	GR	27
Italy	IT	165
Portugal	PT	22
Romania	RO	31
Slovakia	SK	2
Spain	ES	195
United Kingdom	GB	291

Comparing the COSMO-REA6 estimates to the OPSD observations shows the general north-east to southwest CF bias gradient being underestimated in COSMO-REA6 (Fig. 5.8b). The northeast and central countries are rather overestimated and the southwestern rather underestimated. Prominent overestimations between 3.7-2% occur in GB, FR, IT, RO, and SK. The strong overestimation in Italy is supposed to be related to Saharan dust events which are not directly simulated in COSMO-REA6 but known to reduce surface radiation. Comparison of the rather smooth spatial distribution of the desert dust part in the Tanre climatology to Saharan dust advection paths shown by e.g. Israelevich et al. [2012] suggest aerosol underestimations especially in the northern part of Italy. Here, aerosols are blocked physically by the Alps and accumulate. Prominent underestimations of the averaged CF occur mainly at the Iberian Peninsula. Most extreme is the underestimation in Spain with -2.7%. Here, the contribution of CSP might have a slight different production characteristic than PV power plants. Thus, differences between PV power simulations and a reference which considers PV and CSP-power as a sum are expected.

The shown country specific biases motivate the development and application of a calibration in order to arrive most realistic CF time-series of each country. The calibration method and the resulting added value of the post-processing are discussed in the following.

5.3.2.2 Calibration

The developed calibration accounts for the country specific effects like conversion losses at the electricity transformers, systematic biases in the reanalyses input, and power plant aggregation mismatches. A first order approach to correct for these effects is to apply a linear scaling of

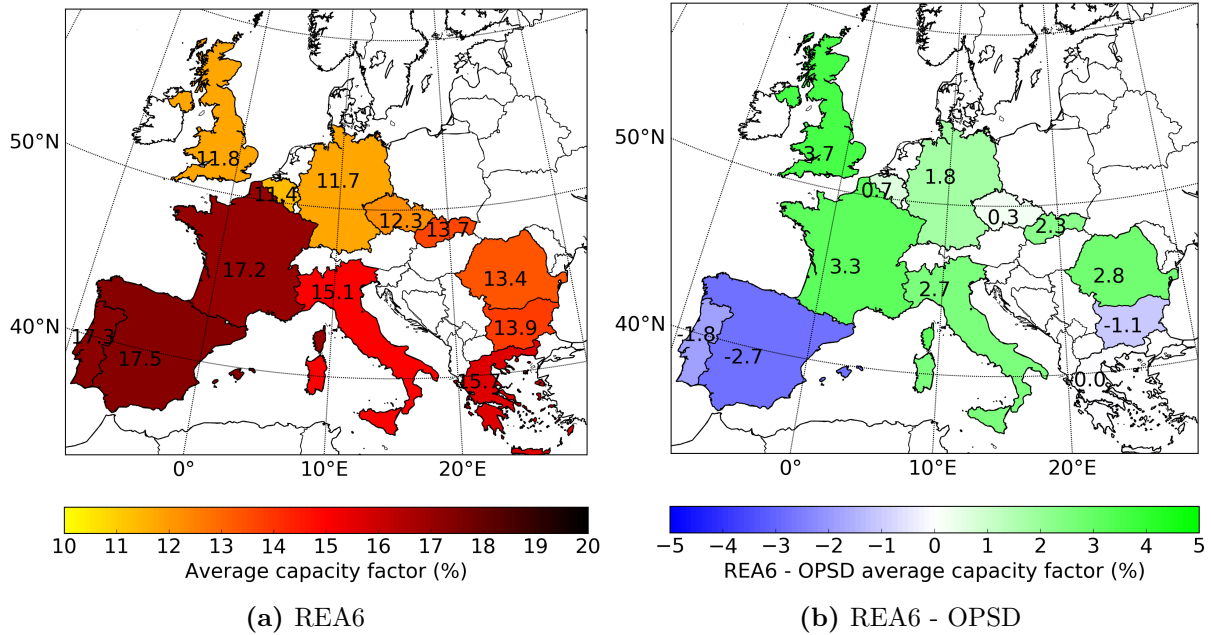


Figure 5.8: a) Averaged PV capacity factors (2015) from site-level data aggregated to country-level and b) the difference of COSMO-REA6 based estimates to OPSD observations for 2015.

the CF values per country. The scaling factors per country i are derived with a least-square regression of the form

$$CF_{OPSD,i} = \alpha_i CF_{REA6pp,i} \quad (5.8)$$

with α the finally applied scaling factors and CF the daily average capacity factors in 2015. A similar approach but by using just one scaling factor for whole Europe is applied in Pfenninger and Staffell [2016] to the MERRA reanalysis.

The resulting scaling factors estimated with the least-square regression per country are listed in Tab. 5.5. In general they vary between 0.68 - 1.18. In compliance to the findings from Fig. 5.8b scaling factors greater one can be found for ES, PT, and BG. In all the other countries the scaling factors are smaller than one.

For the assessment whether the calibration improves the CF estimates, relative bias, relative RMSE, and the earth movers distance (EMD) - a measure for the difference of two cumulative distribution functions - are calculated before and after applying the calibration (Tab. 5.5). The term relative means that the bias and RMSE is expressed with respect to the mean CF of the respective country. For the reason of limited data availability, a comprehensive score calculation for all countries could only be conducted based on the training year 2015 itself. To investigate if the calibration improves the CF estimates also in other years the scores could only be estimated for CZ, FR, DE, and IT in the years 2012-2014.

Table 5.5: Estimated scaling factors α complemented by relative bias (relativ to the mean CF of the country), relative RMSE, and earth movers distance (EMD) of daily CF estimates based on COSMO-REA6pp before (REA6pp) and after applying the country based calibration (REA6pp_cal) for the year 2015 (top) and for the years 2012-2014 (bottom). Reference observations are obtained from the OPSD platform.

		REA6pp			REA6pp_cal			
α	Years	BIAS %	RMSE %	EMD	BIAS %	RMSE %	EMD	
BE	0.87	2015	6.5	35.8	138	-7.1	31.4	96
BG	1.04	2015	-7.1	21.0	88	-3.1	20.5	102
CZ	0.96	2015	2.2	17.3	102	-1.6	16.7	84
FR	0.80	2015	23.5	28.3	166	-1.1	10.0	44
DE	0.83	2015	17.8	30.0	138	-2.3	18.1	92
GR	0.98	2015	-0.2	13.7	162	-2.4	13.5	136
IT	0.81	2015	21.3	27.6	240	-1.4	12.1	84
PT	1.06	2015	-9.3	16.5	134	-3.6	15.3	118
RO	0.77	2015	26.4	35.9	194	-2.1	15.0	58
SK	0.81	2015	20.2	34.3	142	-2.7	21.0	74
ES	1.18	2015	-13.4	24.1	236	2.6	17.0	174
GB	0.68	2015	45.2	67.1	164	-1.8	34.8	74
CZ		2012-2014	6.2	19.2	140	2.4	17.9	126
FR		2012-2014	30.6	36.8	632	9.8	16.4	284
DE		2012-2014	20.6	33.3	300	1.0	20.3	84
IT		2012-2014	17.9	24.5	362	-4.2	13.5	140

Applying the calibration to 2015 reduces the bias in 10 of 12 countries. In 8 of the 12 countries the bias reduced from relative biases between 10 and 46% to biases less than 8%. Bias degradations in BE and GR of 2% relative bias increases are rather small. The EMD, which indicates whether the general distribution is improved, depicts improvements for all countries except Bulgaria. In Bulgaria the EMD value slightly increased. Also the RMSE depicts in general an improvement.

As mentioned before, the deduced scaling factors rely on comparisons based on 2015 only. However, with the aim to apply the scaling factors to the whole time span of COSMO-REA6 Tab. 5.5 is complemented by statistics deduced based on independent years, too. Thus, applicability of the single year derived scaling factors to multi-year time-series can be assessed. The results show for each of these countries with multiple years for assessment, namely CZ, FR, DE, and IT, improved bias, RMSE, and EMD scores. Note, by the limitation to only a subset of countries and only the short time window from 2012-2014 the findings can only be interpreted as hint whether the scaling factors are generally applicable. However, with the lack of further years for comparison at this point no further investigations are possible.

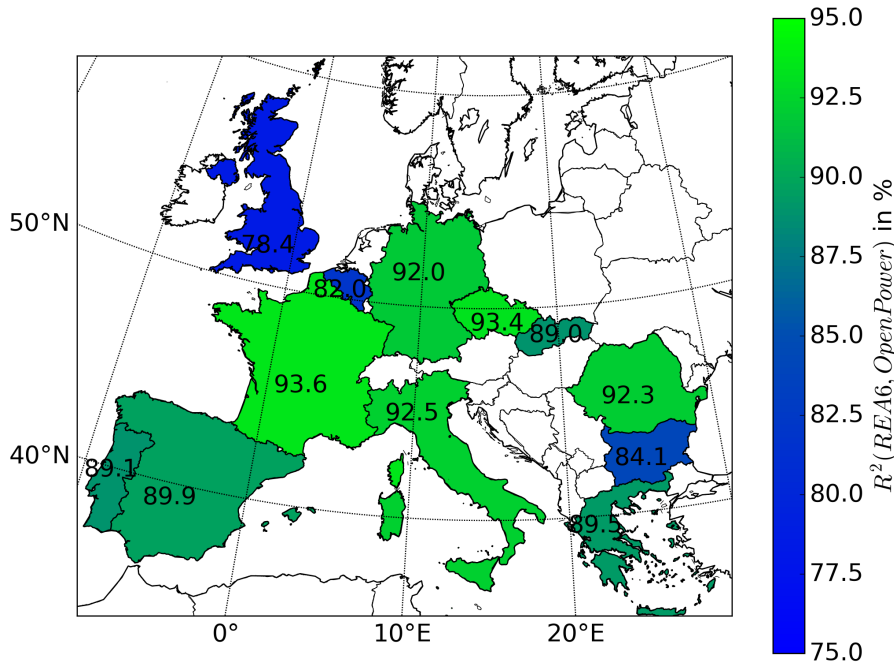


Figure 5.9: Explained variance of COSMO-REA6 simulated daily CF compared to OPSD data in 2015 for various European countries. Considered is only PV power.

5.3.2.3 Variability assessment

With the aim to investigate balancing effects it is crucial to investigate whether the simulated CF variations are similar to the realistic ones. A typical measure representing the similarity of variations is given by the explained variance expressed by the squared correlation. Calculated for the European countries, based on daily CFs 2015, the explained variance varies between 78 and 94% (Fig. 5.9). For most countries COSMO-REA6 simulations capture more than 89% of the observed variance. Only in GB, BE, and BG the values are lower. Thus, COSMO-REA6 simulations represent daily CF variabilities quite well.

However, these high correlations need to be treated with caution: (1) By considering variables fluctuating at different scales it is not known which scale has which contribution to the calculated correlation, e.g. considering a variable with strong annual cycle compared to the daily fluctuations the correlation is mainly determined by the annual cycle. Thus, despite high correlations, daily variances might not be well represented. A second problem of correlations (2) is the need of temporal matching for high correlations. Thus, a temporal mismatch of events decreases the correlation although in a statistical manner the variance is represented well.

Time-series of moving standard deviations (STD) give the opportunity to check for the missing information squared correlations do not capture. Considering a moving time-window before comparing the variances of COSMO-REA6 and OPSD loosens the condition of sharp simul-

taneity. Considering the whole time-series provides information on the variability on different temporal scales.

Fig. 5.10 shows the moving STD exemplarily for two countries, Germany and Italy. Those two countries have been depicted as they are found to be quite well representatives for all considered countries. Before going into detail, the general courses of the resulting moving STD time-series is discussed. The strong annual cycles can be explained by the higher day to night CF differences due to higher sun elevation angles during summer than in winter. Also explained by sun elevation differences but this time by latitudinal differences are the higher STD values in Italy than in Germany.

Comparing the simulated moving STD time-series with the observed ones depicts in general a high correlation on all scales - short as well as long term variabilities seem to be well represented. The deviation between simulated and observed CF STD is typically between -1 and +1% CF with a maximum deviation of 2%. The strong annual cycle is probably the main driver for the high explained variances shown in Fig. 5.9. Nevertheless, also shortest visible variations in Fig. 5.10, which are on the scale of daily variations, show high correlation. Thus, the figure implies also for this short scale variations and all scales up to annual scales a high grade of explained CF variability characteristics.

5.3.2.4 Summary and discussion

The estimated CF of PV from COSMO-REA6pp is shown to have systematic biases compared to observations but high values of explained variance. In terms of variability COSMO-REA6pp derived calibrated CFs are found in high compliance with the reference time-series. With high values of explained variance (>89% for most countries) and a visual evaluation of CF time-series it could be concluded that daily up to annual variations are well represented. This provides a solid basis for the subsequent investigation of spatial balancing effects in Sec. 5.3.3.

Considering biases of the derived CF product the relative bias per country was found to vary between -14% and +46%. Finding the reason for the systematic biases between COSMO-REA6 based CF estimates and OPSD measurements is a difficult task. Possible reasons for the systematic CF biases are manifold:

- I Simulated power plant distribution within a country differs from the real distribution
- II Real-world PV module orientation differs significantly from the simulated ones
- III COSMO-REA6 input variables for the PV estimate may have area specific biases
- IV PV-reference data have unknown uncertainties

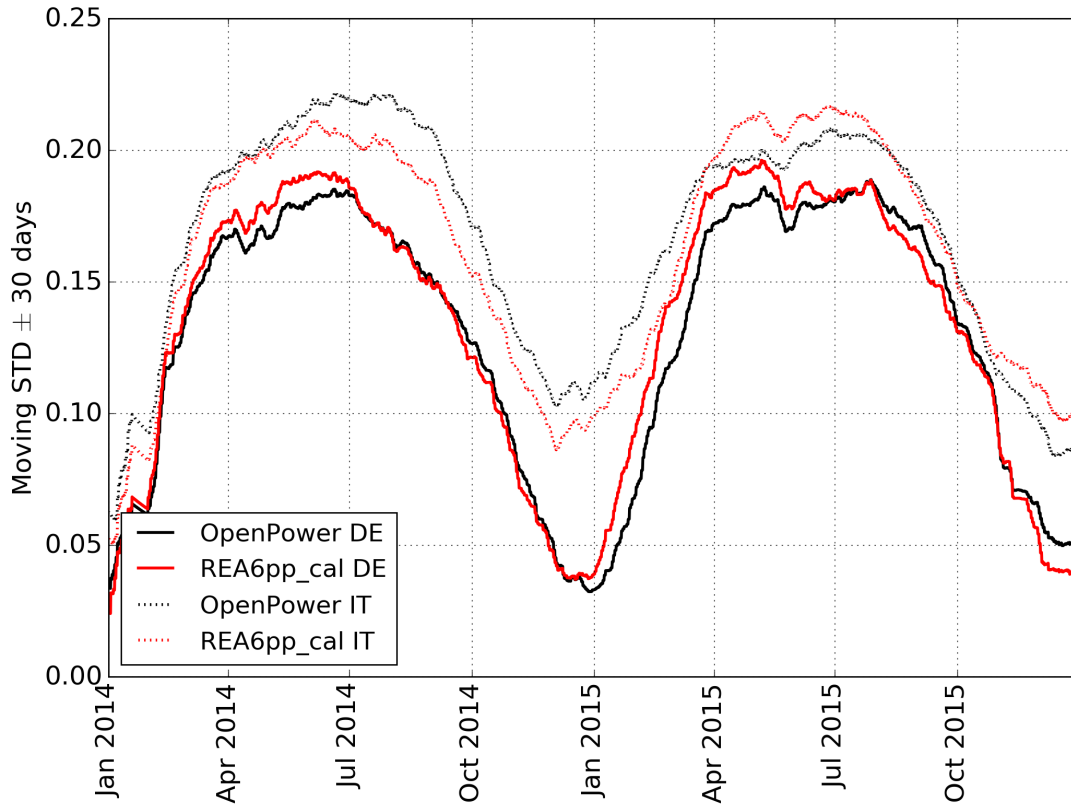


Figure 5.10: Moving standard deviation of OPSP provided CF time-series and of calibrated COSMO-REA6 derived PV CFs for Italy and Germany. Based on hourly time-series of country aggregated CF values.

Most of these possible reasons have been addressed within the scope of this thesis. In order to reduce the effect of different power plant distributions in simulation and reality (I) a power plant register from Wiki-Solar is used. Nevertheless, by providing only large-scale power plants with installed capacities $>4\text{MW}_{AC}$ there is space for improvement here. Especially the large amount of privately installed PV power plants on rooftops are expected to have a considerable impact.

(II) With respect to the module orientation COSMO-REA6 based optimal tilt angles multiplied by 0.7 are used (for more detail see Sec. 2.2.1). Although Küchler [2018] found that the aggregated PV power yields are only slightly sensitive on the exact module orientations (roughly $0.1\% \text{deg}^{-1}$ close to the optimal tilt angle) for short scale and individual areas this aspect might have significant influences. The recent publication of Saint-Drenan et al. [2018] found appropriate relations between optimal and real-world orientations. Unfortunately, they are typically reduced to individual countries and do have only a very small reference set of real-world PV orientations. The most effective way to close this gap would be a publicly available list of all installed PV modules complemented by their orientation.

(III) Biases in the COSMO-REA6 input variables for the conversion scheme are specifically addressed in this thesis. On the one hand COSMO-REA6 underestimates GHI during clear sky situations due the usage of an optically too thick aerosol climatology, and on the other hand it overestimates due to either too few or optically too thin clouds (Sec. 3). In order to reduce the systematic biases a post-processing for GHI but also for direct and diffuse radiation components are developed and applied. Although the post-processing yields clear improvements for PV power estimates, some biases remain. Here, further improvements in the reanalysis are necessary to meet the requirements of the energy industry.

(IV) The problem with the reference data of PV generation is the lack of uncertainty information combined with the diversity of data providers. Most providers cover different areas/countries and use individual methods to monitor/estimate the real-world productions. Thus, uncertainties depending on source and country are expected but no estimates of those are available. A comparison of different sources show large differences implying high uncertainties even up to the country aggregates (not shown here). Therefore, for the study on hand installed capacities listed by EUROSTAT ⁷ only are used. This guarantees at least a uniform data control and estimate procedure of the used reference data. Nevertheless, with respect to the country-specific biases found in this study, the usage of PV-observations with unknown uncertainties might result in misleading results and conclusions. On the way to an optimized European energy transition it is highly recommend to develop a cross-border and uniform monitoring procedure of real-world generation including accurate uncertainty estimates.

Nevertheless, despite the problems with reference power data, in this study the common practise in literature is followed and thus a country based calibration to COSMO-REA6 estimates applied. A comparison of the calibrated and uncalibrated CF estimates with reference data depicted a significant improvement due to the calibration procedure. Here, bias, RMSE, and EMD improved significantly for dependent but also for independent years. With the aim to investigate cross-border PV-extremes, it was decided to apply the calibration also to the long-term simulation (evaluation run) used in Sec. 5.3.3.

5.3.3 Balancing effects and potentials of hybrid wind-solar production

Building up on the radiation post-processing (Sec. 3 and Sec. 5.2.2), the described PV-conversion scheme (Sec. 2.2), and the gained knowledge on how reliable COSMO-REA6 represents PV (Sec. 5.3.2.1) and wind power characteristics (4) in this section European balancing effects of PV and wind power estimates are investigated. Therefore, a long-term simulation (evaluation run) over 20 years (1995-2014) of PV and wind power is used (see Fig. 5.3). In order to investigate the balancing potentials without influences from varying power plant installations in history the main assumption in the evaluation run is a fixed plant installation

⁷<https://ec.europa.eu/eurostat/de/home>

Table 5.6: Pearson correlation between wind- and PV power calculated for daily and hourly CFs. Compared are the country aggregated CFs between 1995 and 2014. Aggregations are performed based on the installed wind fleet end 2014 and the installed PV fleet end 2018.

	R daily	R hourly
BE	-0.38	-0.16
BG	-0.34	-0.05
CZ	-0.34	-0.06
FR	-0.38	-0.04
DE	-0.37	-0.08
GR	-0.13	0.05
IT	-0.25	0.10
PT	-0.31	0.01
RO	-0.22	-0.10
ES	-0.27	0.03
GB	-0.35	-0.08

over the whole simulation time span. For a more detailed description of the construction of the evaluation run the reader is referred to Sec. 5.2.5.

5.3.3.1 Inland balancing

A first important question is which countries do benefit from compensating effects when adding PV generation to wind power. A simple indicator for a beneficial compensation effect is a negative correlation between the wind- and PV power within the considered country (see Tab. 5.6). Analyzing daily mean CFs of 20 years shows for all considered European countries significant negative correlation factors and thus beneficial compensation effects. Countries benefiting most are BE and FR with -0.38 followed by DE with -0.37 on daily scale. With a correlation coefficient of -0.13 the weakest balancing effects occur in GR followed by RO and IT with -0.22 and -0.25, respectively. In summary, the results indicate the highest potential of beneficial wind-solar balancing effects for the northern European countries.

Analyzing the correlation between hourly wind and PV time-series of CFs shows a significantly decreased balancing potential. In IT, GR, ES and PT, wind and solar generation even correlate positively. The reason for the large differences between daily and hourly correlations is the consideration of variations on different temporal scales. For the daily correlations synoptical and annual variations are expected to dominate the results. For hourly correlations the diurnal cycle and local cloud effects become most prominent. Thus, typical day to night variations in wind production are increased by adding PV power. Nevertheless, on daily to annual scales the correlations indicate beneficial smoothing effects. For simplicity and the higher balancing potential on the daily scale in the following questions only daily mean CFs are considered.

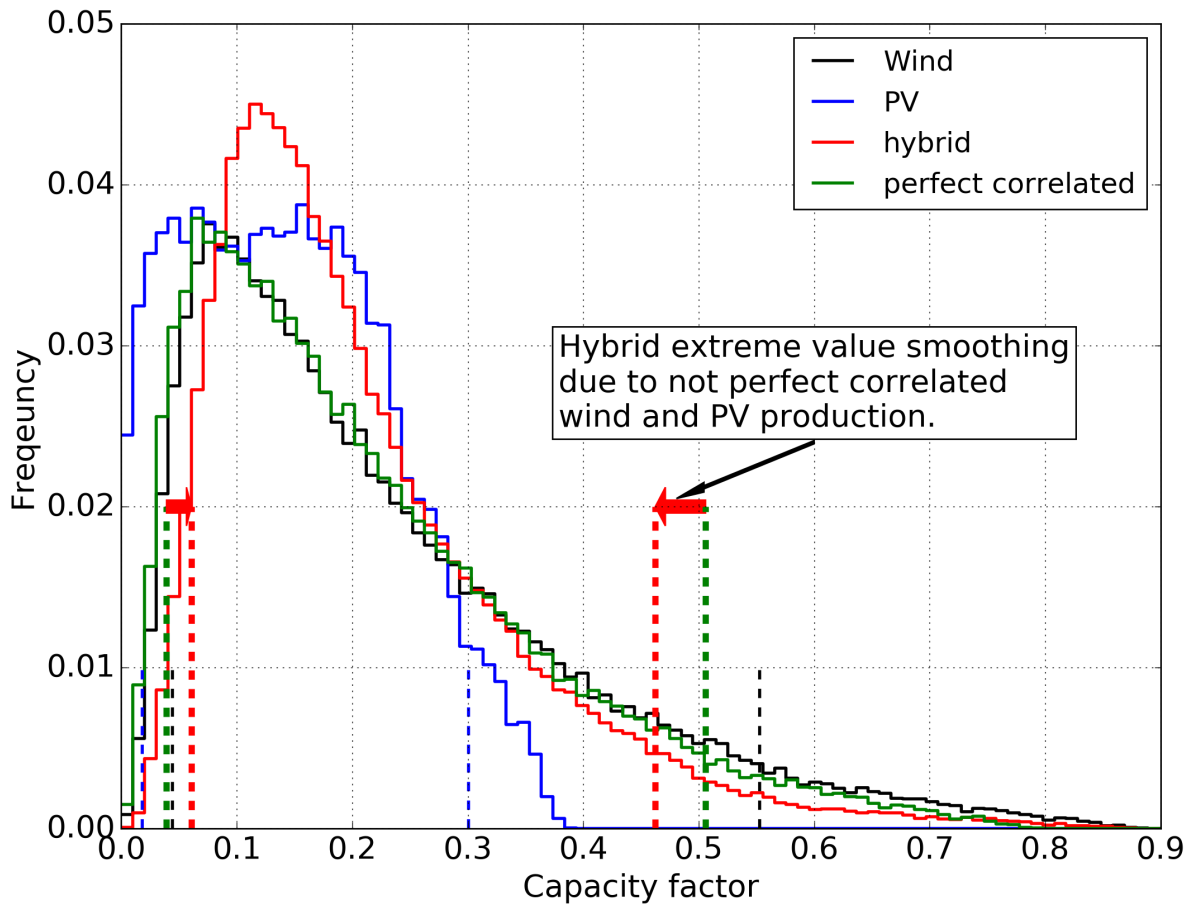


Figure 5.11: Frequency histogram of daily mean CF from wind-, PV-, hybrid wind-solar, and a theoretical scenario with perfect correlated wind and PV production for whole Europe. Vertical dashed lines illustrate the 5th and 95th percentiles. The histograms are based on the simulation of real-world listed power plants comprising 20 GW installed capacity of PV and 76 GW installed capacity of wind power.

A second important question is how extremes of the individual productions by either wind or PV power can be smoothed by hybrid wind-solar power production. One approach to answer this question is to track the changes of the 5th and 95th percentile of the CF distribution when combining wind and PV production. A smoothing would then lead to an increase in the 5th- and a decrease in the 95th percentile. Illustrated for Europe (Fig. 5.11), the 5th percentile increases from the individual 5th percentiles 0.044 and 0.018 for wind and PV, respectively to 0.061 in the hybrid wind-solar production scenario. A further step necessary to quantify the smoothing due to decorrelations of wind and PV power is to relate the hybrid 5th percentile (0,061) to the 5th percentile of a hybrid scenario where no smoothing between wind and PV occurs (the perfect correlation scenario). The exact position of the 5th percentile in the perfect correlation scenario can be calculated by a capacity weighted averaging of the individual 5th percentile of wind and PV. Thus, for Europe the benefit due to decorrelation is an increase of the 5th CF percentile

by 2.2% and an decrease by -4.3% in the 95th percentile (see red arrows in Fig. 5.11). In order to illustrate the distribution changes for all European countries in a concise format only the 5th and 95th percentiles complemented by the benefit values are shown next.

An overview of the extreme thresholds of the CF distributions - 5th and 95th percentiles - per country shows the minimum thresholds of PV and wind ranging between 0.6 - 7.0% and 2.7 - 7.6%, respectively (Fig. 5.12a and 5.12c). The main reason for the general lower PV thresholds compared to those of the wind is the lack of PV production during the night. For PV, the minimum extremes weaken with increasing latitude which is in line with the general higher sun position in the south. The wind minimum thresholds show the expected relation of less extreme values close to the coast.

Analyzing the benefits of the hybrid wind-solar thresholds due to decorrelations show the CF minimum thresholds increased by an absolute value between 0.1 up to 3.7% per country (Fig. 5.12e). Since the hybrid production scenario relies on a specific fleet scenario (Sec. 5.2.5) Fig. 5.12e is complemented by the ratio of installed PV capacity divided by the hybrid installed capacity per country. As expected balancing benefits are related to the ratio of PV and wind installed capacities. For the eleven considered countries a Pearson correlation between the benefit values and the installation ratios of 0.85 is found. Country-to-country threshold variations not explained by the installation ratio obviously depend on the area specific varying balancing potential of wind and PV production. Nevertheless, given the specific fleet scenario with the shown ratios most prominent extreme reductions occur in BG, CZ, and FR with absolute CF 5th percentile increases of 3.7, 3.3, and 3.2%, respectively.

The maximum thresholds of PV ranges between 18 to 36% (Fig. 5.12b). In accordance with the north-south gradient of weakening minimum extremes the maximum extremes increase towards the south. For the maximum thresholds the north-south dependency is less pronounced than for the minimum threshold. An interesting issue is the low maximum threshold of IT being very similar to that of Germany. This issue might be a result of not treated Saharan dust events in the COSMO-REA6 reanalysis (already discussed in 5.3.2.1). The maximum thresholds of wind power vary between 44 to 68%. As expected, with mainly westerly flow in Europe highest 95th CF percentiles occur at the Atlantic Ocean. Considering the hybrid wind-solar CF maximum thresholds show the balancing benefit per country varying between -0.19 and -10.6%. Here, a Pearson correlation between the installed capacity and the benefit values of 0.98 is found. Highest reductions occur for CZ and GB with -10.5 and -5.2%, respectively.

After analyzing to what extent the extremes of the individual countries weaken due to hybrid generation with the "current" installed power plants, the question arises what the maximal weakening would be under a theoretical best installation ratio of PV and wind and what the installation ratio would be. Assuming the same power plant portfolio but with scaled installed

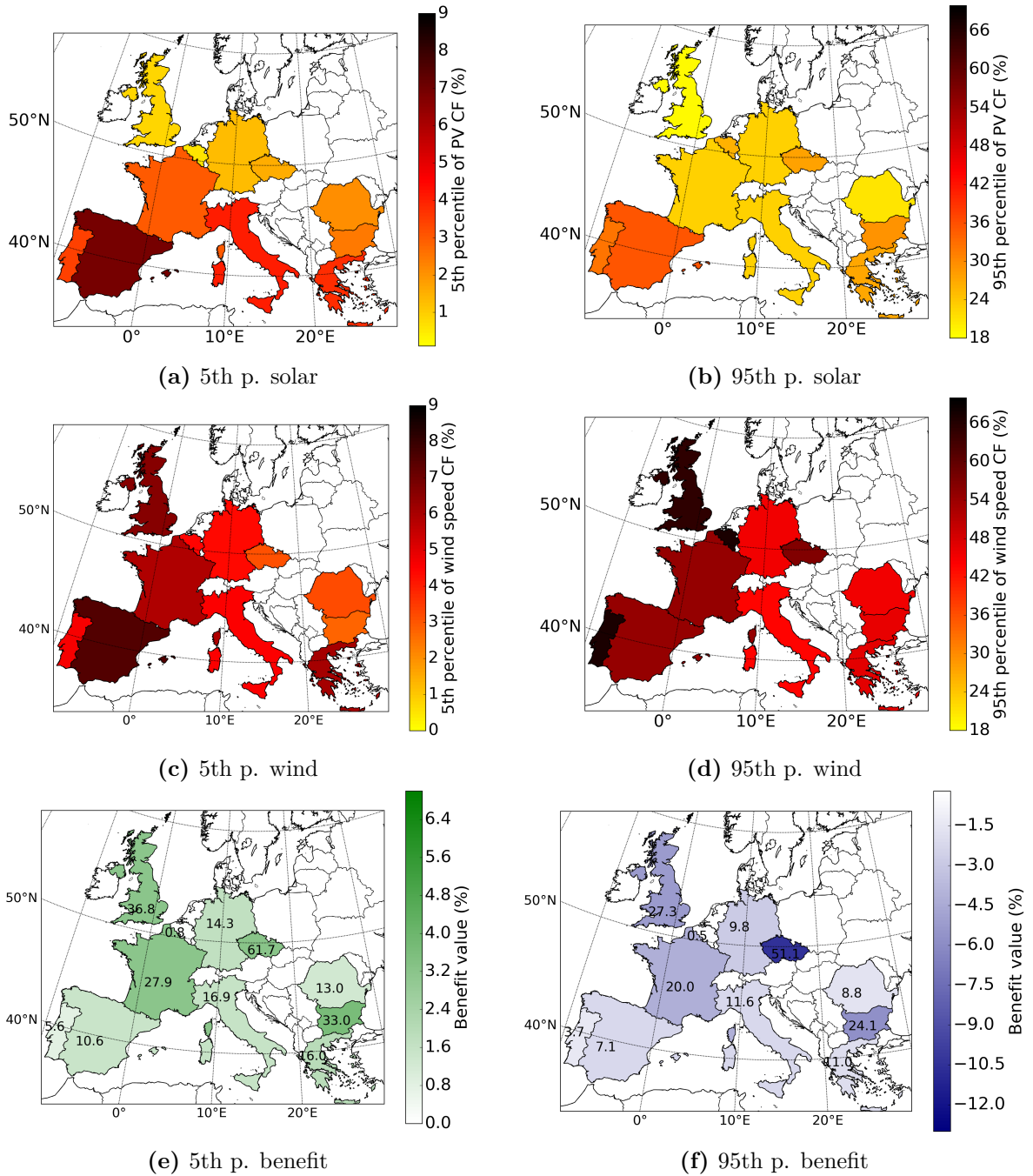


Figure 5.12: Overview of 5th (left) and 95th (right) percentiles of daily PV (top) and daily wind power CFs (middle). The last row shows the benefit values (benefit due to balancing effects between wind and PV) expressed in absolute CF value changes. The numbers in (e) show the ratio of installed PV capacity relative to the total installed capacity of wind plus PV. The numbers in (f) represent the corresponding ratio of PV power production relative to the combined production of wind plus PV.

capacities an optimum ratio is calculated by maximizing the sum of the benefit for the 5th and 95th percentile (Fig. 5.13).

Results show the optimized benefits of the minimum threshold vary between 2.65 (DE) to 5.95% (PT) per country. Optimized benefits in terms of reducing maximum extremes vary between -4.81 (GR) to -12.18% (BE). Interpreting this benefits with respect to the CF distribution width, the distance between the 5th and 95th percentile, of the perfect correlated hybrid scenario this benefits indicates optimized Distribution Width Reductions (DWR) of 29 to 42% due to natural decorrelations (Fig. 5.13c). With other words, variability reduction potentials of hybrid wind-PV production caused by decorrelations between wind and PV power vary between 29 to 42% per country. Considering the spatial distribution of the DWR potential indicates the potential variability reductions due to decorrelations being highest in northern countries of Europe. Relating the optimal installed DWR potentials further to those connected to the "current" ratios provides for each country the individual CF DWR remaining potential yet not made use of (5.13d). Thus, this shows remaining DWR potentials of 20 (BG) up to 42% (BE), except for Czech Republic with 7%.

The installation ratios in the theoretical best installation scenario, again PV over hybrid installed capacities, vary between 57 - 68% (Fig. 5.13a). Expressed in generation ratios this corresponds to about 45-57% of total power generation by PV and the rest by wind power (Fig. 5.13b). In general, spatial correlations of the optimized quantities hardly seem to exist. Only the generation ratios appear to be linked to latitude. The share of PV needs to be higher in the north than in the south. The reader should be aware that although the balancing effects are maximal in this optimized scenario, the absolute generation variation of this hybrid wind-PV scenario can still be higher than in another ratio scenario. This is caused by the differing absolute variability of wind and PV itself which is not considered in the applied optimization scheme.

5.3.3.2 Cross-border balancing

In this section it is aimed to answer the question whether specific countries do especially benefit from the hybrid production of other countries. This can be investigated with e.g. the help of correlation coefficients of power production time-series between the countries. If the correlations between countries decrease when changing from production time-series of either wind or PV to hybrid-production time-series the countries are expected to profit from increased balancing potentials, and if the correlations increase the countries are expected to have degraded balancing potentials.

The correlations between the country-to-country CF time-series (20 years with daily resolution) of the wind power, complemented by the correlation changes due to adding PV power are depicted in Fig. 5.14. Before discussing the effect caused by adding PV power to the wind

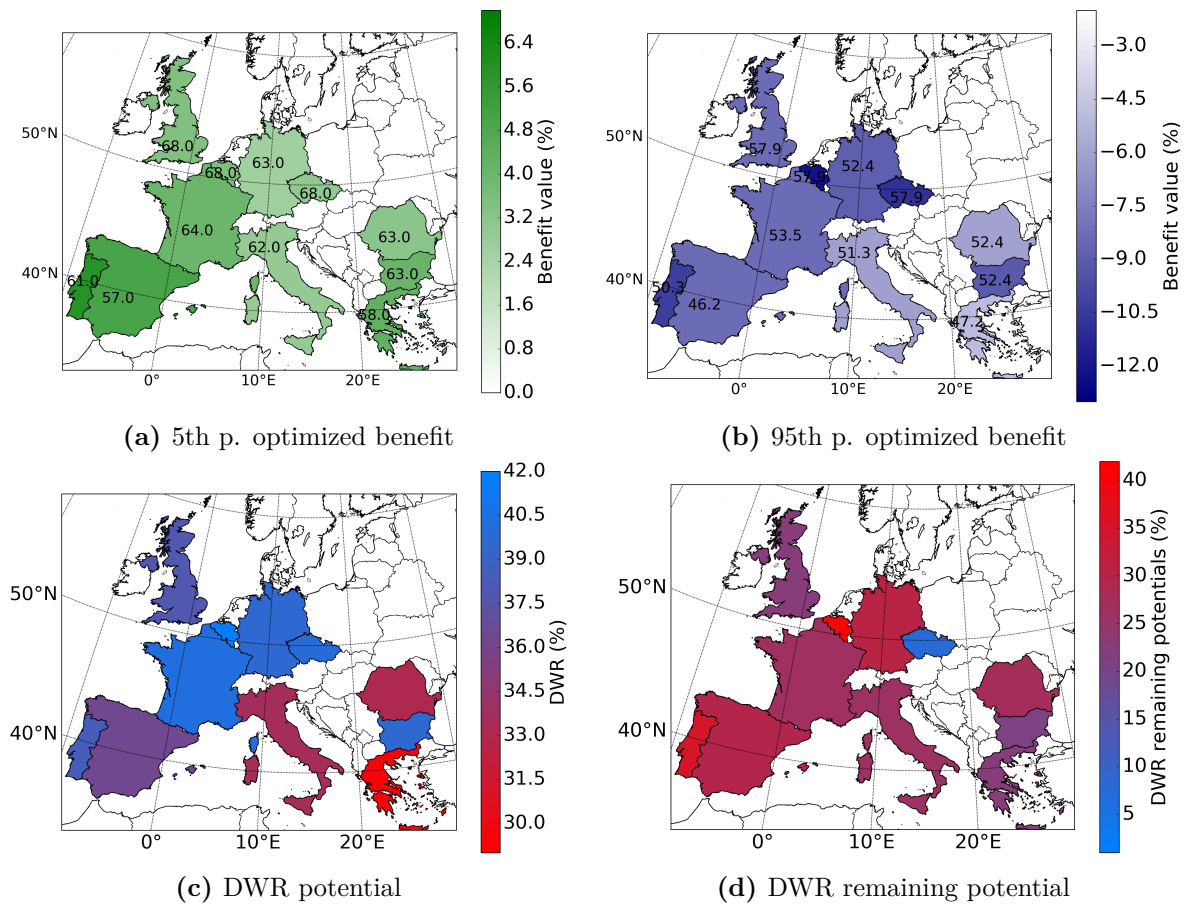


Figure 5.13: Results of an optimized balancing scenario between daily wind and PV production. Here, the wind to PV capacities are varied in order to maximize the summed 5th and 95th percentile benefit values. Fig. (a) and (b) depict the resulting 5th and 95th percentile benefit values, again in absolute CF numbers. Fig. (c) shows the distribution width reduction of the hybrid wind-PV CF distribution relative to the perfect correlated hybrid wind-PV scenario. Fig. (d) relates the findings of (c) with the current installation ratio and shows remaining DWR potentials of the individual countries. Numbers in (a) show the optimal installation ratios. Numbers in (b) give the corresponding ratio of PV power production relative to the combined production of wind plus PV.

power, here the wind power correlations are discussed first. As expected high wind balancing potentials occur in general for countries with higher spatial distance. Even slightly negative correlations are found between GR with BG, FR, DE, CZ, PT and ES. Probably mainly driven by the different role of the westerly flow in middle Europe compared to the countries southward the Alps. Lowest balancing potentials are found for DE with CZ with a correlation of roughly 0.75.

Considering the correlation changes when adding PV to wind production shows for most countries no or slightly increased balancing potential. Country combinations that benefit the most are CZ-BE, CZ-DE, and CZ-FR with -0.26, -0.24, and 0.2, respectively. The reason for the high

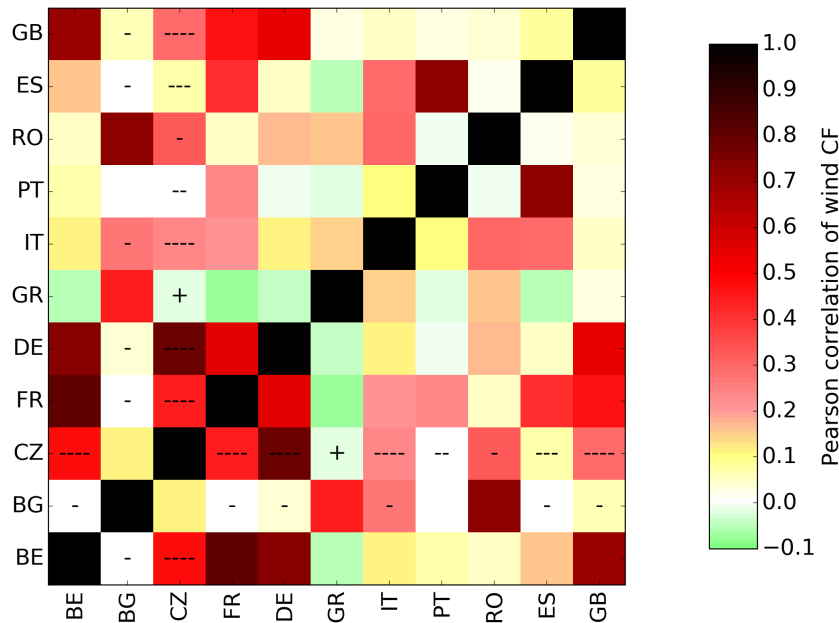


Figure 5.14: Pearson correlation coefficients of daily wind CF between all considered countries. Minus and plus signs illustrate decreasing and increasing correlation coefficients when considering hybrid wind-PV generation compared to wind generation only. No sign illustrates a correlation change below 0.04, one sign a change between 0.04 to 0.08, two signs between 0.08 to 0.12, three signs between 0.12 to 0.16, and four signs a change larger than 0.16. The hybrid correlation coefficients rely on the "current" ratios of wind to PV installations.

benefits for Czech Republic by adding PV power is the high share of PV in CZ. This high share leads to significant changes of the wind power CF time-series when adding PV power. Consequently, the decorrelation of wind with PV dominates when comparing the PV dominated CF time-series of the Czech Republic to countries where the hybrid-CF generation is dominated by wind power (see installation ratios in Fig. 5.12e). The cross-border balancing effects would be different if the total production of wind and radiation per country was equal. In this case, the generally decreasing correlation with increasing distance of hybrid products would determine the cross-border balancing potential. A result of this effect might be seen for example between GB and BG where installation ratios are very similar but due to their distance the balancing potential increases when adding PV to wind power.

The last question addressed is which countries are particularly suited to balance the extremes of other countries. Therefore, the Simultaneous Occurrence Probability of Extremes (SOP) from country-to-country is analyzed. The general idea is that countries with a low number of simultaneous extremes have high balancing potentials. In order to analyze the changes of balancing potentials between countries when combining wind and PV generation the SOP of extremes between the countries are investigated once for PV generation only, once for wind generation only, and once for wind in the one and PV generation in the other country (Fig.

5.15). Again, the 5th and 95th percentiles of the CFs are used to define country specific extreme situations. An advantage of this methodology is that results are completely independent from installation ratios.

The SOP of PV power minima (Fig. 5.15a) vary from country-to-country between 21 and 61%. As expected, nearby countries do have the highest correlations and thus the lowest potential for balancing during extreme minimum production situations. Nevertheless, except three country combinations, RO-BG, DE-CZ, and ES-PT, all other joint probabilities are lower than 40.7%. Minimum values and therefore highest balancing potentials occur between PT-BG, PT-BE, IT-BG, and IT-BE.

Considering the SOP of wind power minima (Fig. 5.15c) best balancing potentials are found for the country combination PT-BG where the SOP reaches only 2.73%. A noticeable deviation from this low SOP can only be seen for the country combination RO-BG which has a SOP value of 42%. When comparing the joint probabilities of PV minima (Fig. 5.15a) with those of wind minima (Fig. 5.15c), wind minima are found to have a significantly lower probability of simultaneous occurrence. The reason for this effect is probably connected to the amplitude of daily production variability relative to the annual cycle amplitude of the individual power types. In case of PV, a low ratio would cause just a small sub-sample of winter days when absolute minimum situation would be possible. Thus, the simultaneous probability occurrence increases by nature.

Considering the simultaneous occurrence probability of wind power minimum situation with PV minimum situations (Fig. 5.15e) a completely different compensation relation from country-to-country occurs. Here, an evident relation of the SOP between northern and southern country becomes visible. Lowest SOP values of only 4% and less are found for the combination of (1) northern country wind minima with southern country PV minima and (2) for all countries PV minima with northern wind minima. With other words, northern wind minima can often be balanced by southern PV production, and all countries PV minima situations can often be balanced by northern wind production. The reasons for this particular suited combinations are most likely the typical annual cycles of wind speed and solar irradiance. In northern countries wind minima are most likely to occur during summer when high pressure systems prevail. Thus, there is a high likelihood that there is no minimum of annual PV production in southern countries and thus the northern wind minima can be balanced by southern PV production. The second case can be explained by the general high likelihood of PV minimums during winter due to the sun elevation angle combined with the low probability of wind minima during the northern winter.

The SOP of high extremes in PV (Fig. 5.15b) is very similar to that of PV minimum extremes. Country combinations with high probability of simultaneous minima do usually also have a high

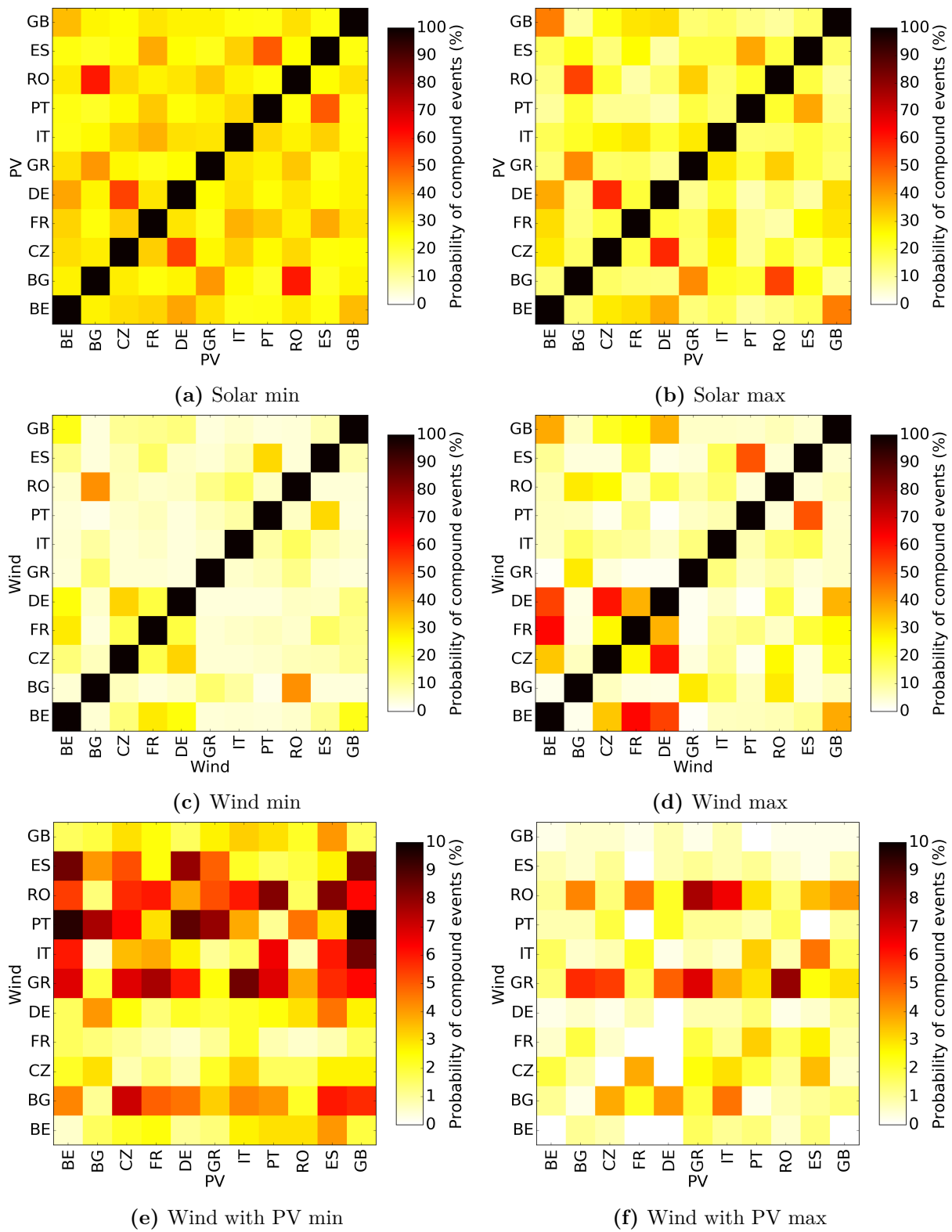


Figure 5.15: Joint probability of low (left), and high CF extremes (right) between European countries. The basis provide daily country-aggregated PV and wind power simulations based on COSMO-REA6.

probability for simultaneous maxima. Nevertheless, country-to-country minimum situations occur more often simultaneously (mean value 30%) than maximum situations (mean value 21%). Minimum situations occur mostly in winter months when large-scale weather conditions dominate the PV availability. In summer, smaller circulations play a greater role, which reduces the spatial correlation of the PV maxima and thus the simultaneous occurrence. Probably for the same reason of dominating weather circulation differences of winter and summer, also the probability of simultaneous wind maximum situations (Fig. 5.15d) is found to be slightly higher compared to that of simultaneous wind minimum situations. Highest probabilities reach about 60% for DE-BE, DE-CZ, and BE-FR. Lowest probabilities are close to 2%, particularly often in combination with GR.

Considering the SOP of wind maximum situations with PV maximum situations (Fig. 5.15f) shows in principle relative low probabilities mainly below 3%. Only combinations with RO and GR have higher values up to 8%. Thus, in these two countries maximum wind extremes seem to appear relatively often during summer time when PV maximum values occur. In terms of high balancing potentials with respect to being balanced by wind production of other countries when a PV maximum occurs is DE. Here, 4 to 5 country connections with Germany are found to have a SOP smaller than 1%.

5.3.4 Discussion

Since there are hardly any studies that deal with the hybrid and transnational balancing effects of wind and solar power in Europe, only parts of this study can be compared and related to other work. Roques et al. [2010] analyzed balancing effects between five European countries based on historical hourly wind generation time-series. They found a high balancing potential between northern and southern European countries with even negative correlation between Germany and Spain. With negative correlations even on daily scale between e.g. Germany and Greece, the special balancing potential between north and south can not only be confirmed, but even completed on a further time scale.

Heide et al. [2010] investigated the optimal mix of PV and wind for Europe with the boundary condition to fit the demand. They find for whole Europe based on an eight year time-series (2000-2008) an optimal mix of power generation being 45% solar and 55% wind power. Unfortunately, a direct comparison to the findings in the study on hand are not possible, since optimal mixes are calculated only for every individual country in Europe and not for Europe as a whole. However, for the individual countries optimal mixes of 46-57% solar and the rest wind power are found. The reason for the difference is expected to be simply in the different optimization approaches. While Heide et al. [2010] optimized in order to reduce hybrid generation differences to an European load curve, the applied approach in this study optimizes in order to reduce the occurrence of hybrid extreme situations without the consideration of load curves. The fact that

the European annual load curve varies in the same phase with annual wind power generation simply increases the share of wind power in Heide et al. [2010]. To our best knowledge, most of the more recent studies investigated the wind-solar ratios for scenarios of e.g. 50% share from renewable energies complemented by conventional produced power and storage. Here, very different ratios of optimal shares are found. In terms of installed capacity ratios, e.g. Tafarte et al. [2014] found in the 50% renewable scenario an optimal ratio of 66% solar and 34% wind. In contrast, Zappa and van den Broek [2018] found in the scenario of 82% renewable energy penetration an optimal ratio of 26% solar and 74% wind. The study on hand adds to this discussion that country specific extreme situations of European countries are optimally balanced for installation ratios of 58-68% solar and 32-42% wind, independent from alternative generation technologies. Thus, with respect to the introduction these installation ratios are expected to be that ratios with the lowest need for backup capacities from conventional power plants.

At this point it should be mentioned that these estimates of optimal installation ratios depend directly on the applied and defined optimization criterion. The applied criterion in this study is to minimize the distribution width of hybrid wind-PV productions. Thus, the criterion optimizes by considering simultaneously both, the smoothing of minimum as well as the smoothing of maximum extremes. If, for example, finding the optimal ratio for maximizing the balancing effects in minimum (drought) situations is of interest, the resulting ratios might be significantly different. Investigations on the resulting differences when considering slightly different optimization criteria might be helpful to understand the sensitivity of the optimal installation ratios on this issue.

5.4 Conclusion

The study on hand contributes one further step to shed light on European wind-solar balancing potentials in Europe. Therefore, the recent regional reanalysis COSMO-REA6 is used. By providing long-term and physically consistent meteorological input variables for renewable power estimates, reanalysis are particularly suited when investigating derived joint distributions of wind- and solar power.

With the aim to estimate most reliable PV power estimates based on the reanalyses radiation components and the knowledge of systematic biases in the summed radiation component field (GHI) of COSMO-REA6 (see Sec. 3), first a post-processing for the individual radiation components has been developed. Although PV estimates based on the post-processed components are found to provide improved CF distributions compared to estimates based on the original reanalysis, still country based biases remain. To correct also for the remaining CF biases simple CF scaling factors per country have been derived. Therefore, simulations have been compared to historical observed CF time-series of the year 2015.

With the need of long-term time-series when analyzing production characteristics and balancing potentials of wind and PV, for this issue the so called evaluation run has been conducted. Based on the post-processed COSMO-REA6 reanalyses in the evaluation run PV estimates are simulated for 20 years. Therein, in order to avoid to analyze variability characteristics induced due to power plant installation changes a fixed power plant distribution of 2018 has been used. Final evaluations of balancing are then based on the country aggregated daily average CF time-series which are calibrated with the previous found scaling factors for 2015.

COSMO-REA6 based wind power CF time-series are those obtained from Henckes et al. [2018]. The provided time-series is generated for a fixed power plant distribution which was active end 2014. Also Henckes et al. [2018] applied a country based calibration.

Given these two 20 year time-series (wind- and PV capacity factors) for most European countries once the balancing potentials between wind and PV power within each country, and once the balancing potentials cross-border are investigated. For both insights a special focus was set to balancing of extreme production phases.

Main findings are:

- The developed post-processing of the COSMO-REA6 radiation components improves the distribution of PV estimates.
- Assuming OPSD data as truth, also high resolution regional reanalysis derived PV estimates need bias corrections, at least on country scale.
- Temporal variations of country aggregated PV estimates are shown to be realistically represented, at least on daily up to annual scale. Here, explained variances of PV estimates based on COSMO-REA6pp reach values up to 94%.
- For all European countries significant negative correlations for daily wind and PV generation time-series are found, slightly more prominent for the northern European countries. Thus, on daily scale all European countries have the potential for beneficial wind-solar compensation effects.
- With respect to extremes, balancing potentials of wind and PV production differ strongly from country-to-country, mainly forced by the installed wind-to-PV installation ratio.
- The balancing potential of extremes due to the decorrelation of wind- and PV generation per country is a noteworthy effect, e.g. the 5th percentile of CF increases due to balancing effects in absolute numbers between 2.7 and 5.9% per country, at least in an optimal installation scenario. The CF value of the 95th percentile reduces between -4.8 and -12.2% per country.

- Potential variability reductions of hybrid wind-PV production caused by decorrelations between wind and PV power vary between 29 to 42% per country.
- Simultaneous extremes of wind in the one and PV in the other country are rather small (<10%). Indicating high potential for cross-border balancing.
- Northern wind minima can often be balanced by southern PV production (joined probability of simultaneous wind-PV extremes is <4%), and PV minimum situations in all European countries can often be balanced by northern wind production (joined probability of simultaneous wind-PV extremes is <4%).

With regard to research suggestions, further investigations on intra-day scale are recommendable. Thus, with respect to e.g. PV power daily cycle effects induced by the sun position and local cloud effects come into play. A reasonable approach to investigate balancing potentials on the intra-day scale might be to start with PV CF values normalized on the sun elevation. This approach provides the opportunity to characterize the production characteristics and balancing potentials induced by clouds only.

Reanalyses have a great potential to characterize the generation variability of renewable energies. With the opportunity to derive realistic multi-year power simulations based on reanalyses they are prerequisite for current state analysis and also for future planning steps of the electricity system. While the explained variance on aggregated scales already reaches high values of roughly 90%, systematic biases can still be quite high. Thus, further improvements of reanalyses in terms of representing renewable related variables are desirable, especially in terms of absolute values. However, in the field of balancing effects, where variabilities of wind power and PV are the central quantity of interest, reanalyses provide unique opportunities.

5.5 Annex

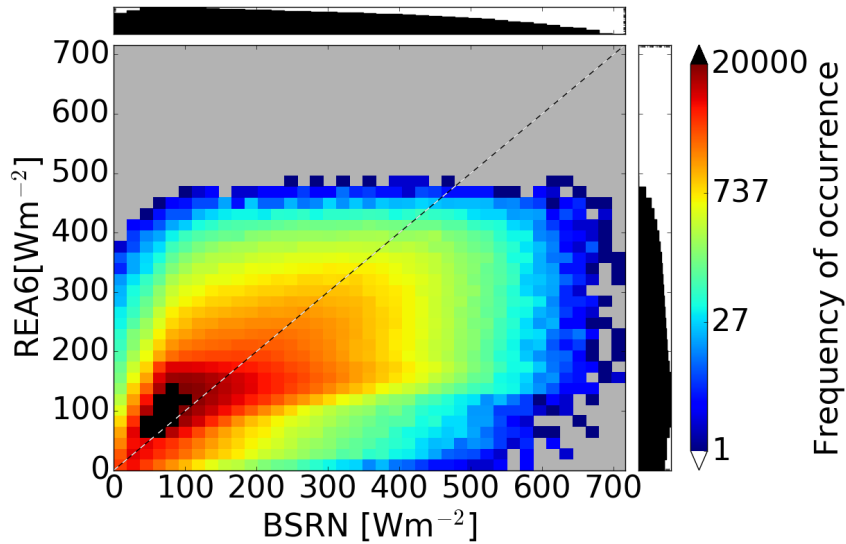


Figure 5.16: Joint distribution of diffuse horizontal irradiance provided by BSRN and COSMO-REA6. Considered are measurements at eight BSRN sites. The contribution of the number of data from the individual stations is shown in Tab. 5.2.

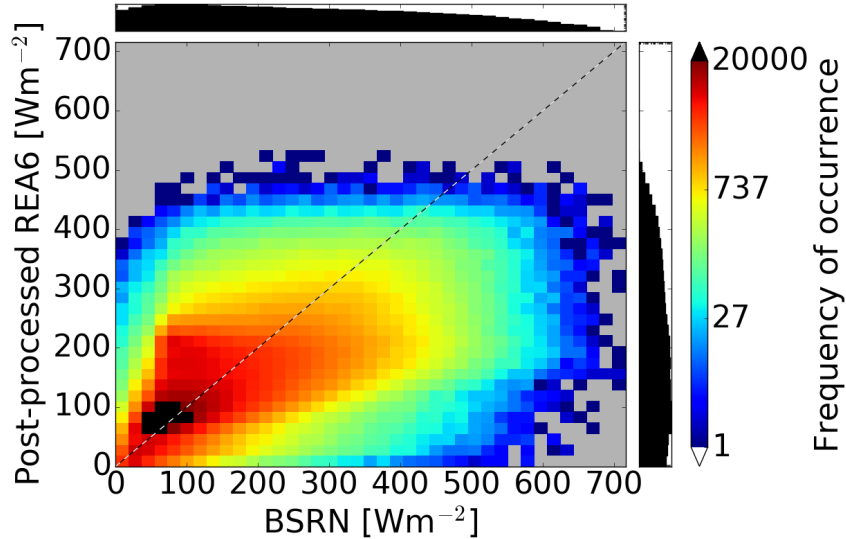


Figure 5.17: Joint distribution of diffuse horizontal irradiance provided by BSRN and COSMO-REA6pp. Considered are measurements at eight BSRN sites. The contribution of the number of data from the individual stations is shown in Tab. 5.2.

Table 5.7: Same as Tab. 5.1 but for clear sky situations only (both GHI transmissivity values -observed and reanalyzed - are simultaneously above the threshold 0.5).

			COSMO-REA6		COSMO-REA6pp	
	Station name	N values	BIAS	MAE	BIAS	MAE
LIN	Lindenberg	59774	-22.95	87.09	18.98	81.69
CAM	Camborne	47115	-2.28	100.46	46.40	102.40
CAR	Carpentras	138175	-78.28	109.55	-35.07	84.62
CNR	Cener	33882	-69.26	112.05	-28.79	93.24
CAB	Cabauw	35721	-16.66	88.04	28.51	86.80
PAL	Palaiseau	35521	-29.40	94.46	14.79	86.55
TOR	Toravere	53589	-63.54	88.13	-33.82	73.08
PAY	Payerne	71481	-53.71	93.64	-20.06	79.77
All	All sites	475258	-49.50	98.45	-8.85	84.91

Table 5.8: Same as Tab. 5.2 but for clear sky situations only (both GHI transmissivity values -observed and reanalyzed - are simultaneously above the threshold 0.5).

			COSMO-REA6		COSMO-REA6pp	
	Station name	N values	BIAS	MAE	BIAS	MAE
LIN	Lindenberg	59774	-18.33	53.70	-16.41	57.45
CAM	Camborne	47115	-32.58	68.14	-35.97	73.57
CAR	Carpentras	138175	24.82	58.38	28.03	63.35
CNR	Cener	33882	14.36	61.49	21.42	69.49
CAB	Cabauw	35721	-25.48	56.09	-27.22	61.42
PAL	Palaiseau	35521	-12.73	55.97	-11.90	60.28
TOR	Toravere	53589	21.12	46.29	35.79	58.13
PAY	Payerne	71481	2.44	50.61	16.47	60.01
All	All sites	475258	2.59	56.10	7.62	62.59

Table 5.9: Same as Tab. 5.1 but for cloudy sky situations only (both GHI transmissivity values -observed and reanalyzed - are simultaneously below the threshold 0.5).

			COSMO-REA6		COSMO-REA6pp	
	Station name	N values	BIAS	MAE	BIAS	MAE
LIN	Lindenberg	91886	17.69	24.25	10.94	19.03
CAM	Camborne	72483	19.31	25.08	12.42	19.39
CAR	Carpentras	59010	18.13	28.18	9.62	22.12
CNR	Cener	23981	15.99	26.04	8.40	20.49
CAB	Cabauw	63626	14.55	23.37	8.29	18.62
PAL	Palaiseau	49965	16.72	26.45	9.45	20.88
TOR	Toravere	75198	11.72	18.60	6.98	14.99
PAY	Payerne	47340	27.59	34.22	17.77	26.18
All	All sites	483489	17.43	25.15	10.42	19.74

Table 5.10: Same as Tab. 5.2 but for cloudy sky situations only (both GHI transmissivity values -observed and reanalyzed - are simultaneously below the threshold 0.5).

			COSMO-REA6		COSMO-REA6pp	
	Station name	N values	BIAS	MAE	BIAS	MAE
LIN	Lindenberg	91886	-1.49	48.66	-10.95	47.97
CAM	Camborne	72483	-10.95	58.07	-20.42	58.47
CAR	Carpentras	59010	3.15	52.43	-6.56	51.45
CNR	Cener	23981	-8.04	58.12	-19.44	58.41
CAB	Cabauw	63626	-12.28	55.36	-21.75	56.07
PAL	Palaiseau	49965	-4.74	56.41	-15.11	56.09
TOR	Toravere	75198	3.32	47.56	-6.11	46.24
PAY	Payerne	47340	4.00	50.70	-5.61	49.60
All	All sites	483489	-3.14	52.71	-12.83	52.28

6 Conclusions and Outlook

The first part of this section summarizes the results and conclusions of the individual studies. Moreover, answers to the key questions raised in the introduction (Sec. 1) are given. The second part contains an overall outlook on the application of reanalyses in the field of renewable energy.

6.1 Conclusions

Regional reanalyses are a new tool providing comprehensive meteorological data with great potential for a variety of applications. However, before these data can be used for renewable energy applications, e.g. balancing effects of wind- and PV-power, their quality needs to be assessed. Thus, in the first two studies of this thesis surface radiation and wind speed on relevant turbine heights of the new regional reanalyses COSMO-REA6 and COSMO-REA2 have compared to reference observations. After demonstrating the added value of the regional reanalyses compared to global reanalysis, a detailed analysis of the balancing effects of wind and solar energy based on reanalyses only was carried out.

Given the added value of the new reanalyses to estimate power in both power sectors, wind and PV, combined with the unique characteristic of reanalyses to provide wind and solar radiation physically consistent laid the foundation for new and more accurate insights to balancing potentials of wind and PV power. One important new aspect in this thesis was to investigate the balancing effects between different European countries. Moreover, new metrics were defined to investigate which additional balancing potential could be gained by optimizing the share between wind and PV installed capacities. In the following, for the sake of clarity, the conclusions are presented separately for the three sub-themes below. However, results of study I and II directly influenced methods and potentials for study III.

Study I - Radiation study

Study I addressed the suitability of the new high resolution regional reanalyses COSMO-REA for solar energy simulations and was published in Frank et al. [2018]. One of the central question was whether the new regional reanalyses have an improved performance compared to global reanalyses with respect to PV applications. Using ground measurements of the global horizontal irradiance - which is the central VRE variable for PV estimates - the estimates of reanalyses were assessed and the reliability of the different products compared. Multiple validation scores

like bias, RMSE, correlation, and variance showed the regional reanalyses outperforming the global reanalyses ERA-Interim and MERRA-2. The median of 10 BSRN sites of the daily mean bias for example improved from roughly 10 Wm^{-2} in the global reanalyses to less than 3 Wm^{-2} in the COSMO-reanalyses. This first central finding - which is confirmed by e.g. Urraca et al. [2018] - has motivated during the last years since publication several follow-up studies that used the new regional reanalyses as basis. Camargo et al. [2019] for example used COSMO-REA6 data in an potential study with the aim to cover the electricity demand of residential users in two countries in central Europe only by PV, battery systems and micro-generation wind turbines. Further, Peter [2019] uses the COSMO-REA6 data as basis for investigations with respect to the question how climate change affects the optimal allocation of variable renewable energy. These studies illustrate how urgent and valuable assessment studies like conducted in this thesis are.

Another central finding of the study is that the performance of representing GHI by the regional reanalyses is comparable to that of satellite derived products, even on local scale. This finding complements that of Molod et al. [2015] who showed that on aggregated country-scale PV output simulations based on the MERRA and MERRA-2 are comparable in quality to satellite based estimates. Our new finding that the regional reanalyses provide GHI with comparable quality as the satellite product SARAH also on local scale becomes of special interest in the field of hybrid wind-solar production studies, as GHI estimates in reanalyses are physically consistent with the wind estimates.

A third central finding, with respect to the question for the accuracy of the GHI provided by COSMO-REA6, is a cloud situation dependent systematic bias. In particular, GHI values are systematically underestimated in clear sky situations (by roughly -50 Wm^{-2}) and overestimated in cloudy situations (by roughly $+15 \text{ Wm}^{-2}$). In the long term, these effects compensate each other. Nevertheless, especially the underestimation in clear sky situations was shown in study III to have significant impact on the realistic representation of simulated PV production distributions. Thus, at this point a recommendation to use post-processed radiation components as derived in study I and study III is made here.

The fourth and last main finding is that the systematic GHI biases found in COSMO-REA6 can be successfully mitigated by post-processing. An algorithm using high quality GHI measurements from BSRN sites has been developed and the results have extensively been assessed. With a bias reduction during clear sky from -47 to -2 Wm^{-2} , and during cloudy sky from $+15$ to -1 Wm^{-2} , the post-processed GHI shows a significant reduction of systematic biases. In addition to the bias improvements also marginal distribution comparisons of e.g. ramp rates revealed significant improvements in the post-processed product. The new COSMO-REA6pp GHI is recommended for all applications which consider absolute values of GHI. In particular, studies working with instantaneous reanalysis output will profit from the post-processed GHI, as those studies do not aggregate and therefore do not mix different cloud situations.

Study II - Wind study

This second main study complemented the solar study by assessing the other most relevant VRE variable, namely the wind speed. The two regional reanalyses COSMO-REA are again evaluated on their quality, including an added value investigation compared to global reanalyses. Moreover, a comparison of hub-height wind speed provided by reanalyses and vertically extrapolated wind speed estimates with tower observations revealed the suitability of the regional reanalyses for wind power site assessment studies. As reference four well established wind towers with maximum measurements heights up to 280 m located in central Europe were used.

Concerning the question whether regional reanalyses perform better in representing hub-height wind speed than global reanalyses, the study revealed that the regional reanalyses COSMO-REA performs better or at least similar to the global reanalyses ERA-Interim and MERRA-2. The significance of the result is found to be strongly dependent on many factors such as considered site, height, atmospheric stability, and the applied validation metric. With a focus on significant improvements, especially marginal distributions of wind speed, ramp rates (wind speed changes within tree hours), and vertical wind gradients are found to be better represented in regional reanalyses. As an example, the most extreme observed ramp rates (lowest 5% + highest 5%) at levels above 98 m, global reanalyses are found to underrepresent these extremes by -80 to -43% while COSMO-REA6 and COSMO-REA2 represent them with relative errors between -28% to +2%, and between -14 to +9%, respectively. Thus, the regional reanalyses are the first reanalyses providing a reliable base for ramp rate analyses at a three hour scale.

Considering joint distribution scores like the bias, the mean absolute error, and the correlation most prominent improvements were found close to ground and at sites with increased complexity of the surrounding terrain. The bias corrected mean absolute error (BC_MAE) in 100 m above ground at the complex terrain site Karlsruhe for example improved from roughly 1.45 ms^{-1} in the global to 1.25 ms^{-1} in the regional reanalyses. While in Karlsruhe these improvements were found up to 200 m in other areas with less complex terrain improvements occurred rather close to ground. Thus, as expected the regional reanalyses improve compared to the global reanalyses especially in those areas where the local conditions become more dominant and thus the spatial resolution of the models is more important.

A second part of the wind study is concerned with the application potential of regional reanalyses for wind power site assessment. For this topic the use of reanalyses is of special interest as there is currently no gridded data set available which provides the wind information with the accuracy required from the economical perspective. With a shown improvement from global to regional reanalyses to represent wind characteristics, the question rises if the accuracy of the regional reanalyses now might fit the economical requirements for site assessment. In order to answer this question a pragmatical way was chosen. As defined in the German site assessment guidelines,

wind measurements obtained in 2/3 of hub-height with subsequent vertical extrapolation fulfill the required conditions. Therefore, in this study the reanalyses' reliability is directly compared to that of extrapolated measurements. The overall reference is given by meteorological towers. The main conclusion based on the conducted comparisons is that also the regional reanalyses are still not accurate enough to replace local tower measurements with subsequent extrapolation. Instead of reaching the extrapolation accuracy in heights of 3/2 above the measurement height reanalyses become equal in heights of roughly two to three times above the measurement height, at least at three out of four considered towers.

Study III - Balancing study of wind and PV power

In study III the regional reanalysis COSMO-REA6 has been used and exploited directly in one of its most promising applications in the renewable sector, namely the hybrid wind-solar balancing application. In order to conduct the hybrid investigations based on most realistic and unbiased irradiance estimates, the COSMO-REA6 irradiances have been post-processed before performing further analyses.

Comprehensive investigations concerned with the question if the post-processing of the direct and diffuse radiation improve the COSMO-REA6 derived PV estimates show especially the post-processed direct component leading to improvements. This can be seen by significant bias and MAE reductions of the direct radiation component during clear sky situations (from -50 to -9 Wm^{-2} and 98 to 85 Wm^{-2} , respectively), and an significantly improved frequency distribution of derived power estimates due to the post-processing when comparing to power observations. Given this main finding subsequent estimates of PV power for hybrid wind-solar balancing investigations have been calculated based on the post-processed radiation components.

To answer the second main question, to which extent extreme productions of the individual sources (wind or PV power) can be balanced out by adding the other source, daily power time-series of 20 years for 12 European countries derived from COSMO-REA6 were used. The central question is how well decorrelation effects of wind and PV lead to compensation effects, especially for extremes. This was investigated by tracking the 5th and 95th percentile changes between the hybrid wind-PV distribution of the 20 year power time-series and a theoretical wind-PV distribution where wind and PV productions were perfectly correlated. Comparisons of the distances of the 5th and 95th generation percentile between these two distributions showed distribution width reductions and therefore variability reduction potentials between 29 to 42% per country, at least for an optimized installation ratio scenario of wind an PV power plants. Thus, here the decorrelation potentials of wind and PV power generation have been found to be a relevant effect for all European countries.

With respect to the question whether specific countries do benefit more from hybrid production than other countries the main finding is that actually especially those countries benefit which have outstanding PV to wind installation ratios compared to the European mean. As this investigation was conducted with predefined fixed installation ratios of wind and PV, here further investigations of potentials under optimized installation ratio scenarios are recommended. For the installation scenario with the wind fleet installed end 2014 and the PV fleet installed end 2018, Czech Republic was found to have an outstanding installation ratio and therefore benefits most from hybrid production of other countries.

In the field of cross-border balancing potentials of extremes main conclusions are in principle threefold. First, simultaneous wind with PV extremes from country-to-country in Europe are rather seldom ($<10\%$), which indicates a high potential for cross-border balancing of extremes. Second, northern wind minima can often be balanced by southern PV production (joint probability of simultaneous wind-PV extremes is $<4\%$). Third, PV minimum situations in all European countries can often be balanced by northern wind production (joined probability of simultaneous wind-PV extremes is $<4\%$).

6.2 Overall picture and outlook

This thesis assessed new high resolution reanalyses (COSMO-REA6 and COSMO-REA2) and their applicability and added value for the renewable energy sector in comparison to other reanalyses. The comprehensive study showed why high resolution reanalyses should be preferred in general, but also for specific applications like in measure-correlate-predict approaches in site assessments studies, wind and PV ramp rate investigations, and wind drought evaluations. Benefits of regional reanalyses have been found in many aspects. Significant improvements compared to global reanalyses were found close to ground and in regions with complex surface characteristics. Moreover, a spatio-temporal representation study of GHI fields showed that cloud distributions as well as the connected atmospheric processes are significantly improved at all scales up to the synoptic scale. However, it has to be kept in mind that these findings are statistical and thus there are still some individual situations and sites where the global reanalyses provide more realistic estimates. However, the general conclusion that the regional reanalyses perform better than global reanalyses in representing wind speed and irradiance measurements is expected to be particularly important for upcoming studies which struggle with the question which reanalyses might be the best for their application.

Beside the *new insights* of the applicability of the reanalyses the thesis on hand also provides *improvements*, particularly achieved by the development of a new post-processing method for the COSMO-REA provided GHI, as well as direct and diffuse radiation. Comprehensive evaluations using both, post-processed radiation fields and derived PV estimates showed significant

achieved improvements due to the developed post-processing. The significant improvements were found to be especially caused by the adaptation of the direct radiation component. The simple methodology enables a fast implementation and is easy to apply. A special characteristic of the developed post-processing is its applicability to the whole reanalysis domain. Thus, not only site specific improvements are achieved but improvements for whole Europe. Sectors expected to benefit most from the developed post-processing are the PV, as well as the solar concentrating power sector.

The application of regional reanalyses in the field of European hybrid wind-solar balancing effects revealed variability reduction potentials from 29 to 42% per country when having an optimized share of installed wind and PV power. The investigations showed the potential being slightly higher in northern than in southern European countries. Further, when focusing on cross-border balancing potentials, occurrence probabilities of less than 10% were found for simultaneous extreme productions of wind in the one and PV in the other country. Even higher is the balancing potential of northern wind minimums by southern PV production. Here, the probability of simultaneous occurrence reduces to 4%. Thus, from a meteorological perspective especially cross-Alp electricity inter-connectors seem to be promising for an effective electricity production balancing.

Although the COSMO reanalyses provide enhanced information for energy related applications, further improvements would be desirable. Starting from the view of PV applications further improvements of the radiation reliability are necessary in order to satisfy the economic requirements. In case of a new reanalyses development it is highly recommended to update the used aerosol climatology. Also from the perspective of wind power especially for site assessment studies further improvements would be necessary. A central problem for site assessment studies is still the problem of systematic site dependent biases in the reanalyses products. To improve this issue further data assimilation and improved representations of roughness and land use might be useful. In terms of data assimilation, new reanalyses might profit from wind lidar assimilation or in future also from the wind observations retrieved from the AEOLUS satellite [Stoffelen et al., 2005]. Moreover, the wind as well as the solar energy sector would profit from a longer time span than the actual 23 years of COSMO-REA6. With the knowledge that ERA-Interim and with it the COSMO reanalyses will end in August 2019 it is desirable to set up a new regional reanalyses which covers a longer time period. Here, ERA5 of the European Centre for Medium-Range Weather Forecasts might be a good choice for providing boundary condition.

With the increased resolution of the new regional reanalyses down to the kilometer scale, reanalyses are expected to become now also of interest for applications like island networks and local self-sufficiency. It is expected that these research topics will play an increasing role for the energy industry and thus there will be an increased need for weather data with high resolution and high accuracy to tackle these questions.

Bibliography

- Allen, M. R., Dube, O. P., Aragon-Durand, F., Cramer, W., Humphreys, S., Kainuma, M., Kala, J., Mahowald, N., Mulugetta, Y., Perez, R., Wairiu, M., and Zickfeld, K. (2018). Framing and context, in: Global warming of 1.5°C. an ipcc special report on the impacts of global warming of 1.5°C above pre-industrial levels and related global greenhouse gas emission pathways, in the context of strengthening the global response to the threat of climate change, sustainable development, and efforts to eradicate poverty [masson-detmotte et al.]. Technical report.
- Bañuelos-Ruedas, F., Angeles-Camacho, C., and Rios-Marcuello, S. (2010). Analysis and validation of the methodology used in the extrapolation of wind speed data at different heights. *Renewable and Sustainable Energy Reviews*, 14(8):2383–2391.
- Bett, P. E. and Thornton, H. E. (2016). The climatological relationships between wind and solar energy supply in Britain. *Renewable Energy*, 87:96–110.
- Bett, P. E., Thornton, H. E., and Clark, R. T. (2013). European wind variability over 140 yr. *Advances in Science and Research*, 10(April):51–58.
- Beyrich, F. and Adam, W. K. (2007). *Site and Data Report for the Lindenberg Reference Site in CEOP - Phase I*.
- Blanc, P., Gschwind, B., Lefèvre, M., and Wald, L. (2011). The HelioClim project: Surface solar irradiance data for climate applications. *Remote Sensing*, 3(2):343–361.
- Boilley, A. and Wald, L. (2015). Comparison between meteorological re-analyses from ERA-Interim and MERRA and measurements of daily solar irradiation at surface. *Renewable Energy*, 75:135–143.
- Bollmeyer, C. (2015). *A high-resolution regional reanalysis for Europe and Germany*. PhD thesis, University of Bonn.
- Bollmeyer, C., Keller, J. D., Ohlwein, C., Wahl, S., Crewell, S., Friederichs, P., Hense, A., Keune, J., Kneifel, S., Pscheidt, I., Redl, S., and Steinke, S. (2015). Towards a high-resolution regional reanalysis for the European CORDEX domain. *Quarterly Journal of the Royal Meteorological Society*, 141(686):1–15.
- Borsche, M., Kaiser-Weiss, A. K., and Kaspar, F. (2016). Wind speed variability between 10 and 116 m height from the regional reanalysis COSMO-REA6 compared to wind mast measurements over Northern Germany and the Netherlands. *Advances in Science and Research*, 13:151–161.
- Bowen, B., Dewart, J., and Chen, A. (1983). Stability Class Determination: A Comparison for one site. pages 211–214, Boston, MA. American Meteorological Society.

- Brümmer, B., Lange, I., and Konow, H. (2012). Atmospheric boundary layer measurements at the 280 m high Hamburg weather mast 1995-2011: Mean annual and diurnal cycles. *Meteorologische Zeitschrift*, 21(4):319–335.
- Bundesnetzagentur (2014). Monitoringbericht 2014. Technical report, Bundesnetzagentur für Elektrizität, Gas, Telekommunikation, Post und Eisenbahnen, Bonn.
- Bundesnetzagentur (2018). Monitoringbericht 2018. Technical report, Bundesnetzagentur für Elektrizität, Gas, Telekommunikation, Post und Eisenbahnen, Bonn.
- Camargo, L. R., Gruber, K., and Nitsch, F. (2018). Assessing variables of regional reanalysis data sets relevant for modelling small-scale renewable energy systems. *Renewable Energy*.
- Camargo, L. R., Gruber, K., Nitsch, F., and Dorner, W. (2019). Hybrid renewable energy systems to supply electricity self-sufficient residential buildings in Central Europe. *Energy Procedia*, 158:321–326.
- Cannon, D., Brayshaw, D. J., Methven, J., Coker, P. J., and Lenaghan, D. (2014). Using reanalysis data to quantify extreme wind power generation statistics: a 33 year case study in Great Britain. *Renewable Energy*, 75:767–778.
- Carta, J. A., Velázquez, S., and Cabrera, P. (2013). A review of measure-correlate-predict (MCP) methods used to estimate long-term wind characteristics at a target site. *Renewable and Sustainable Energy Reviews*, 27:362–400.
- Child, M., Kemfert, C., Bogdanov, D., and Breyer, C. (2019). Flexible electricity generation, grid exchange and storage for the transition to a 100% renewable energy system in Europe. *Renewable Energy*, 139:80–101.
- Dabernig, M., Mayr, G. J., and Messner, J. W. (2015). Predicting wind power with reforecasts. *Weather and Forecasting*, 30(6):1655–1662.
- Dee, D. P., Uppala, S. M., Simmons, a. J., Berrisford, P., Poli, P., Kobayashi, S., Andrae, U., Balmaseda, M. a., Balsamo, G., Bauer, P., Bechtold, P., Beljaars, a. C. M., van de Berg, L., Bidlot, J., Bormann, N., Delsol, C., Dragani, R., Fuentes, M., Geer, a. J., Haimberger, L., Healy, S. B., Hersbach, H., Hólm, E. V., Isaksen, L., Kållberg, P., Köhler, M., Matricardi, M., McNally, a. P., Monge-Sanz, B. M., Morcrette, J. J., Park, B. K., Peubey, C., de Rosnay, P., Tavolato, C., Thépaut, J. N., and Vitart, F. (2011). The ERA-Interim reanalysis: Configuration and performance of the data assimilation system. *Quarterly Journal of the Royal Meteorological Society*, 137(656):553–597.
- Dittmann, S., Friesen, G., Williams, S., Betts, T., Gottschalg, R., Beyer, H. G., Guerin de Montgareuil, A., van der Borg, N., Burgers, A., Huld, T., Müller, B., Reise, C., Kurnik, J., Topic, M., Zdanowicz, T., and Fabero, F. (2010). Results of the 3rd modelling round robin

- within the European project ' PERFORMANCE ' - Comparison of module energy rating methods. page tba.
- Efron, B. and Tibshirani, R. J. (1994). *An Introduction to the Bootstrap*. CRC Press Book.
- EPA (1994). An evaluation of a solar radiation/delta-t method for estimating Pasquill-Gifford (P-G) stability categories. Technical report, U.S. Environmental Protection Agency, Research Triangle Park, NC.
- Faiman, D. (2008). Assessing the outdoor operating temperature of photovoltaic modules. *Progress in Photovoltaics: Research Applications*, 16(4):307–315.
- Fernandez, G., Usabiaga, H., and Vandepitte, D. (2018). An efficient procedure for the calculation of the stress distribution in a wind turbine blade under aerodynamic loads. *Journal of Wind Engineering and Industrial Aerodynamics*, 172(November 2017):42–54.
- Fördergesellschaft Windenergie und andere Erneuerbare Energien (2011). Technische Richtlinien für Windenergieanlagen: Teil 6 Bestimmung von Windpotenzial und Energieertägen. Technical report, Berlin.
- Frank, C. W., Pospichal, B., Wahl, S., Keller, J. D., Hense, A., and Crewell, S. (2019). The added value of high resolution regional reanalyses for wind power applications. *Renewable Energy*.
- Frank, C. W., Wahl, S., Keller, J. D., Pospichal, B., Hense, A., and Crewell, S. (2018). Bias correction of a novel European reanalysis data set for solar energy applications. *Solar Energy*, 164:12–24.
- Gelaro, R., McCarty, W., Suárez, M. J., Todling, R., Molod, A., Takacs, L., Randles, C. A., Darmenov, A., Bosilovich, M. G., Reichle, R., Wargan, K., Coy, L., Cullather, R., Draper, C., Akella, S., Buchard, V., Conaty, A., da Silva, A. M., Gu, W., Kim, G. K., Koster, R., Lucchesi, R., Merkova, D., Nielsen, J. E., Partyka, G., Pawson, S., Putman, W., Rienecker, M., Schubert, S. D., Sienkiewicz, M., and Zhao, B. (2017). The modern-era retrospective analysis for research and applications, version 2 (MERRA-2). *Journal of Climate*, 30(14):5419–5454.
- Gilleland, E., Ahijevych, D., Brown, B. G., Casati, B., and Ebert, E. E. (2009). Intercomparison of Spatial Forecast Verification Methods. *Weather and Forecasting*, 24(5):1416–1430.
- Graabak, I. and Korpås, M. (2016). Variability Characteristics of European Wind and Solar Power Resources-A Review. *Energies*, 9(6):449.
- Grams, C. M., Beerli, R., Pfenninger, S., Staffell, I., and Wernli, H. (2017). Balancing Europe's wind-power output through spatial deployment informed by weather regimes. *Nature Climate Change*, 7(8):557–562.

- Gualtieri, G. and Secci, S. (2011). Comparing methods to calculate atmospheric stability-dependent wind speed profiles: A case study on coastal location. *Renewable Energy*, 36(8):2189–2204.
- Gueymard, C. A. and Myers, D. R. (2009). Evaluation of conventional and high-performance routine solar radiation measurements for improved solar resource, climatological trends, and radiative modeling. *Solar Energy*, 83(2):171–185.
- Hadi, F. A. (2015). Diagnosis of the Best Method for Wind Speed Extrapolation. *International Journal of Advanced Research in Electrical Electronics and Instrumentation Engineering*, 4(10):8176–8183.
- Heide, D., von Bremen, L., Greiner, M., Hoffmann, C., Speckmann, M., and Bofinger, S. (2010). Seasonal optimal mix of wind and solar power in a future, highly renewable Europe. *Renewable Energy*, 35(11):2483–2489.
- Heimo, A., Vernez, A., and Wasserfallen, P. (1993). Baseline Surface Radiation Network (BSRN). Concept and Implementation of a BSRN Station.
- Henckes, P., Frank, C. W., Küchler, N., Peter, J., and Wagner, J. (2019). Uncertainty estimation of investment planning models under high shares of renewables using reanalysis data. *Working Paper, Submitted in April 2019 to Energy*.
- Henckes, P., Knaut, A., Obermüller, F., and Frank, C. (2018). The benefit of long-term high resolution wind data for electricity system analysis. *Energy*, 143:934–942.
- Huld, T., Friesen, G., Skoczek, A., Kenny, R. P., Sample, T., Field, M., and Dunlop, E. D. (2011). A power-rating model for crystalline silicon PV modules. *Solar Energy Materials and Solar Cells*, 95(12):3359–3369.
- Huld, T. and Gracia Amillo, A. M. (2015). Estimating PV module performance over large geographical regions: The role of irradiance, air temperature, wind speed and solar spectrum. *Energies*, 8(6):5159–5181.
- IEC (2005). International Standard IEC 61400-1. Technical report.
- Irwin, J. S. (1979). A theoretical variation of the wind profile power law exponent as a function of surface roughness length and stability. *Atmospheric Environment*, 13:191–194.
- Israelevich, P., Ganor, E., Alpert, P., Kishcha, P., and Stupp, A. (2012). Predominant transport paths of Saharan dust over the Mediterranean Sea to Europe. *Journal of Geophysical Research Atmospheres*, 117(2):1–11.
- Jacob, D., Petersen, J., Eggert, B., Alias, A., Christensen, O. B., Bouwer, L. M., Braun, A., Colette, A., Déqué, M., Georgievski, G., Georgopoulou, E., Gobiet, A., Menut, L., Nikulin, G., Haensler, A., Hempelmann, N., Jones, C., Keuler, K., Kovats, S., Kröner, N., Kotlarski,

- S., Kriegsmann, A., Martin, E., van Meijgaard, E., Moseley, C., Pfeifer, S., Preuschmann, S., Radermacher, C., Radtke, K., Rechid, D., Rounsevell, M., Samuelsson, P., Somot, S., Soussana, J. F., Teichmann, C., Valentini, R., Vautard, R., Weber, B., and Yiou, P. (2014). EURO-CORDEX: New high-resolution climate change projections for European impact research. *Regional Environmental Change*, 14(2):563–578.
- Jia, B., Xie, Z., Dai, A., Shi, C., and Chen, F. (2013). Evaluation of satellite and reanalysis products of downward surface solar radiation over East Asia: Spatial and seasonal variations. *Journal of Geophysical Research Atmospheres*, 118(9):3431–3446.
- Kaigh, W. D. (1983). Quantile interval estimation. *Communications in Statistics - Theory and Methods*, 12(21):2427–2443.
- Kaiser-Weiss, A. K., Kaspar, F., Heene, V., Borsche, M., Tan, D. G. H., Poli, P., Obregon, a., and Gregow, H. (2015). Comparison of regional and global reanalysis near-surface winds with station observations over Germany. *Advances in Science and Research*, 12:187–198.
- Kaspar, F., Borsche, M., Pfeifroth, U., Trentmann, J., Drücke, J., and Becker, P. (2019). A climatological assessment of balancing effects and shortfall risks of photovoltaics and wind energy in Germany and Europe. *Advances in Science and Research*, 16(July):119–128.
- Killinger, S., Lingfors, D., Saint-Drenan, Y.-M., Moraitis, P., Sark, W. V., Taylor, J., Engerer, N. A., and Bright, J. M. (2018). On the search for representative characteristics of PV systems: Data collection and analysis of PV system azimuth, tilt, capacity, yield and shading. *Solar Energy*, 173(April):1087–1106.
- Kleissl, J. (2013). *Solar energy forecasting and resource assessment*. Academic Press.
- Klucher, T. M. (1979). Evaluation of models to predict insolation on tilted surfaces. *Solar Energy*, 23(2):111–114.
- Koehl, M., Heck, M., Wiesmeier, S., and Wirth, J. (2011). Modeling of the nominal operating cell temperature based on outdoor weathering. *Solar Energy Materials and Solar Cells*, 95(7):1638–1646.
- Koepke, P., Hess, M., Schult, I., and Shettle, E. P. (1997). Global Aerosol Dataset. Technical report, Max-Planck-Institut für Meteorologie, Hamburg, Germany.
- Kohavi, R. (1995). A Study of Cross-Validation and Bootstrap for Accuracy Estimation and Model Selection. *International Joint Conference on Artificial Intelligence*, 14(12):1137–1143.
- Kohler, M., Metzger, J., and Kalthoff, N. (2018). Trends in temperature and wind speed from 40 years of observations at a 200-m high meteorological tower in Southwest Germany. *International Journal of Climatology*, 38(1):23–34.

- König-Langlo, G., Sieger, R., Schmithüsen, H., Bücken, A., Richter, F., and Dutton, E. (2013). The Baseline Surface Radiation Network and its World Radiation Monitoring Centre at the Alfred Wegener Institute.
- Kubik, M. L., Brayshaw, D. J., Coker, P. J., and Barlow, J. F. (2013). Exploring the role of reanalysis data in simulating regional wind generation variability over Northern Ireland. *Renewable Energy*, 57:558–561.
- Küchler, N. (2018). *Ground-based remote sensing of warm low-level stratified clouds - new perspectives and applications*. PhD thesis, University of Cologne.
- Lan, C. W., Lo, M. H., Chen, C. A., and Yu, J. Y. (2019). The mechanisms behind changes in the seasonality of global precipitation found in reanalysis products and CMIP5 simulations. *Climate Dynamics*, 53(7):4173–4187.
- Linares-Rodríguez, A., Ruiz-Arias, J. A., Pozo-Vázquez, D., and Tovar-Pescador, J. (2011). Generation of synthetic daily global solar radiation data based on ERA-Interim reanalysis and artificial neural networks. *Energy*, 36(8):5356–5365.
- Lohmann, S., Schillings, C., Mayer, B., and Meyer, R. (2006). Long-term variability of solar direct and global radiation derived from ISCCP data and comparison with reanalysis data. *Solar Energy*, 80(11):1390–1401.
- Long, C. N. and Dutton, E. G. (2002). BSRN Global Network recommended QC tests, V2.
- Lubitz, W. D. (2006). Accuracy of vertically extrapolating meteorological tower wind speed measurements. In *Canadian Wind Energy Association*, Winnipeg, Manitoba, Canada.
- Markovsky, I. and Huffel, S. V. (2007). Overview of total least-squares methods. *ScienceDirect*, 87:2283–2302.
- Martin, N. and Ruiz, J. M. (2001). Calculation of the PV modules angular losses under field conditions by means of an analytical model. *Solar Energy Materials and Solar Cells*, 70(1):25–38.
- Masters, G. M. (2004). *Renewable and Efficient Electric Power Systems*. Wiley.
- Michaelsen, J. (1987). Cross-Validation in Statistical Climate Forecast Models. *Journal of Climate and Applied Meteorology*, 26(11):1589–1600.
- Mohan, M. and Siddiqui, T. A. (1998). Analysis of various schemes for the estimation of atmospheric stability classification. *Atmospheric Environment*, 32(21):3775–3781.
- Molod, A., Takacs, L., Suarez, M., and Bacmeister, J. (2015). Development of the GEOS-5 atmospheric general circulation model: Evolution from MERRA to MERRA2. *Geoscientific Model Development*, 8(5):1339–1356.

- Mulder, F. M. (2014). Implications of diurnal and seasonal variations in renewable energy generation for large scale energy storage. *Journal of Renewable and Sustainable Energy*, 033105(2014):1–14.
- Müller, R., Pfeifroth, U., Träger-Chatterjee, C., Trentmann, J., and Cremer, R. (2015). Digging the METEOSAT treasure—3 decades of solar surface radiation. *Remote Sensing*, 7(6):8067–8101.
- Muneer, T. (1990). Solar radiation model for Europe. *Building Services Engineering Research & Technology*, 11(4):153–163.
- Nelson, J., Johnston, J., Mileva, A., Fripp, M., Hoffman, I., Petros-Good, A., Blanco, C., and Kammen, D. M. (2012). High-resolution modeling of the western North American power system demonstrates low-cost and low-carbon futures. *Energy Policy*, 43:436–447.
- Ohmura, A., Gilgen, H., Hegner, H., Müller, G., Wild, M., Dutton, E., Forgan, B., Fröhlich, C., Philipona, R., Heimo, A., König-Langlo, G., McArthur, B., Pinker, R., Whitlock, C., and Dehne, K. (1998). Baseline Surface Radiation Network (BSRN/WCRP): New Precision Radiometry for Climate Research. *Bulletin of the American Meteorological Society*, 79:2115–2136.
- OPSD (2019a). Open Power System Data, Data package National generation capacity, DOI: https://doi.org/10.25832/national_generation_capacity/2019-02-22.
- OPSD (2019b). Open System Power Data, Data Package Time series, DOI: https://doi.org/10.25832/time_series/2019-06-05.
- Perez, M. J. and Fthenakis, V. M. (2015). On the spatial decorrelation of stochastic solar resource variability at long timescales. *Solar Energy*, 117:46–58.
- Perez, R., Kivalov, S., Schlemmer, J., Hemker, K., and Hoff, T. E. (2012). Short-term irradiance variability: Preliminary estimation of station pair correlation as a function of distance. *Solar Energy*, 86(8):2170–2176.
- Perez, R., Stewart, R., Arbogast, C., Seals, R., and Scott, J. (1986). An anisotropic hourly diffuse radiation model for sloping surfaces: Description, performance validation, site dependency evaluation. *Solar Energy*, 36(6):481–497.
- Peter, J. (2019). How Does Climate Change Affect Optimal Allocation of Variable Renewable Energy? EWI Working Papers 2019-3, Energiewirtschaftliches Institut an der Universität zu Köln (EWI).
- Petrik, R., Geyer, B., and Rockel, B. (2019). Atmospheric variability in PBL depicted by most recent regional hindcasts. *in preparation for submission*.

- Pfenninger, S. (2017). Dealing with multiple decades of hourly wind and PV time series in energy models: A comparison of methods to reduce time resolution and the planning implications of inter-annual variability. *Applied Energy*, 197:1–13.
- Pfenninger, S. and Staffell, I. (2016). Long-term patterns of European PV output using 30 years of validated hourly reanalysis and satellite data. *Energy*, 114:1251–1265.
- Poli, P., Hersbach, H., Tan, D., Dee, D., Thépaut, J.-N., Simmons, A., Peubey, C., Laloyaux, P., Komori, T., Berrisford, P., and Dragani, R. (2013). The data assimilation system and initial performance evaluation of the ECMWF pilot reanalysis of the 20th-century assimilating surface observations only (ERA-20C). *ERA report series*, 14:59.
- Posselt, R., Mueller, R. W., Stöckli, R., and Trentmann, J. (2012). Remote sensing of solar surface radiation for climate monitoring - the CM-SAF retrieval in international comparison. *Remote Sensing of Environment*, 118:186–198.
- Quaschnig, V. (2013). *Regenerative Energiesysteme - Technologie – Berechnung – Klimaschutz*. Hanser Verlag München, 8. aktualisierte edition.
- Rabin, J., Delon, J., and Gousseau, Y. (2008). Circular Earth Mover ' s Distance for the comparison of local features. In *2008 19th International Conference on Pattern Recognition*, pages 1–4.
- Randles, C. A., da Silva, A. M., Buchard, V., Darmenov, A., Colarco, P. R., Aquila, V., Bian, H., Nowottnick, E. P., Pan, X., Smirnov, A., Yu, H., and Govindaraju, R. (2016). The MERRA - 2 Aerosol Assimilation. *Technical Report Series on Global Modeling and Data Assimilation*, 45(December).
- Ranjha, R., Svensson, G., Tjernström, M., and Semedo, A. (2013). Global distribution and seasonal variability of coastal low-level jets derived from ERA-Interim reanalysis. *Tellus A: Dynamic Meteorology and Oceanography*, 65.
- Richardson, D. B. and Andrews, R. W. (2014). Validation of the MERRA dataset for solar PV applications. *2014 IEEE 40th Photovoltaic Specialist Conference, PVSC 2014*, pages 809–814.
- Rienecker, M. M., Suarez, M. J., Gelaro, R., Todling, R., Bacmeister, J., Liu, E., Bosilovich, M. G., Schubert, S. D., Takacs, L., Kim, G. K., Bloom, S., Chen, J., Collins, D., Conaty, A., Da Silva, A., Gu, W., Joiner, J., Koster, R. D., Lucchesi, R., Molod, A., Owens, T., Pawson, S., Pegion, P., Redder, C. R., Reichle, R., Robertson, F. R., Ruddick, A. G., Sienkiewicz, M., and Woollen, J. (2011). MERRA: NASA's modern-era retrospective analysis for research and applications. *Journal of Climate*, 24(14):3624–3648.
- Ritter, B. and Geleyn, J.-F. (1992). A Comprehensive Radiation Scheme for Numerical Weather Prediction Models with Potential Applications in Climate Simulations. *Monthly Weather Review*, 120(2):303–325.

- Ritter, M., Shen, Z., Cabrera, B. L., Odening, M., and Deckert, L. (2015). A New Approach to Assess Wind Energy Potential. *Energy Procedia*, 75:671–676.
- Roques, F., Hiroux, C., and Saguan, M. (2010). Optimal wind power deployment in Europe - A portfolio approach. *Energy Policy*, 38(7):3245–3256.
- Rose, S. and Apt, J. (2015). What can reanalysis data tell us about wind power? *Renewable Energy*, 83:963–969.
- Saint-Drenan, Y.-M., Wald, L., Ranchin, T., Dubus, L., and Troccoli, A. (2018). An approach for the estimation of the aggregated photovoltaic power generated in several European countries from meteorological data. *Advances in Science and Research*, 15:51–62.
- Santos-Alamillos, F. J., Pozo-Vázquez, D., Ruiz-Arias, J. A., Lara-Fanego, V., and Tovar-Pescador, J. (2012). Analysis of spatiotemporal balancing between wind and solar energy resources in the southern Iberian Peninsula. *Journal of Applied Meteorology and Climatology*, 51(11):2005–2024.
- Schättler, U. and Doms, G. (2011). A Description of the Nonhydrostatic Regional COSMO-Model Part I: Dynamics and Numerics. Technical report, Deutscher Wetterdienst.
- Schraff, C. H. (1997). Mesoscale data assimilation and prediction of low stratus in the Alpine region. *Meteorology and Atmospheric Physics*, 64(1-2):21–50.
- Simmer, C., Adrian, G., Jones, S., Wirth, V., Göber, M., Hohenegger, C., Janjić, T., Keller, J., Ohlwein, C., Seifert, A., Trömel, S., Ulbrich, T., Wapler, K., Weissmann, M., Keller, J., Masbou, M., Meilinger, S., Reiß, N., Schomburg, A., Vormann, A., and Weingärtner, C. (2016). Herz: The german hans-ertel centre for weather research. *Bulletin of the American Meteorological Society*, 97(6):1057–1068.
- Simmons, A. J., Berrisford, P., Dee, D. P., Hersbach, H., Hirahara, S., and Thépaut, J. N. (2017). A reassessment of temperature variations and trends from global reanalyses and monthly surface climatological datasets. *Quarterly Journal of the Royal Meteorological Society*, 143(702):101–119.
- Smedman-Högström, A.-S. and Högström, U. (1978). A Practical Method for Determining Wind Frequency Distributions for the Lowest 200 m from Routine Meteorological Data. *Journal of Applied Meteorology*, 17(7):942–954.
- Spera, D. A. (1994). *Wind Turbine Technology: Fundamental Concepts of Wind Turbine Engineering*. ASME Press, New York.
- Staffell, I. and Pfenninger, S. (2016). Using bias-corrected reanalysis to simulate current and future wind power output. *Energy*, 114:1224–1239.

- Steinke, S., Wahl, S., and Crewell, S. (2019). Benefit of high resolution COSMO reanalysis : The diurnal cycle of column-integrated water vapour over Germany. *Meteorologische Zeitschrift*, submitted.
- Stephan, K., Klink, S., and Sraff, C. (2008). Assimilation of radar-derived rain rates into the convective-scale model COSMO-DE at DWD. *Quarterly Journal of the Royal Meteorological Society*, 134:1315–1326.
- Stoffelen, A., Pailleux, J., Källén, E., Vaughan, J. M., Isaksen, L., Flamant, P., Wergen, W., Andersson, E., Schyberg, H., Culoma, A., Meynart, R., Endemann, M., and Ingmann, P. (2005). The atmospheric dynamics mission for global wind field measurement. *Bulletin of the American Meteorological Society*, 86(1):73–87.
- Stone, M. (1974). Cross-Validatory Choice and Assessment of Statistical Predictions. *Journal of the Royal Statistical Society*, 36(2):111–147.
- Stull, R. B. (1988a). Mean Boundary Layer Characteristics. In *An Introduction to Boundary Layer Meteorology*, pages 1–27.
- Stull, R. B. (1988b). Similarity Theory. In *An Introduction to Boundary Layer Meteorology*, pages 347–404.
- Tafarte, P., Das, S., Eichhorn, M., and Thrän, D. (2014). Small adaptations, big impacts: Options for an optimized mix of variable renewable energy sources. *Energy*, 72:80–92.
- Tanre, D., Geleyn, J. F., and Slingo, J. (1984). First results of the introduction of an advanced aerosol-radiation interaction in the ECMWF low resolution global model. In *Aerosols and their climatic effects*, pages 133–177. A. DEEPAC Publishing.
- UBA (2018). Berichterstattung unter der Klimarahmenkonvention der Vereinten Nationen und dem Kyoto-Protokoll 2018.
- Urraca, R., Huld, T., Lindfors, A. V., Riihelä, A., Martinez-de Pison, F. J., and Sanz-Garcia, A. (2018). Quantifying the amplified bias of PV system simulations due to uncertainties in solar radiation estimates. *Solar Energy*, 176(June):663–677.
- Van Ulden, A. P. and Wieringa, J. (1996). Atmospheric boundary layer research at Cabauw. *Boundary-Layer Meteorology*, 78(1-2):39–69.
- Vasilj, J., Sarajcev, P., and Jakus, D. (2016). Estimating future balancing power requirements in wind - PV power system. *Renewable Energy*, 99:369–378.
- von Storch, H. and Zwiers, F. W. (2003). *Statistical Analysis Climate Research*. Cambridge University Press, netlibrary edition.

- Wahl, S., Bollmeyer, C., Crewell, S., Figura, C., Friederichs, P., Hense, A., Keller, J. D., and Ohlwein, C. (2017). A novel convective-scale regional reanalysis COSMO-REA2: Improving the representation of precipitation. *Meteorologische Zeitschrift*, 26(4):345–361.
- WMO (2008). *Guide to Meteorological Instruments and Methods of observation*, volume I & II.
- Zappa, W. and van den Broek, M. (2018). Analysing the potential of integrating wind and solar power in Europe using spatial optimisation under various scenarios. *Renewable and Sustainable Energy Reviews*, 94(May):1192–1216.
- Zhang, H., Cao, Y., Zhang, Y., and Terzija, V. (2018). Quantitative synergy assessment of regional wind-solar energy resources based on MERRA reanalysis data. *Applied Energy*, 216(February):172–182.
- Zubler, E. M., Lohmann, U., Lüthi, D., and Schär, C. (2011). Intercomparison of aerosol climatologies for use in a regional climate model over Europe. *Geophysical Research Letters*, 38(15):1–5.

Danksagung

An erster Stelle gilt mein Dank meiner Doktormutter Prof. Dr. Susanne Crewell, die mich während der Bearbeitungszeit dieser Dissertation intensiv begleitete und unterstützte. Durch ihre Hilfestellungen und ihre konstruktiven Anregungen wurde diese Arbeit in der vorliegenden Form erst möglich.

Ein besonderer Dank gilt auch meinen Betreuern Bernhard Pospichal und Sabrina Wahl für ihre sowohl intensive wissenschaftliche als auch persönliche Begleitung während meiner Promotion. Eure unzähligen Denkanstöße, wertvollen Diskussionbeiträge, Korrekturen und Ratschläge waren mir eine besondere Unterstützung.

Desweiteren möchte ich mich bei Andreas Hense bedanken, der mich seit Beginn meines Meteorologiestudiums stets motivierte über den eigenen Tellerrand zu blicken und insbesondere die Welt der Statistik zu begreifen.

Zudem möchte ich meinen Dank an das HErZ Projekt (grant number BMVI/DWD DWD2014P5A) des deutschen Wetterdienstes, als auch an das ET-CC Projekt (grant number ZUK 81/1) aussprechen, welche mir die finanziellen Mittel für die Anfertigung dieser Doktorarbeit bereitstellten. Über die finanzielle Unterstützung hinaus ermöglichten mir diese Projekte ein interdisziplinäres Netzwerk vieler helfender Köpfe aufzubauen. Hier möchte ich mich insbesondere bei Frank Kaspar des deutschen Wetterdienstes, sowie Herrn Höffler vom Energiewirtschaftlichen Institut an der Universität zu Köln bedanken.

Ebenfalls bedanke ich mich für die Bereitstellung verschiedenster historischer Wetterdaten vom deutschen Wetterdienst, sowie die Bereitstellung von Rechenzeit auf dem HPC Cray des ECMWFs. In diesem Zusammenhang möchte ich mich auch bei den Wettermastbetreibern der Masten in Lindenberg, Cabauw, Karlsruhe und Hamburg sowie bei Gerd König-Langlo für die Bereitstellung der qualitativ hochwertigen BSRN Messungen der Strahlung bedanken, die solche Studien wie die hier durchgeführte erst möglich machen.

Maria, Philipp, Nils und Rosa, danke für die Zeit mit euch, die zahlreichen angenehmen wissenschaftlichen sowie privaten Gespräche und die immer entspannte Atmosphäre.

Chris und Clari, es ist schön euch auch nach der Studienzeit noch als enge Freunde zu haben. Vielen Dank für eure Korrekturen und die Hilfe bezüglich technischer Fragen.

Mein Dank gilt ferner allen Kolleginnen und Kollegen der Arbeitsgruppe INFERNO sowie dem kompletten Institut für Meteorologie der Universität zu Köln für das kollegiale, angenehme Arbeitsklima und die konstruktive Zusammenarbeit.

Neben den zahlreichen fachlichen Beiträgen, die mich auf dem Weg zur fertigen Arbeit immer wieder neue Aspekte und Ansätze entdecken ließen, möchte ich mich bei allen zuvor genannten Personen und jenen, die hier nicht aufgelistet sind, aber genannt hätten werden sollen, für die gemeinsame bunte Zeit und die vielen außerdisziplinären Gespräche bedanken.

Last but not least möchte ich mich an dieser Stelle auch bei meinen Eltern und Schwiegereltern, meinen Geschwistern, meiner Schwägerin und meinen Freunden, für die Begleitung und moralische Unterstützung während meiner Dissertation bedanken. Ein Dank auch an meinen Sohn Leonas, der mir in den letzten Zügen der Dissertation den notwendigen Ansporn gab, meine Dissertation zeitnah fertig zu stellen. Meiner Frau Mima, danke ich besonders für ihre unermüdliche Stärkung und Motivierung und ihr stets offenes Ohr für meine Gedanken. Danke, dass du bist wie du bist.

Erklärung

Ich versichere, dass ich die von mir vorgelegte Dissertation selbständig angefertigt, die benutzten Quellen und Hilfsmittel vollständig angegeben und die Stellen der Arbeit - einschließlich Tabellen, Karten und Abbildungen -, die anderen Werken im Wortlaut oder dem Sinn nach entnommen sind, in jedem Einzelfall als Entlehnung kenntlich gemacht habe; dass diese Dissertation noch keiner anderen Fakultät oder Universität zur Prüfung vorgelegen hat; dass sie - abgesehen von unten angegebenen Teilpublikationen - noch nicht veröffentlicht worden ist sowie, dass ich eine solche Veröffentlichung vor Abschluss des Promotionsverfahrens nicht vornehmen werde. Die Bestimmungen der Promotionsordnung sind mir bekannt. Die von mir vorgelegte Dissertation ist von Prof. Dr. Susanne Crewell betreut worden.

Köln, den 04. Oktober 2019

CHRISTOPHER W. FRANK

Teilpublikationen

Christopher W. Frank et al. (2018): "A novel data set for solar energy applications based on high resolution reanalysis". In: *Solar Energy*, 164, pp. 12-24. ISSN: 0038-092X, DOI: doi.org/10.1016/j.solener.2018.02.012.

Christopher W. Frank et al. (2019): "The added value of high resolution regional reanalyses for wind power applications". In: *Renewable Energy*, DOI: doi.org/10.1016/j.renene.2019.09.138

Henckes, P., A. Knaut, F. Obermüller, C. Frank (2018): "The benefit of long-term high resolution wind data for electricity system analysis". In: *Energy*, 143, pp. 934-942, DOI: [10.1016/j.energy.2017.10.049](https://doi.org/10.1016/j.energy.2017.10.049)

